UC San Diego

UC San Diego Electronic Theses and Dissertations

Title

Printed Wearable Electrochemical Sensors for Healthcare Monitoring

Permalink

https://escholarship.org/uc/item/3nf886hp

Author

Bandodkar, Amay Jairaj

Publication Date

2016

Peer reviewed|Thesis/dissertation

eScholarship.org Powered by the California Digital Library
University of California

UNIVERSITY OF CALIFORNIA, SAN DIEGO

Printed Wearable Electrochemical Sensors for Healthcare Monitoring

A dissertation submitted in partial satisfaction of the requirements for the degree

Doctor of Philosophy

in

NanoEngineering

by

Amay J. Bandodkar

Committee in charge:

Professor Joseph Wang, Chair
Professor Michael J. Heller
Professor Darren Lipomi
Professor Yu-Hwa Lo
Professor Patrick Mercier

2016

©
Amay J. Bandodkar, 2016
All rights reserved

The Dissertation of Amay J. Bandodkar is approved, and it is acceptable in quality and form for publication on microfilm and electronically:

_____

_____

_____

_____

_____

Chair

University of California, San Diego

2016

Dedication

To my family.

Epigraph

If you are not willing to risk the usual you will have to settle for the ordinary.
Jim Rohn

Table of Contents

Signature Page iii
Dedication iv
Epigraph v
Table of Contents vi
List of Figures ix
Acknowledgements xiv
Vita xvii
Abstract of the dissertation xx
Chapter 1 Introduction 1
1.1 Importance of wearable chemical sensing 1
1.2 Typical components of (bio)chemical sensors 2
1.2.1 Classification of (bio)chemical sensors 3
1.3 Wearable electrochemical sensors 5
1.3.1 Saliva-based sensors 5
1.3.2 Tears-based sensors 6
1.3.3 Sweat and skin interstitial fluid-based sensors 8
1.4 Fabrication protocols for wearable electrochemical sensors 9
1.4.1 Lithography 9
1.4.2 Printing 10
1.5 Requirements and challenges for all-printed wearable electrochemical sensors 12
1.5.1 Sensor-based challenges 13
1.5.2 Other challenges 18
1.6 References 21
Chapter 2 All-Printed Stretchable Electrochemical Devices 27
2.1 Devices possessing intrinsic stretchability 27
2.1.1 Introduction 27
2.1.2 Experimental section 29

2.1.3 Results and discussion 31
2.1.4 Conclusions 39
2.2 Devices possessing combined intrinsic and design-induced stretchability 41
2.2.1 Introduction 41
2.2.2 Experimental section 43
2.2.3 Results and discussion 48
2.2.4 Conclusions 60
2.3 References 61
Chapter 3 All-Printed Self-healing Electrochemical Devices 65
3.1 Microcapsules-based devices 65
3.1.1 Introduction 65
3.1.2 Experimental section 67
3.1.3 Results and discussion 70
3.1.3 Conclusions 77
3.2 References 78
Chapter 4 Printed Wearable Pontentiometric Sensors 81
4.1 Wearable pH sensor 81
4.1.1 Introduction 81
3.1.2 Experimental section 84
b. Instrumentation: 85
c. Fabrication of temporary tattoo sensors: 85
4.1.2 Experimental section 87
a. *In vitro* characterization: 87
b. Epidermal studies: 91
4.1.3 Conclusions 94
4.2 Wearable sodium sensor 95
4.2.1 Introduction 95
4.2.2 Experimental section 98
4.2.3 Results and discussion 103
4.2.3 Conclusions 111
4.3 References 112
Chapter 5 Printed Wearable Amperometric Sensors 115

5.1 Wearable lactate sensor 115
5.1.1 Introduction 115
5.1.2 Experimental section 118
5.1.3 Results and discussion 122
5.1.4 Conclusion 132
5.2 Wearable glucose sensor 133
5.2.1 Introduction 133
5.2.2 Experimental section 136
5.2.3 Results and discussion 139
5.2.4 Conclusion 144
5.3 References 145
Chapter 6 Printed Wearable Hybrid Sensors 149
6.1 Wearable lactate and electrocardiogram sensor 149
6.1.1 Introduction 149
6.1.2 Experimental section 153
6.1.3 Results and discussion 156
6.1.4 Conclusions 163
6.2 References 164
Chapter 7 Conclusions and Future Prospects 166

List of Figures

Figure 1.1.1 Schematic showing typical components of a chemical sensor…… 3

Figure 1.1.2 Scheme illustrating screen printing process……..... 12

Figure 1.1.3 Current status and challenges in wearable chemical sensors……... 13

Figure 1.1.4 Scheme showing a typical multi-nodal wireless network for wearable sensors…….. 19

Figure 2.1.1 (A) Image of the printing stencil containing the different electrodes, contact pads and interconnect patterns. (B) Scheme depicting the screen printing of the stretchable device using tailor-made stretch-enduring inks.……... 29

Figure 2.1.2 Mechanical (stretch-and-release) deformation study performed on the printable electrochemical device fabricated by pristine (A) and modified (B) Ag/AgCl and PEDOT:PSS inks…… 33

Figure 2.1.3 Images of the stretchable electrochemical sensor when (A) stretched linearly by 100%, (B) stretched radially by 150%, and (C) bent by 90^0. CVs obtained by the sensor…….. 36

Figure 2.1.4 Scanning electron micrographs (A) before (B) after 100% linear stretching and (C) effect of stretching on the resistance of a printed stretchable Ag/AgCl trace. Scanning electron micrographs (A) before (B) after 100% linear stretching……... 38

Figure 2.1.5 (A) Phase shift versus applied frequency data recorded for a stretchable sensor after successive increment of linear strain up to 200% (increment step = 25%) and (B) corresponding phase shift measured at 1Hz (obtained from A)…….. 39

Figure 2.2.1 (A) Image of the stencil employed for printing the stress-enduring stretchable devices. Schematics showing (B) large-scale printed stretchable device arrays along with their various applications (Inset shows an image of a printed CNT-based array device)……... 43

Figure 2.2.2 SEM images of printed stretchable CNT ink-based trace at different magnifications……. 50

Figure 2.2.3 Comparison of the effect of applied strain on the resistance of printed (**A**) free-standing Ag/AgCl-based trace possessing different contacting angles (θ); (B) Ag/AgCl-based free-standing (black plot) and surface-bound (red plot) serpentine traces ($\theta = 30^0$)……. 52

Figure 2.2.4 (A) Optical and (B, C) SEM images showing macroscopic and microscopic cracks and morphology of the printed trace fabricated using non-stretchable CNT ink…… 53

Figure 2.2.5 Images showing (A) non-stretchable and (B) stretchable Ag/AgCl ink-based trace under 200% strain……. 54

Figure 2.2.6 SEM image of stretchable CNT ink-based trace (A) before and (B) after being stretched by 500%..... 54

Figure 2.2.7 (A) Photographs of the printed stretchable array under increasing levels of applied strain (scale bar = 1cm). CVs recorded before (black plot) and after (red plot) applying (B) increasing levels of strain from 0 to 500% with increments of 100%..... 56

Figure 2.2.8 (A) Schematic of a stretchable ion-selective NH_4^+ sensor. (B) Voltage vs time data recorded for increasing NH_4^+ concentration (0.1 – 100 mM) and (C) Calibration plot recorded after application of 10 cycles of 300% strain for a total of 40 cycles…….. 58

Figure 3.1.1 Printed electrochemical devices with a built-in healing function. Schematic showing the (A) preparation of the self-healing carbon ink and screen printing procedure…….. 67

Figure 3.1.2 Real-time resistance study examining the conductivity restoration ability of a self-healing (A) carbon, (A') Ag/AgCl and pristine (A'') carbon and (A''') Ag/AgCl electrode respectively. Respective insets show schematics of the self-healed carbon (A)……... 73

Figure 3.1.3 Self-restoring the electrochemical performance. In-situ CV study of the damage and healing processes for (A) self-healing and (A') normal carbon electrodes. Inset (A) shows individual CVs (i) before damage, (ii) during the damage, and (iii) after……... 75

Figure 3.1.4 In-situ CV study of the repair process for a complete self-healing electrochemical device when the (A) reference (B) counter and (C) working electrodes are damaged in their respective Ag/AgCl connector region.……... 77

Figure 4.1.1 (i) Schematic representation of the fabrication protocol employed in the production of temporary transfer tattoo-based solid-contact ion-selective electrode (ISE) sensors…….. 83

Figure 4.1.2 (i) Response of the ISE tattoo sensor, *in vitro*, upon calibration with unit decrease of pH using standard McIlvaine's buffers. (ii) Potential-time response of the ISE tattoo sensors,*in vitro*, demonstrates the reproducibility of the sensors in response to large pH fluctuations……. 88

Figure 4.1.3 Influence of repeated mechanical strain (bending) upon the response of

the tattoo ISE: (i) pH-responsive behavior of the ISE tattoo sensor over the 3–7 pH range prior to stretching (black) and following the 50th (red) bending on GORE-TEX……..... 90

Figure 4.1.4 Influence of repeated mechanical strain (stretching) upon the response of the tattoo ISE: (i) pH-responsive behavior of the ISE tattoo sensor prior to stretching (black) and following the 40th (red) stretch on GORE-TEX…….. 91

Figure 4.1.5 Real-time response (black) of the ISE tattoos applied to (i) neck, (ii) wrist and (iii) lower back. The plot in blue represents the pH measured by the conventional pH meter. (iv) Photograph showing the entire device (tattoo and digital multimeter)…….. 92

Figure 4.2.1 Schematic showing the fabrication and transfer process for the Na-tattoo sensor. The first step involves (A) screen printing an insulator coating (light gray) on the tattoo paper (dark gray) followed by laser printing the "Tiger Face"……. 97

Figure 4.2.2 Response of the Na-tattoo sensor to (A) NaCl solutions (0.1–100 mM range), (B) artificial sweat with increasing sodium concentration (30–110 mM).…….. 104

Figure 4.2.3 Effect of (A) bending, (B) stretching and (C) poking stress iterations on the Na-tattoo sensor response for NaCl solutions over the 0.1–100 mM range. Note: In the stretching study, an increasing strain from 0% to 26% was applied after every 20 stretching cycles……..... 106

Figure 4.2.4 Effect of temperature on sensor response…… 107

Figure 4.2.5 Photographs showing (A) pinching and (B) poking of the Na-tattoo sensor whist applied to the skin……... 108

Figure 4.2.6 Real-time monitoring of sweat sodium levels for two subjects over a period of 36 min (30 min exercise activity (cycling) followed by 3 min of cool down and another 3 min of complete rest) by the skin-worn Na-tattoo sensor coupled with an electrochemical analyzer…….. 109

Figure 4.2.7 Wirelessly transmitted analytical sensor response (A) for NaCl solutions of varying concentrations (0.1–100 mM) and (B) during carry-over study using 0.1 and 100 mM NaCl solutions……. 110

Figure 4.2.8 Photographs of wireless transceiver (A) worn by a subject along with the Na-tattoo (inset: a zoomed image of the entire device), (B) when encapsulated in an armband (inset: image showing a quarter dollar kept close to wireless transceiver for size comparison)……... 111

Figure 5.1.1 (A) Schematic illustration of a three-electrode "NE" tattoo biosensor for electrochemical epidermal monitoring of lactate. (B) Constituents 118

of the reagent layer of the working electrode which is coated by biocompatible polymer (chitosan). See the text for further details……..

Figure 5.1.2 (A) Amperometric response for increasing concentrations of lactate (1 mM increments) over the 0–20 mM range; Eapplied = +0.05 V (vs Ag/AgCl). (B) Calibration plot up to 30 mM lactate, based on sampling the current at 60 s…….. 124

Figure 5.1.3 (A) Stability of the response of the tattoo biosensor to 8 mM lactate at 30 min intervals over a 8 h period. The inset is the corresponding current–time plot of the chronoamperometric response. The tattoo sensor kept at ambient conditions between such successive runs…… 125

Figure 5.1.4 Electrochemical response of tattoo lactate sensor transferred onto a flexible GORE TEX textile undergoing repeated bending (A) and stretching (B) to 8 mM lactate at +0.05 V (vs Ag/AgCl) and their normalized current (C) and (D), respectively…….. 127

Figure 5.1.5 Photos of a bare 'NE' tattoo on a human neck (A) endured by mechanical strain tests (B) during and subsequent to 100 stretching (i), bending (ii) and twisting (iii) iterations……... 128

Figure 5.1.6 Monitoring of sweat lactate during 33 min of cycling exercise while changing the work intensity. (A) Exercise resistance profile on a stationary cycle……. 129

Figure 5.1.7 (A) Real-time response of the tattoo biosensor during a cycling exercise (left y-axis) and corresponding lactate concentrations (right y-axis)……... 132

Figure 5.2.1 Tattoo-based platform for non-invasive glucose sensing. (A) Schematic of the printable iontophoretic-sensing system displaying the tattoo-based paper……... 139

Figure 5.2.2 (A) Chronoamperometric response of the tattoo-based glucose sensor to increasing glucose concentrations from 0 μM (dash) to 100 μM (plot 'l') in buffer in 10 μM increments…… 141

Figure 5.2.3 Amperograms obtained for non-invasive glucose detection obtained from two human subjects, wearing simultaneously the glucose tattoo sensor (A, A') with and (B, B') without the IP operation…… 144

Figure 5.2.4 Combined data obtained from glucose tattoo sensors (plots 'a_i', 'a_{ii}' and 'a_{iii}'), No-GOx sensors (plots 'b_i', 'b_{ii}' and 'b_{iii}') and No-IP sensors (plots 'c_i', 'c_{ii}' and 'c_{iii}') before and after meal consumption. Conditions, as in Figure 5.2.3…….. 144

Figure 6.1.1 Fabrication and function of the Chem–Phys hybrid sensor patch.(a) Schematic showing the screen-printing process. (b) Image of the 152

Chem–Phys printing stencil……..

Figure 6.1.2 In-vitro characterization of Chem–Phys hybrid patch.(a) Amperometric response to increasing lactate concentration from 0 to 28 with 2 mM additions in phosphate buffer (pH 7.0)……. 159

Figure 6.1.3 On-body test configuration.(a) A photograph of Chem–Phys hybrid patch. (b) Location of the Chem–Phys patch for mounting on the human body—the fourth intercostal space of the chest…… 160

Figure 6.1.4 Real-time on-body evaluation of the Chem-Phys hybrid patch showing the lactate levels and H.R. for three human subjects. The corresponding 'blue plots' represent the real-time lactate concentration profiles for each subject, while, the 'red plots' depict the H.R……... 162

Acknowledgements

First of all, I would like to thank my thesis advisor professor Joseph Wang, for his advice, and support which made my dissertation possible. His enthusiasm and persistence have inspired me and have allowed me to accomplish more than I ever would have expected as a graduate student.

I also thank my other committee members, professor Patrick Mercier, professor Michael Heller, professor Darren Lipomi and professor Yu-Hwa Lo for guiding me through the journey. I would like to take this opportunity to thank professor Patrick Mercier and his research group for developing wireless wearable electronics for various wearable chemical sensors developed in my lab.

In the past five years, I have been fortunate to work with so many wonderful colleagues. Here I would like to thank Dr. Wenzhao Jia, Dr. Gabriela Valdés-Ramírez, Dr. Vinu Mohan, Dr. Jung-Min You, Dr. Joshua Windmiller, Julian Ramírez, Rogelio Nuñez-Flores, Cristian Silva López, Somayeh Imani, Rajan Kumar, Itthipon Jeerapan, JaYoung Kim, Alexandra Martinez and all the wonderful colleagues who helped me throughout my entire thesis work. I wish to thank my parents and my sister. I owe my success to my family's consistent support and countless sacrifices.

Chapter 1 is based, in part, on the material as it appears in Trends in Biotechnology, 2014, by Amay J. Bandodkar and Joseph Wang; in part on the material as it appears in Electroanalysis, 2015, by Amay J. Bandodkar, Wenzhao Jia and Joseph Wang; in part on the material as it appears in ACS Sensors, 2016, by Amay J. Bandodkar, Itthipon Jeerapan and Joseph Wang. The dissertation author was the primary investigator and corresponding author of this paper.

Chapter 2 is based, in part, on the material as it appears in Advanced Materials, 2015, by Amay J. Bandodkar, Rogelio Nuñez-Flores, Wenzhao Jia, and Joseph Wang; in part on the material as it appears in Nano Letters, 2016, by Amay J. Bandodkar, Itthipon Jeerapan, Jung-Min You, Rogelio Nuñez-Flores, and Joseph Wang. The dissertation author was the primary investigator and corresponding author of these papers.

Chapter 3 is based, in part, on the material as it appears in Advanced Electronic Materials, 2015, by Amay J. Bandodkar, Vinu Mohan, Cristian S. López, Julian Ramírez, and Joseph Wang. The dissertation author was the primary investigator and corresponding author of this paper.

Chapter 4 is based, in part, on the material as it appears in Analyst, 2013, by Amay J. Bandodkar, Vinci W.S. Hung, Wenzhao Jia, Gabriela Valdés-Ramírez, Joshua R. Windmiller, Alexandra G. Martinez, Julian Ramírez, Garrett Chan, Kagan Kerman, and Joseph Wang; in part on the material as it appears in Biosensors and Bioelectronics, 2014, by Amay J. Bandodkar, Denise Molinnus, Omar Mirza, Tomás Guinovart, Joshua R. Windmiller, Gabriela Valdés-Ramírez, Francisco J. Andrade, Michael J. Schöning, and Joseph Wang. The dissertation author was the primary investigator and corresponding author of these papers.

Chapter 5 is based, in part, on the material as it appears in Analytical Chemistry, 2013, by Wenzhao Jia, Amay J. Bandodkar, Gabriela Valdés-Ramírez, Joshua R. Windmiller, Zhanjun Yang, Julian Ramírez, Garrett Chan, and Joseph Wang; in part on the material as it appears in Analytical Chemistry, 2015, by Amay J Bandodkar, Wenzhao Jia, Ceren Yardımcı, Xuan Wang, Julian Ramirez, and Joseph Wang. The dissertation author was the primary investigator and corresponding author of these papers.

Chapter 6 is based on the material as it appears in Nature Communications, 2016, by Somayeh Imani, Amay J. Bandodkar, A. M. Vinu Mohan, Rajan Kumar, Shengfei Yu, Joseph

Wang, and Patrick P. Mercier. The dissertation author and Prof. Patrick Mercier were the co-principle investigators and co-corresponding authors of this paper.

Vita

2011 Integrated Masters in Technology, Indian Institute of Technology – Banaras Hindu University

2016 Doctor of Philosophy, University of California, San Diego

Publications

1. "Highly Stretchable Fully-Printed CNT-based Electrochemical Sensors and Biofuel Cells: Combining Intrinsic and Design-induced Stretchability", A. J. Bandodkar, I. Jeerapan, J. M. You, R. N. Flores and J. Wang, ***Nano Lett.*** 2016, **16**, 721.

2. "Self-healing Inks for Autonomous Repair of Printable Electrochemical Devices", A. J. Bandodkar, V. Mohan, C. S. López, J. Ramírez and J. Wang, ***Adv. Electron. Mat.*** 2015, **1**, 1500289.

3. "All-Printed Stretchable Electrochemical Devices", A. J. Bandodkar, R. Nuñez-Flores, W. Jia and J. Wang, ***Adv. Mat.*** 2015, **27**, 3060.

4. "Biocompatible Enzymatic Roller Pens for Direct Writing of Biocatalytic Materials: "Do-it-Yourself" Electrochemical Biosensors", A. J. Bandodkar, W. Jia, J. Ramírez and J. Wang, ***Adv. Health. Mat.*** 2015, **4**, 1215.

5. "Tattoo-based Non-invasive Glucose Monitoring: a Proof-of-Concept Study", A. J. Bandodkar, W. Jia, C. Yardımcı, X. Wang, J. Ramírez and J. Wang, ***Anal. Chem.*** 2015, **87**, 394.

6. "Tattoo-based Wearable Electrochemical Devices: A Review", A. J. Bandodkar, W. Jia and J. Wang, ***Electroanal.*** 2015,**27**, 562.

7. "Wearable temporary tattoo sensor for real-time trace-metal monitoring in human sweat", J. Kim, W. R. de Araujo, I. A. Samek, A. J. Bandodkar, W. Jia, B. Brunetti, Thiago R.L.C. Paixão and J. Wang, ***Electrochem. Commun.*** 2015, **51**, 41.

8. "Wearable textile biofuel cells for powering electronics", W. Jia, X. Wang, S. Imani, A. J. Bandodkar, J. Ramírez, P. P. Mercier and J. Wang, ***J. Mat. Chem. A***, 2014, **2**, 18184.

9. "Microneedle-based self-powered glucose sensor", G. Valdés-Ramírez, Y. C. Li, J. Kim, W. Jia, A. J. Bandodkar, R. Nuñez-Flores, P. R. Miller, S. Y. Wu, R. Narayan, J. R. Windmiller, R. Polsky and J. Wang, ***Electrochem. Commun.***, 2014, **47**, 58.

10. "An epidermal alkaline rechargeable Ag–Zn printable tattoo battery for wearable electronics", S. Berchmans, A. J. Bandodkar, W. Jia, J. Ramírez, Y. S. Meng, J. Wang, ***J. Mat. Chem. A***, 2014, **2**, 15788.

11. "Non-invasive wearable electrochemical sensors: a review", A. J. Bandodkar, J. Wang, ***Trends Biotechnol.***, 2014, **32**, 363.

12. "Non-invasive mouthguard biosensor for continuous salivary monitoring of metabolites", J. Kim, G. Valdés-Ramírez, A. J. Bandodkar, W. Jia, A.G. Martinez, J. Ramírez, P. Mercier, J. Wang, ***Analyst,*** 2014, **139**, 1632.

13. "Epidermal tattoo potentiometric sodium sensors with wireless signal transduction for continuous non-invasive sweat monitoring", A. J. Bandodkar, D. Molinnus, O. Mirza, T. Guinovart, J. R. Windmiller, G. Valdés-Ramírez, F. J. Andrade, M. J. Schöning, J. Wang, ***Biosens. Bioelectron.***, 2014, **54**, 603.

14. "Electrochemical Tattoo Biosensors for Real-Time Noninvasive Lactate Monitoring in Human Perspiration", W. Jia, A. J. Bandodkar, G. Valdes-Ramirez, J. R. Windmiller, Z. Yang, J. Ramirez, G. Chan, J. Wang, ***Anal. Chem.***, 2013, **85**, 6553.

15. "Epidermal Biofuel Cells: Energy Harvesting from Human Perspiration", W. Jia, G. Valdés-Ramírez, A. J. Bandodkar, J. R. Windmiller, J. Wang, ***Angew. Chem. Int. Ed.***, 2013, **52**, 7233.

16. "A potentiometric tattoo sensor for monitoring ammonium in sweat", T. Guinovart, A. J. Bandodkar, J. R. Windmiller, F. J. Andrade, J. Wang***, Analyst***, 2013, **138**, 7031.

17. "Solid-state Forensic Finger sensor for integrated sampling and detection of gunshot residue and explosives: towards 'Lab-on-a-finger'", A. J. Bandodkar, A. M. O'Mahony, J. Ramírez, I. A. Samek, S. M. Anderson, J. R. Windmiller, J. Wang, ***Analyst***, 2013, **138**, 5288.

18. "Tattoo-based potentiometric ion-selective sensors for epidermal pH monitoring", A. J. Bandodkar, V. W. S. Hung, W. Jia, G. Valdés-Ramírez, J. R. Windmiller, A. G. Martinez, J. Ramírez, G. Chan, K. Kerman, J. Wang, ***Analyst***, 2013, **138**, 123.

19. "Electrochemical sensing based on printable temporary transfer tattoos", J. R. Windmiller, A. J. Bandodkar, G. Valdés-Ramírez, S. Parkhomovsky, A. G. Martinez, J. Wang, ***Chem. Commun.***, 2012, **48**, 6794.

20. "Stamp transfer electrodes for electrochemical sensing on non-planar and oversized surfaces", J. R. Windmiller, A. J. Bandodkar, S. Parkhomovsky, J. Wang, ***Analyst***, 2012, **137**, 1570.

21. “Swipe and Scan”: Integration of sampling and analysis of gunshot metal residues at screen-printed electrodes”, A. M. O'Mahony, J. R. Windmiller, I. A. Samek, A. J. Bandodkar, J. Wang, ***Electrochem. Commun.***, 2012, **23**, 52.

FIELDS OF STUDY

Major Field: Biomedical Nanotechnology

Studies in Nanoengineering

Professor Joseph Wang

Abstract of the dissertation

Printed Wearable Electrochemical Sensors for Healthcare Monitoring

by

Amay J. Bandodkar

Doctor of Philosophy in NanoEngineering

University of California, San Diego, 2016

Professor Joseph Wang, Chair

With an expected compound annual growth rate of 35% over the next five years, the global wearables market is poised to reach 148 million annual shipments in 2019. One of the alluring factors of wearables is the incorporation of sensors that can monitor a people's well-being and their surroundings in a continuous autonomous fashion. Such continuous stream of vital data thus offers unprecedented avenue in healthcare, defense and environmental domains. Though the attractiveness of wearable sensors is indubitable, this nascent field is marred with several challenges and not much has been done to address these. A major challenge is the

unavailability of important wearable sensors. For example, the wearable sensor field is dominated by sensors that monitor physical parameters, for example, motion, pressure, temperature, heart rate and brain-activity sensors etc. One must monitor chemicals in addition to physical parameters in order to obtain a comprehensive knowledge of a person's well-being. Continuous chemical monitoring is important for analyzing fitness levels, alerting people about serious medical conditions, e.g., diabetes, traumatic brain injury, soft tissue injury etc. At present only blood analyzers are available to measure these chemicals. But the intrusive nature of these analyzers, due to blood sampling step, render then impractical for continuous, everyday use. Sensors that can perform continuous non-invasive monitoring of vital chemical biomarkers are thus highly desired, yet missing. The present thesis focuses on filling this technological vacuum by developing body-compliant, skin-worn electrochemical sensors that can detect physiologically relevant chemicals directly on the human skin in a completely non-invasive fashion.

Chapter 1 Introduction

1.1 Importance of wearable chemical sensing

Continuous monitoring of a person's health status can provide unprecedented levels of important data that can help users and health providers in maintaining one's well-being.[1] The medical interest for wearable systems arises from the need for monitoring patients over long periods of time. These devices have the potential to continuously collect continuously vital health information from a person's body and provide this information to them or their healthcare provider in a timely fashion. Such on-body monitoring can alert the wearer of any imminent health hazard and hence to facilitate rapid corrective clinical action (outside of the hospital environment).[2] The past decade has thus witnessed exceptional growth in research activity pertaining to the development of wearable health monitors that continuously track the fitness levels of the wearer.[3] These developments hold considerable promise for maintaining and improving the quality of life while reducing medical costs. This is particularly true for monitoring older adults or patients with chronic diseases in home settings, in general, and particularly in remote locations (with limited or no personal access to doctors). On-body monitoring of performance markers (coupled to smartphone platforms) has also received a considerable recent attention in connection to variety of sports and fitness applications.

Although the information provided by such sensors is necessary, it is not sufficient to get a complete picture of a person's health status majority of the success in this field has been in developing wearable sensors that monitor physical and electro-physiological parameters, such as, body motion, temperature, heart rate, blood pressure etc.[1, 3] One must also concurrently monitor physiologically relevant chemicals in order to obtain comprehensive personal health information.[2, 4] Unfortunately, most of the chemical sensors rely on painful

fingersticks for blood sampling. For example, widely-used enzyme-electrode strips for the management of diabetes depend on detecting glucose via finger-pricking blood collection. The intrusive nature of these biosensors poses a major hurdle to the patient and impedes temporal information acquisition desired for diverse biomedical applications. This is especially true in the case of neonatals, elderly and hemophobic patients where blood sampling is challenging. Continuous biomarker monitoring is of particular importance in different areas. For example, optimum diabetes management can be achieved by continuous glucose measurements in skin interstitial fluid (ISF),[5] tears[6] or saliva.[7] Similarly, continuous measurements of lactate and electrolyte levels in saliva[8] and sweat[9] can be used for real-time fitness monitoring. Real-time detection of pathogens in saliva[10] or on the skin can alert the person about plausible onset of disease. Monitoring drug efficacy is another scenario where continuous measurements are of great importance. In the above mentioned cases, invasive sensors have obvious limitations since continuous availability of the required sampling media (blood, urine, serum, etc) is impractical. Thus, wearable chemical sensors that can non-invasively monitor chemicals directly on the human body are highly desired, yet missing.[2] Researchers have been working on miniaturized (bio)chemical sensors for several decades and developments in the field of portable (bio)chemical sensors can be exploited towards realization of wearable (bio)chemical sensors.

1.2 Typical components of (bio)chemical sensors

IUPAC defines a chemical sensor as “is a device that transforms chemical information, ranging from the concentration of a specific sample component to total composition analysis, into an analytically useful signal.” A typical chemical sensor contains two basic functional units: a receptor part and a physico-chemical transducer part. The receptor transforms the analyte concentration, into a chemical or physical output signal with a

defined sensitivity. The main role of the receptor is to provide high selectivity towards the desired analyte in presence of potentially interfering chemical species. The receptors thus help in obviating false positive results. The transducer is another crucial component of a sensor that serves to convert the signal generated by the receptor to a readable value. Chemical sensors can be distinguished based on receptors as either catalytic or affinity-based. Similarly, they can be called as electrochemical, optical, piezoelectric and calorimetric sensors when classified depending on the type of transducer used. A typical schematic of a chemical sensor is shown in Figure 1.1.1.

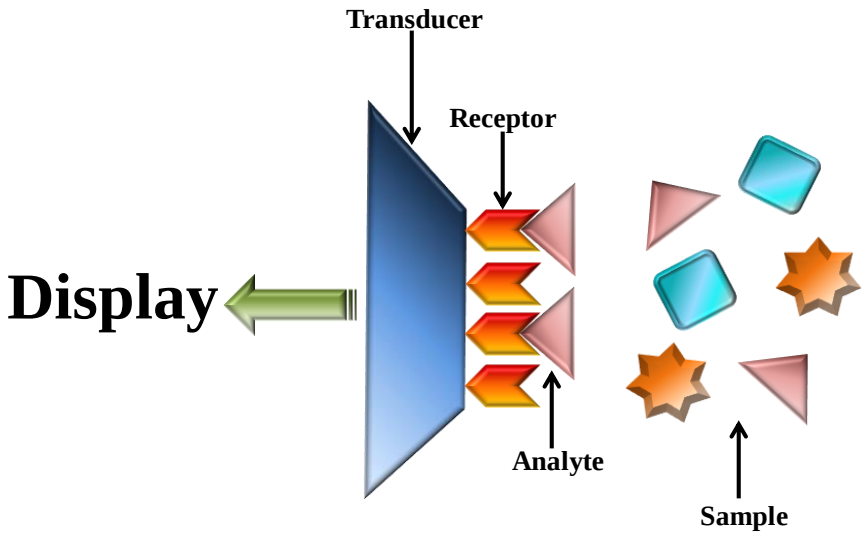


Figure 1.1.1: Schematic showing typical components of a chemical sensor. (Reprinted with permission from ref. 27. Copyright 2014 Elsevier).

1.2.1 Classification of (bio)chemical sensors

On the Basis of Transducer:

a. Electrochemcial (Bio)chemical sensors:

Electrochemical sensors have gained a dominating role in clinical diagnostics owing to their high performance, portability, simplicity and low-cost. Substantial progress in the electrochemical sensors domain has led to the development of highly successful commercial

hand-held analyzers, such as the Accu-Check®, Abbott iSTAT or Lactate Scout®, devices, for detecting different metabolites and electrolytes. The present thesis research work thus leverages the attributes of electrochemical techniques towards realization of body-worn non-invasive sensors. Electrochemical sensors can be broadly classified as follows:

i. Amperometric (Bio)chemical sensors:

These sensors measure the current produced during the oxidation or reduction of a reactant at a constant applied potential. This current is linearly proportional to the concentration of the electroactive product, which in turn is proportional to the non-electroactive enzyme substrate. The electron transfer between catalytic molecules (usually oxidase or dehydrogenase) is the most important factor which affects the functioning of amperometric biosensors.

ii. Potentiometric (Bio)chemical sensors:

These sensors are used to measure the potential at constant current which may be used to detect the concentration of the analyte.

iii. Impedimetric (Bio)chemical sensors:

These sensors rely on detecting chemicals by monitoring the variation of the impedance of the electrode-electrolyte interface.

b. Conductometric (Bio)chemical sensors:

These sensors are used to measure the changes in the conductance of the biological component arising between a pair of metal electrodes.

c. Calorimetric (Bio)chemical sensors:

These sensors are based on the measurement of the heat evolved or absorbed as a result of a biochemical reaction.

d. Piezoelectric (Bio)chemical sensors:

The basic principle of these sensors lies in the binding of molecular species to the surface of crystal resulting in a mass change which eventually leads to a change in the frequency of oscillation of the crystal.

e. Optical (Bio)chemical sensors:

These sensors detect the chemical analyte based on variation in optical properties, such as, measurement of absorbance, reflectance, or fluorescence emissions that occur in the ultraviolet (UV), visible, or near-infrared (NIR), occurring due to the interaction between the chemical analyte and the sensor.

1.3 Wearable electrochemical sensors

The field of wearable electrochemical sensors can be broadly classified based on biofluids into tears, saliva, sweat or skin interstitial fluid-based sensors. The following sub-sections deal with this classification along with representative examples of wearable electrochemical sensors.

1.3.1 Saliva-based sensors

Saliva is a complex biofluid comprising of numerous constituents permeating from blood via transcellular or paracellular paths. Hence, sialochemistry offers an excellent non-invasive alternative to blood analysis for monitoring emotional, hormonal, nutritional, and metabolic state of the human body. Saliva is also readily available compared to blood and requires fewer pretreatment steps. These virtues of saliva have attracted the attention of several researchers to develop portable *in-vitro* salivary diagnostic tools.[11]

The field of wearable salivary sensing has experienced considerable progress primarily aiming towards the incorporation of sensors within partial dentures. The first examples of such wearable sensors were demonstrated already in the 1960s for monitoring

mastication. Recently, Emorine *et al* described the fabrication of miniaturized conductivity and temperature sensors that can be easily attached to one's tooth for analyzing variations in electrolyte and temperature during mastication.[12] Mannoor *et al*. demonstrated a dental tattoo for continuous wireless monitoring of bacteria by bio-functionalizing anti-microbial peptides on graphene-modified silk tattoo substrates.[10] The tattoo was then transferred to bovine tooth enamel for *in-vitro* detection of bacteria in human saliva. Yet, real-time on-body applications have not been described.

Though the progress in wearable salivary sensors has been promising, there are still many exciting avenues to be explored. While *in-vitro* measurements of glucose, lactate, heavy metals, diseases and drugs in saliva have been demonstrated, wearable analogs for on-body detection of these chemicals can provide plethora of vital information about a person's well-being to an individual, doctor or sports coach.

1.3.2 Tears-based sensors

Tears are a complex extracellular fluid encapsulating the surface epithelial cells and forming the anterior component of the ocular surface. Tears contain proteins/peptides, electrolytes, lipids, and metabolites from lacrimal glands, ocular surface epithelial cells, Meibiomian glands, goblet cells, and blood.[13] Since blood is one of the sources of these constituents, tears can be used as an attractive fluid for non-invasive monitoring. Conventional bench-top instruments, like MS, HPLC and NMR, have been traditionally used for detecting amino acids,[14] antioxidants[15] and metabolites[16] in human tears. However *in-vitro* tears analysis involves several road-blocks. Evaporation of collected tears (commonly 5-10 μL) during transport to laboratories represents a major factor affecting the accuracy of such centralized tear analyses. Considering the delicate nature of the human eye, utmost care much be taken

during the sample collection. Additionally, the measured analyte concentration often depends upon collection method utilized.

Wearable sensors that detect analytes directly on the human retina may circumvent the aforementioned limitations. However, such sensing devices should satisfy several critical requirements. For example, the sensor should conform well on the highly curved eyeball, and should be soft and innocuous to avoid eye damage. The sensor should perform accurately using ultra-low sample volume. The entire sensor and the supporting electronics should be confined within a small area. Recent advances in electronic miniaturization and nanobiotechnology have facilitated the development of such wearable ocular chemical sensors. The earliest forms of these sensors were fabricated on strip-based flexible substrates.[17]

Continuous non-invasive monitoring of glucose is highly desired for optimal diabetes management. Tears prove to be a suitable media for diabetes management as there exists a correlation between glucose levels in tears and blood.[18] Extensive efforts in the wearable ocular sensing domain have thus focused on the development of tear glucose biosensors.[19, 20] Wearing strip-based ocular sensors is cumbersome and thus continuous measurement is a challenge. This limitation can be addressed by developing a soft contact lens-based sensor with integrated wireless electronics. For example, Parviz's team developed contact lens glucose sensors with in-built wireless electronics for continuous data transmission.[21]

A major challenge in wearable ocular sensors is obtaining a suitable powering source. The lachrymal fluid contains several metabolites that can be used as potential biofuels for powering the ocular sensors. Such biofuel cells must be integrated within the contact-lens together with the accompanying sensor. Recently Falk *et al* have demonstrated biofuels cells capable of generating usable energy from lycramal glucose.[22] The biofuel cell relied on gold microwire anode and cathode modified with cellobiose dehydrogenase and bilirubin oxidase,

respectively (along with gold nanoparticles). A similar biofuel cell for harvesting power from lycramal ascorbate was recently demonstrated by the same Swedish team.[23]

1.3.3 Sweat and skin interstitial fluid-based sensors

Sweat offers another attractive fluid for non-invasive monitoring of the wearer's physiological state. The human sweat and skin interstitial fluid (ISF) contain abundant information about a person's health status and thus are excellent biofluids for non-invasive chemo-sensing.[24, 25] Electrolyte loss during perspiration is a major cause of muscle cramps.[26] Thus, monitoring electrolyte imbalance is of utmost importance to athletes,[27] individuals working in hot climate[28] and cystic fibrosis (CF) patients.[29] Similarly, exhaustive exercise causes muscle break-down leading to increased ammonia level in sweat,[30] while elevated calcium levels in sweat indicate bone mineral loss for athletes involved in endurance exercise[31] and Osteoporosis patients.[32] The pH of the human sweat is an indicator of dehydration. Additionally, sweat lactate is an attractive biomarker for physical stress.[33] Thus, quantifying sweat lactate levels is crucial in sports and military domains. On the other hand, ISF contains vital biomarkers whose concentration correlates well with blood levels and can thus be used for non-invasively monitoring several physiological conditions.[25, 34] Tremendous progress has been made in the development of wearable electrochemical sensors in the past several years.[2] Yet, much needs to be done to make these devices commercially-viable. The following sections and chapters will discuss the fabrication protocols utilized to develop these sensors, the challenges faced in this field and how the present work attempts to address these issues.

1.4 Fabrication protocols for wearable electrochemical sensors

Lithography and printing have been utilized to realize various types of wearable electrochemical sensors. The following sub-sections will discuss the basics of these fabrication techniques.

1.4.1 Lithography

Lithography has been a crucial technology towards the manufacturing of integrated circuits (ICs) and microchips. It has been used to develop patterns with a feature size ranging from a few nanometers up to tens of millimeters. Lithography is regularly combined with other fabrication processes such as deposition and etching to create high-resolution topographies. Lithography techniques are divided into two genres: masked lithography and maskless lithography. Masked lithography utilizes masks/molds to transfer patterns over a large area simultaneously, thus, enabling a high-throughput fabrication. The forms of masked lithography include photolithography, soft lithography, and nanoimprint lithography. Whereas, maskless lithography, such as electron beam lithography, focused ion beam lithography, and scanning probe lithography, fabricates patterns by a serial writing sans the use of masks. Of these various techniques, photolithography has been recently used by researchers to develop wearable electrochemical sensors due to their relatively low-cost of production and ease of fabrication.[35, 36]

Optical lithography is a process used in microfabrication to selectively remove parts of a thin film or the bulk of a substrate. It uses light to transfer a geometric pattern from a photo mask to a light-sensitive chemical called “photoresist” or simply "resist" on the substrate. A series of chemical treatments then engraves the exposure pattern into the material

underneath the photoresist. In a complex integrated circuit for example, modern CMOS, a wafer will go through the photolithographic cycle up to 50 times.

Optical lithography shares some fundamental principles with photography, in that the pattern in the etching resist is created by exposing it to light, either using a projected image or an optical mask. This step is like an ultra high precision version of the method used to make printed circuit boards. Optical lithography is used because it has exact control over the shape and size of the objects it creates, and because it can create patterns over an entire surface simultaneously. The basic procedure for optical lithography comprises of cleaning, photoresist application, exposure and development and photoresist removal.

1.4.2 Printing

The process of printing comprises of the reproduction of a pattern on a substrate by transferring material, in the form of inks, onto the substrate. Conventional printing methods, including, flexography, gravure, ink-jet and screen printing, have evolved over several centuries and can now achieve remarkable levels of quality at very low cost. All these processes share a common feature: the pattern to be printed is embodied on a roll, plate, or screen and transferred from this template through direct or indirect contact with the substrate. The important printing parameters are accuracy, resolution, uniformity, wetting control and interface formation, compatibility of inks with printing process, throughput and cost-effectiveness.

It is extremely critical that one employs optimal wetting control on substrate faces, which can both promote and prevent the spread of printed inks. Chemical treatment and physical treatment are the two ways to control wetting and spreading. These techniques are widely utilized in the graphic printing industry. Chemical treatment involves modulating the energy state of the surface. Plasma cleaning of substrate surfaces usually creates a high-energy

state on most surfaces, resulting in the promotion of wetting and spreading. On the other hand, CF_4 plasma treatment, creates a fluorinated layer on the surface. Thus leading to a very low-energy state. Apart from wetting the substrate surface with the ink, drying conditions also play a crucial role in printed technology. In the case of printing methodologies, such as inkjet, offset-gravure, and flexo, the viscosity of inks and the concentrations of metallic nanoparticle inks are quite low, while the amount of solvent is large. Due to the presence of large quantities of solvents, the solvent must undergo complete evaporation to achieve printed devices with optimal resolution and performance. Although, most of the printing techniques can be utilized for realizing wearable electrochemical sensors, screen printing has acquired the greatest attention due to its low-cost, high precision and ease of fabrication.[2, 4, 8]

a. Screen printing:

Screen printing is one of the most common printing methods and has been used for decades in electronics manufacturing. The most attractive attribute of this thick film printing technology as compared to other printing methods is the high aspect ratio of printed patterns.[37] By changing the stencil thickness, one can print traces with thickness ranging from few tens to few hundreds of microns with a single pass of printing. In contrast, for other methods such as inkjet or flexo printing, the typical thickness is less than 5 μm. Screen printing involves printing at a low printing pressure using a screen mesh with a designed pattern of uniform thickness (Figure 1.1.2). A metal squeegee or rubber squeegee is used for squeezing the thixotropic fluidic paste through the mesh and onto the substrate. The stencil can be made of polyamide/polyester, or stainless steel. The thixotropic fluidic ink contains a variety of substances including fillers, binders, solvent and other additives. The inks utilized in screen printing have a high viscosity but when forced through the screen mesh by the squeegee blade, the ink undergoes sheer thinning allowing it to penetrate through the screen mesh which defines the final shape/design. Upon contact with the substrate, typically a

ceramic, plastic, paper, polymeric material, the ink returns to its viscous state forming the intended shape/design with definition.

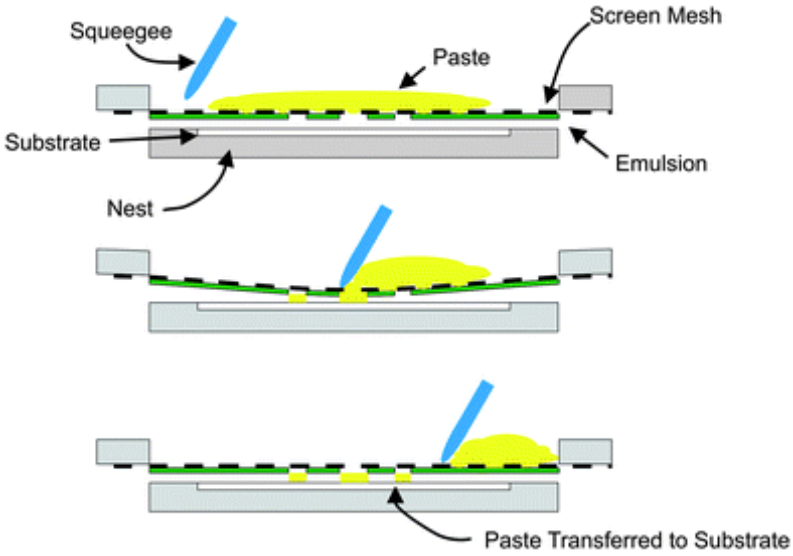


Figure 1.1.2: Scheme illustrating screen printing process. (Reprinted with permission from ref. 37. Copyright 2011 Royal Society of Chemistry).

1.5 Requirements and challenges for all-printed wearable electrochemical sensors

The recent advances in the field of wearable electrochemical sensors are indeed quite commendable. However, there are several daunting challenges faced by this field. It is only by addressing these issues that the wearable sensors field can progress towards maturity. The bottlenecks in the wearable sensors domain can be broadly classified into challenges in materials, power, data acquisition, processing, security, communication and analytical requirements (Figure 1.1.3). The following sub-sections will briefly discuss these.

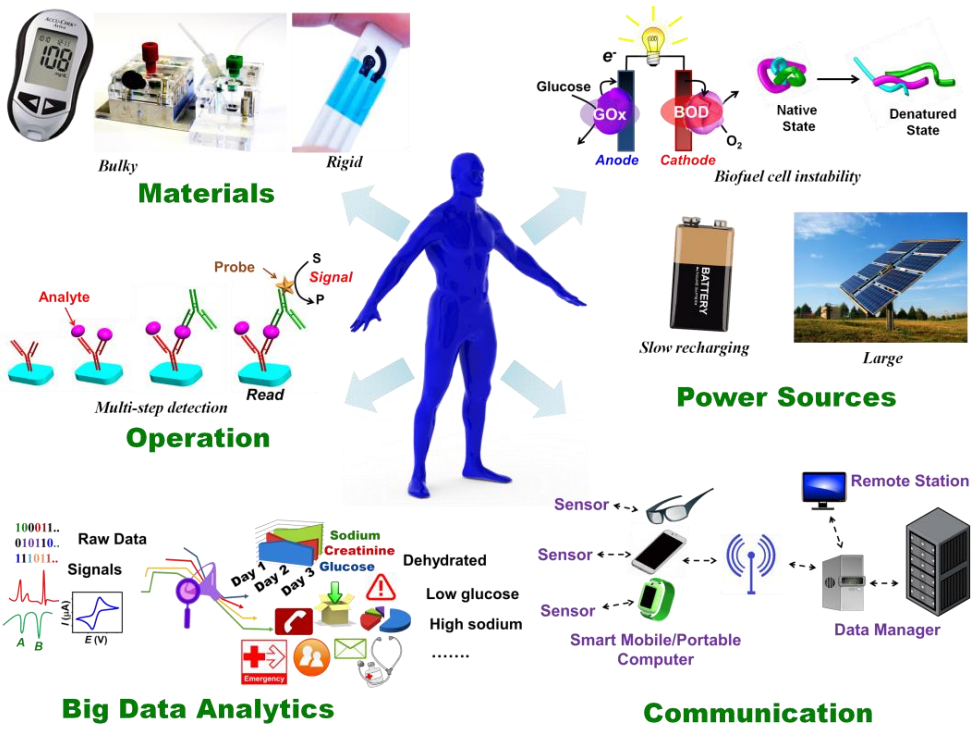


Figure 1.1.3: Current status and challenges in wearable chemical sensors. (Reprinted with permission from ref. 38. Copyright 2016 Americal Chemical Society).

1.5.1 Sensor-based challenges

Sensor based challenges can further be classified into materials and operational based challenges.

a. Materials-based challenges:

Limitations due to absence of viable materials for realizing high performance devices is one of the most critical challenges in the field of wearable chemical sensors. Although state-of-the-art chemical sensors have been in the markets for several decades, the materials, fabrication techniques and device form-factor utilized for developing such traditional sensors are often incompatible for realizing their wearable counterparts. For example, conventional chemical sensors are bulky and heavy[38, 39] and hence cannot be used for wearable applications. Thus, in order to target the wearables market, there is a need to develop sensors that are small

and light for seamless integration with the human body for daily life. Similarly, common chemical sensors are fabricated on rigid surfaces and therefore they cannot be easily mated with the soft, curvilinear human tissues.[40, 41] Conformal contact between the device and the tissue is also essential for acquiring low noise sensor response. This is especially true in cases of wearable/implantable devices that are intended to integrate with highly non-linear biological structures, such as sensors for brain activity monitoring,[42] ocular sensors[21] etc.

The rigidity of the conventional chemical sensors leads also to poor mechanical resiliency against repeated complex deformations commonly experienced by the human body.[3] The human tissue is soft and curvilinear in nature and undergoes regular multi-axes deformations. Recognizing the rigidity of existing chemical sensors, direct chemical sensing on the skin requires soft and stretchable sensor materials able to conform to the non-planar features characteristic of human anatomy. The wearable chemical sensors thus must have mechanical properties similar to the tissues so that they can be anatomically compliant with the contours of the skin, without causing any somatosensory response.[43] In extreme cases, stretchability is not enough and the wearable device must possess self-healing ability to quickly recover itself after mechanical damage.[44] Smart wearable chemical sensors that have autonomous self-healing ability will have a major impact in improving the life-span of such devices since they will self-repair upon mechanical damage and thus allow uninterrupted sensing. In this regard, the wearable sensor community should thus look into recent demonstrations of self-healing devices.[45, 46]

b. Operational challenges:

In addition to above unique challenges, chemical sensors have other issues that have hindered easy transformation of conventional devices to their wearable formats.

i. Pre-treatment and special condition:

Several sensors, such as potentiometric sensors, require calibration before every use and incubation in conditioning solution when not in use.[47] Such conditions are incompatible with wearable technology. Furthermore, potentiometric sensors have the issue of drift that causes significant error in calculating analyte concentration. Therefore, these sensors need to be re-calibrated at regular intervals. Researchers are addressing this issue by developing calibration-free potentiometric sensors.[48, 49] Such requirements are unattractive for wearable applications. Equally challenging for on-body operation is the use of sensors that mandate pre-treatment of sample solution before detection.[47] Similarly, several sensors can detect chemicals only under extreme conditions. For example, several gas sensors detect toxic gases at temperatures much higher than ambient temperature.[50, 51] Thus, such sensors are incapable of being utilized for direct detection of chemical analytes under conditions experienced by wearable devices.

ii. Stability:

Since chemical biosensors rely on biological recognition elements, the stability of these bioreceptors represents a major problem with these devices' long-term storage and use. Biological recognition elements, such as enzymes, DNA, antibodies, and aptamers are very sensitive to their local environments.[52-55] Factors like local temperature, pH, ionic strength, humidity, or pressure have shown to greatly affect these biomolecules. Deviation from optimal conditions can lead to denaturation of the bioreceptors, thus decreasing their sensing ability. High stability of biological recognition element is particularly crucial for wearable applications since (unlike well controlled lab testing) wearable sensors are exposed to varying temperature, pH, ionic strength, humidity, or pressure during prolonged indoor and outdoor activities of the user. At present, the chemical biosensors are incapable of performing optimally in such fast changing environments for long durations.

iii. Sensitivity, limit of detection:

Various wearable chemical sensing applications require detection of low concentrations of analytes. For example, glucose concentration in tears and in extracted skin interstitial fluid is in the micromolar range, which is two orders of magnitude lower than its level in blood. Low concentration detection is especially crucial for environmental and defense applications. Several toxic pollutants,[56, 57] chemical warfare agents,[54] explosives,[58, 59] or contraband drugs[60, 61] must be detected at extremely low levels with high precision, selectivity and rapidity. At present, state-of-the-art, centralized, bench-top analyzers that meet these requirements are available[39] and wearable versions that can compete with these are yet to be developed. Continuous monitoring of analytes is the most attractive aspect of wearable technology. Thus, wearable chemical sensors must be able to detect chemicals rapidly, with short response times corresponding to the dynamic concentration variation of the analyte. This requirement mandates also that wearable sensors will possess reversible response with no carry over so that they can provide accurate data with negligible hysteresis.

iv. Bio-affinity sensing based challenges:

Plethora of important chemical sensors that have immense significance in the wearables market mandates bio-affinity assays. For example, the detection of detection of a wide variety of physiologically relevant biomarkers depends on bio-affinity based sensors.[62, 63] Similarly, environmental sensors for detecting toxic chemicals,[53] and chemical warfare agents[54] require bio-affinity receptors. The development of reliable wearable formats of such bio-affinity sensors has the potential to radically change the landscape of the wearable chemical sensors field. Such sensors will usher in a new and important phase in the field of IoT for critical healthcare, security and environmental monitoring. However, realizing bio-affinity based wearable chemical sensors is challenging (due to their slow response, analytical requirements, and limited re-usability) and hence such wearable devices have not yet been demonstrated. For starters, bio-affinity receptors, such as antibodies,[62] DNA,[64] RNA,[65] PNA,[66]

aptamers[67] are quite labile and denature rather quickly when subjected for long durations to environments common for wearable applications. These bio-receptors rely on "lock-and-key" mechanism to detect the analyte and even minute variations in the receptor's 3D structure greatly affect its ability to recognize the analyte.[68] This leads to reduction in the device's sensing performance.

As mentioned earlier, the most enticing aspect of wearable chemical sensors is their ability to continuously monitor the desired chemical parameters. Meeting this crucial requirement is indeed challenging in the case of bio-affinity sensors since the bio-receptors bind strongly to the analyte, and regeneration of the sensor surface is difficult without damaging the bio-receptors. The need for continuous sensor response also puts the condition of rapid detection on wearable chemical sensors. This requirement is relatively easy to satisfy in case of enzymatic sensors, since these catalytic reactions are fast. However, in case of bio-affinity sensors, the incubation time is usually long (>15 min) and this weakens the chances of developing a continuous and rapid bio-affinity based wearable sensor. Furthermore, in order to achieve accurate and precise information, the bio-affinity sensors must be washed thoroughly after the incubation phase to reduce non-specific binding of interfering species to the sensor surface. Satiating this condition is again daunting in case of wearable applications with the need for human intervention.

The concentrations of the chemical analytes that these wearable bio-affinity sensors are expected to detect are usually low (nM to aM range).[53] Thus, these sensors must offer very low limits of detection. This condition is inherently tied to the above mentioned challenges. For example, in order to achieve low limits of detection, the binding affinity of the receptor to its analyte must be strong; this implies that regeneration of the sensor surface will be extremely difficult. Similarly, low limit of detection mandates thorough washing of the sensor surface for mitigating non-specific adsorption – a complicating step for wearable application.

Researchers achieve low limit of detection for bio-affinity sensors by relying on sandwich-based systems.[64, 69, 70] These are multi-step protocols which cannot be easily implemented using wearable platforms.

1.5.2 Other challenges

Other challenges faced by wearable chemical sensors include issues related to power source, data transmission, security and analytics. These are briefly discussed in the following sub-sections.

a. Power source:

As the demand for wearable sensors grows, so too does the demand for relevant power sources. Wearable sensors are increasingly becoming "energy-hungry" in order to meet the increasing demands of detecting multiple parameters simultaneously, performing complex data analysis, communicating with other sensors, devices and data transmission. The scientific community that has interest in solving this issue has broadly focused on three aspects – develop low-power energy efficient devices,[71, 72] compact, energy dense wearable power sources[73, 74] and adaptive algorithms for intelligent, low-power consuming electronics.[75, 76] Advances in the field of wearable energy devices have not been able to cope with the speed at which wearable sensor technology has progressed. Limitation caused by inefficient wearable power sources is a common roadblock for effective adaptation of wearable sensors. It is thus imperative to develop wearable power sources that are in the vicinity of the target wearable electronic device in order to obviate the need for long wires and ease of complete device integration with the body. In this regard, several avenues, such as wearable batteries,[77, 78] supercapacitors,[79] solar cells,[80] biofuel cells,[81, 82] thermoelectric,[83] piezoelectric/triboelectric,[84] have been explored by researchers to realize wearable power devices.

b. Communication:

Similar to any disruptive technology, the field of wearable sensors is also expected to witness an exponential boom in its demand. As the markets warm up towards wearable sensors, the need to develop faster, more compact, multi-functional, smart wearable sensors will only grow with time. One of the most attractive aspects of the wearable sensor field is uninterrupted streaming of information from various sensor nodes to the wearer. Such sensors will also be expected to continuously interact with a nearby computing device (such as a mobile phone) that automatically classifies certain events in order to provide timely intervention (e.g., message to a remote caregiver or alert to the user). Some wearable sensor applications do not require real-time wireless connectivity, and the data can be logged locally on the sensor platform for several days. The connectivity requirements are amplified in scenarios common to residential or commercial setups, where several individuals have multiple wearable sensors, interacting with each other at high rates, thus requiring high density wireless communication (Figure 1.1.4). Such conditions mandate by wearable sensors with unprecedented connectivity.

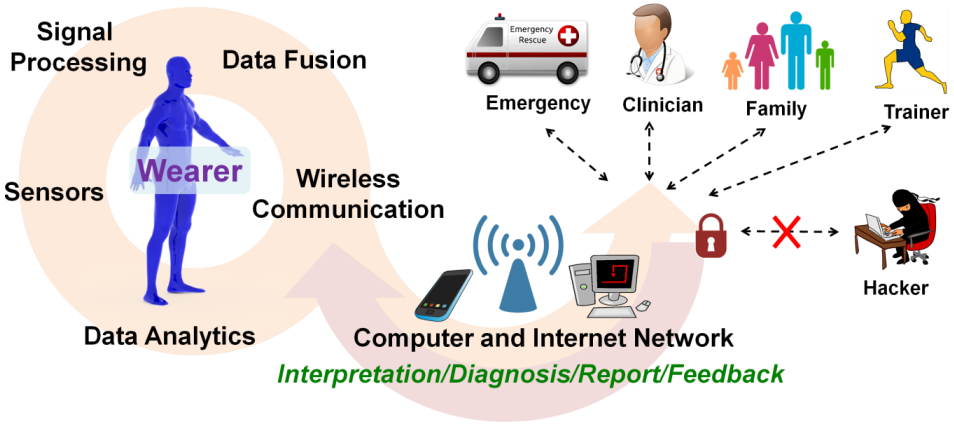


Figure 1.1.4: Scheme showing a typical multi-nodal wireless network for wearable sensors. (Reprinted with permission from ref. 38. Copyright 2016 Americal Chemical Society).

To date, Bluetooth low energy (BLE),[85, 86] and near-field communication (NFC)[10, 87] technologies have been explored the most for wearable sensors applications. Researchers,

including our group, have exploited BLE and RF technologies for developing wearable chemical sensors for detecting analytes on the skin[85] in tears[6] and saliva.[88] While these protocols are suitable for low density data transmission, they fare poorly when it comes to smooth streaming of data within a complex network of high density wearable sensors.

c. Data security and analytics:

With the widespread market penetration of wearable sensors, developers will have to inevitably grapple with the challenges of big data analytics and data security. As wearable sensors increasingly become an integral part of humans, these devices are expected to generate unprecedented volumes of un-structured, low quality information originating from a wide variety of heterogeneous sources, such as different physical and chemical sensors. The information that wearable sensors collect and report to their wearer is highly individual. As more consumers rely on wearable sensors, they expose themselves to potential security breaches. Data protection has thus become one of the most crucial factors for the operation of mobile and wearable devices.

Directly sending huge amounts of this unprocessed sensor data will only overwhelm and confuse the user, thus leading to underuse of the wearable device. Providing the most pertinent and relevant analytical information in an easy-to-understand manner is thus essential for widespread adoption of wearable sensor technology. This involves intelligent big data mining to unearth relevant information before presenting it to the user. However, present data mining algorithms will not be able to handle the huge volumes of data that wearable sensor networks are expected to generate.[89] Researchers are making efforts towards developing effective strategies to address these issues. For example, data miners are working on new algorithms for data cleaning and filtering[90] and expanding data mining protocols for handling heterogeneous information.[91]

This chapter is based, in part, on the material as it appears in Trends in Biotechnology, 2014, by Amay J. Bandodkar and Joseph Wang; in part on the material as it appears in Electroanalysis, 2015, by Amay J. Bandodkar, Wenzhao Jia and Joseph Wang; in part on the material as it appears in ACS Sensors, 2016, by Amay J. Bandodkar, Itthipon Jeerapan and Joseph Wang. The dissertation author was the primary investigator and corresponding author of this paper.

1.6 References

1. Kim, D. H.; Ghaffari, R.; Lu, N.; Rogers, J. A. *Annu. Rev. Biomed. Eng.* **2012,** *14*, 113.

2. Bandodkar, A. J.; Wang, J. *Trends Biotechnol.* **2014,** *32*, 363.

3. Rogers, J. A.; Someya, T.; Huang, Y. *Science* **2010,** *327*, 1603.

4. Bandodkar, A. J.; Jia, W.; Wang, J. *Electroanalysis* **2015,** *27*, 562.

5. Bandodkar, A. J.; Jia, W.; Yardımcı, C.; Wang, X.; Ramirez, J.; Wang, J. *Anal. Chem.* **2015,** *87*, 394.

6. Yao, H.; Shum, A. J.; Cowan, M.; Lahdesmaki, I.; Parviz, B. A. *Biosens. Bioelectron.* **2011,** *26*, 3290.

7. Liu, J.; Sun, S.; Shang, H.; Lai, J.; Zhang, L. *Electroanalysis* **2016,** DOI: 10.1002/elan.201501179.

8. Kim, J.; Valdes-Ramirez, G.; Bandodkar, A. J.; Jia, W.; Martinez, A. G.; Ramirez, J.; Mercier, P.; Wang, J. *Analyst* **2014,** *139*, 1632.

9. Jia, W.; Bandodkar, A. J.; Valdés-Ramírez, G.; Windmiller, J. R.; Yang, Z.; Ramírez, J.; Chan, G.; Wang, J. *Anal. Chem.* **2013,** *85*, 6553.

10. Mannoor, M. S.; Tao, H.; Clayton, J. D.; Sengupta, A.; Kaplan, D. L.; Naik, R. R.; Verma, N.; Omenetto, F. G.; McAlpine, M. C. *Nat Commun* **2012,** *3*, 763.

11. Vasudev, A.; Kaushik, A.; Tomizawa, Y.; Norena, N.; Bhansali, S. *Sens. Actuators, B* **2013,** *182*, 139.

12. Emorine, M.; Mielle, P.; Maratray, J.; Septier, C.; Thomas-Danguin, T.; Salles, C. *IEEE Sens. J.* **2012,** *12*, 3124.

13. Zhou, L.; Beuerman, R. W. *Prog. Ret. Eye Res.* **2012,** *31*, 527.

14. Nakatsukasa, M.; Sotozono, C.; Shimbo, K.; Ono, N.; Miyano, H.; Okano, A.; Hamuro, J.; Kinoshita, S. *Am. J. Ophthalmol.* **2011,** *151*, 799.

15. Choy, C. K. M.; Cho, P.; Chung, W.-Y.; Benzie, I. F. F. *Invest. Ophthalmol. Vis. Sci.* **2001,** *42*, 3130.

16. Gogia, R.; Richer, S. P.; Rose, R. C. *Curr. Eye Res.* **1998,** *17*, 257.

17. Iguchi, S.; Mitsubayashi, K.; Uehara, T.; Ogawa, M. *Sens. Actuators, B* **2005,** *108*, 733.

18. Sen, D. K.; Sarin, G. S. *Br. J. Ophthalmol.* **1980,** *64*, 693.

19. Kudo, H.; Sawada, T.; Kazawa, E.; Yoshida, H.; Iwasaki, Y.; Mitsubayashi, K. *Biosens. Bioelectron.* **2006,** *22*, 558.

20. Chu, M.; Shirai, T.; Takahashi, D.; Arakawa, T.; Kudo, H.; Sano, K.; Sawada, S.; Yano, K.; Iwasaki, Y.; Akiyoshi, K.; Mochizuki, M.; Mitsubayashi, K. *Biomed. Microdevices* **2011,** *13*, 603.

21. Yao, H.; Liao, Y.; Lingley, A. R.; Afanasiev, A.; Lähdesmäki, I.; Otis, B. P.; Parviz, B. A. *J. Micromech. Microeng.* **2012,** *22*, 075007.

22. Falk, M.; Andoralov, V.; Blum, Z.; Sotres, J.; Suyatin, D. B.; Ruzgas, T.; Arnebrant, T.; Shleev, S. *Biosens. Bioelectron.* **2012,** *37*, 38.

23. Falk, M.; Andoralov, V.; Silow, M.; Toscano, M. D.; Shleev, S. *Anal. Chem.* **2013,** *85*, 6342.

24. Mitsubayashi, K.; Suzuki, M.; Tamiya, E.; Karube, I. *Anal. Chim. Acta* **1994,** *289*, 27.

25. Vashist, S. K. *Anal. Chim. Acta* **2012,** *750*, 16.

26. Bergeron, M. F. *J. Sci. Med. Sport.* **2003,** *6*, 19.

27. Rosner, M. H.; Kirven, J. *Clin. J. Am. Soc. Nephrol.* **2007,** *2*, 151.

28. Ladell, W. S. S. *J. Physiol.* **1955,** *127*, 11.

29. Stern , R. C. *New Eng. J. Med.* **1997,** *336*, 487.

30. Ravier, G.; Dugue, B.; Grappe, F.; Rouillon, J. D. *Int. J. Sports Med.* **2006,** *27*, 810.

31. Klesges, R. C.; Ward, K. D.; Shelton, M. L.; Applegate, W. B.; Cantler, E. D.; Palmieri, G. M.; Harmon, K.; Davis, J. *J. Am. Med. Assoc.* **1996,** *276*, 226.

32. Heaney, R. P. *J. Intern. Med.* **1992,** *231*, 169.

33. Pilardeau, P.; Vaysse, J.; Garnier, M.; Joublin, M.; Valeri, L. *Br. J. Sports Med.* **1979,** *13*, 118.

34. Nixon, S.; Sieg, A.; Delgado-Charro, M. B.; Guy, R. H. *J. Pharm. Sci.* **2007,** *96*, 3457.

35. Lee, H.; Choi, T. K.; Lee, Y. B.; Cho, H. R.; Ghaffari, R.; Wang, L.; Choi, H. J.; Chung, T. D.; Lu, N.; Hyeon, T.; Choi, S. H.; Kim, D.-H. *Nat Nano* **2016,** DOI: 10.1038/nnano.2016.38.

36. Gao, W.; Emaminejad, S.; Nyein, H. Y. Y.; Challa, S.; Chen, K.; Peck, A.; Fahad, H. M.; Ota, H.; Shiraki, H.; Kiriya, D.; Lien, D.-H.; Brooks, G. A.; Davis, R. W.; Javey, A. *Nature* **2016,** *529*, 509.

37. Metters, J. P.; Kadara, R. O.; Banks, C. E. *Analyst* **2011,** *136*, 1067.

38. Bandodkar, A. J.; Jeerapan, I.; Wang, J. *ACS Sensors* 2016 DOI: 10.1021/acssensors.6b00250.

39. Musso, J.; Buchmann, W.; Gonnet, F.; Jarroux, N.; Bellon, S.; Frydman, C.; Brunet, D.-L.; Daniel, R. *Anal. Bioanal. Chem.* **2014,** *407*, 1285.

40. Choi, S.; Lee, H.; Ghaffari, R.; Hyeon, T.; Kim, D. H. *Adv. Mater.* **2016**, DOI: 10.1002/adma.201504150.

41. Chan, M.; Estève, D.; Fourniols, J.-Y.; Escriba, C.; Campo, E. *Artif. Intell. Med.* **2012,** *56*, 137.

42. Kang, S.-K.; Murphy, R. K. J.; Hwang, S.-W.; Lee, S. M.; Harburg, D. V.; Krueger, N. A.; Shin, J.; Gamble, P.; Cheng, H.; Yu, S.; Liu, Z.; McCall, J. G.; Stephen, M.; Ying, H.; Kim, J.; Park, G.; Webb, R. C.; Lee, C. H.; Chung, S.; Wie, D. S.; Gujar, A. D.; Vemulapalli, B.; Kim, A. H.; Lee, K.-M.; Cheng, J.; Huang, Y.; Lee, S. H.; Braun, P. V.; Ray, W. Z.; Rogers, J. A. *Nature* **2016,** *530*, 71.

43. Hattori, Y.; Falgout, L.; Lee, W.; Jung, S.-Y.; Poon, E.; Lee, J. W.; Na, I.; Geisler, A.; Sadhwani, D.; Zhang, Y.; Su, Y.; Wang, X.; Liu, Z.; Xia, J.; Cheng, H.; Webb, R. C.; Bonifas, A. P.; Won, P.; Jeong, J.-W.; Jang, K.-I.; Song, Y. M.; Nardone, B.; Nodzenski, M.; Fan, J. A.; Huang, Y.; West, D. P.; Paller, A. S.; Alam, M.; Yeo, W.-H.; Rogers, J. A. *Adv. Healthc. Mat.* **2014,** *3*, 1597.

44. Bandodkar, A. J.; Mohan, V.; López, C. S.; Ramírez, J.; Wang, J. *Adv. Electron. Mat.* **2015,** *1*, DOI: 10.1002/aelm.201500289.

45. Yang, Y.; Zhu, B.; Yin, D.; Wei, J.; Wang, Z.; Xiong, R.; Shi, J.; Liu, Z.; Lei, Q. *Nano Energy* **2015,** *17*, 1.

46. Tee, B. C. K.; Wang, C.; Allen, R.; Bao, Z. *Nat Nano* **2012,** *7*, 825.

47. David-Parra, D. N.; Bocchi, N.; Teixeira, M. F. S. *Electrochim. Acta* **2015,** *174*, 640.

48. Zou, X. U.; Zhen, X. V.; Cheong, J. H.; Bühlmann, P. *Anal. Chem.* **2014,** *86*, 8687.

49. Cisternas, R.; Kahlert, H.; Scholz, F.; Wulff, H. *Electrochem. Commun.* **2015,** *60*, 17.

50. Gupta Chatterjee, S.; Chatterjee, S.; Ray, A. K.; Chakraborty, A. K. *Sens. Actuators, B* **2015,** *221*, 1170.

51. Deng, J.; Ma, J.; Mei, L.; Tang, Y.; Chen, Y.; Lv, T.; Xu, Z.; Wang, T. *J. Mater. Chem. A* **2013,** *1*, 12400.

52. Chen, C.; Xie, Q.; Yang, D.; Xiao, H.; Fu, Y.; Tan, Y.; Yao, S. *RSC Advances* **2013,** *3*, 4473.

53. Loyprasert, S.; Hedström, M.; Thavarungkul, P.; Kanatharana, P.; Mattiasson, B. *Biosens. Bioelectron.* **2010,** *25*, 1977.

54. Gaylord, S. T.; Dinh, T. L.; Goldman, E. R.; Anderson, G. P.; Ngan, K. C.; Walt, D. R. *Anal. Chem.* **2015,** *87*, 6570.

55. Bankar, S. B.; Bule, M. V.; Singhal, R. S.; Ananthanarayan, L. *Biotechnol. Adv.* **2009,** *27*, 489.

56. Cho, E. S.; Kim, J.; Tejerina, B.; Hermans, T. M.; Jiang, H.; Nakanishi, H.; Yu, M.; Patashinski, A. Z.; Glotzer, S. C.; Stellacci, F.; Grzybowski, B. A. *Nat. Mater.* **2012,** *11*, 978.

57. Lu, R.; Li, W.-W.; Mizaikoff, B.; Katzir, A.; Raichlin, Y.; Sheng, G.-P.; Yu, H.-Q. *Nat. Protocols* **2016,** *11*, 377.

58. Wang, Y.; La, A.; Ding, Y.; Liu, Y.; Lei, Y. *Adv. Funct. Mater.* **2012,** *22*, 3547.

59. Peters, K. L.; Corbin, I.; Kaufman, L. M.; Zreibe, K.; Blanes, L.; McCord, B. R. *Anal. Methods* **2015,** *7*, 63.

60. Taghdisi, S. M.; Danesh, N. M.; Emrani, A. S.; Ramezani, M.; Abnous, K. *Biosens. Bioelectron.* **2015,** *73*, 245.

61. Choodum, A.; Parabun, K.; Klawach, N.; Daeid, N. N.; Kanatharana, P.; Wongniramaikul, W. *Forensic. Sci. Int.* **2014,** *235*, 8.

62. Kadimisetty, K.; Malla, S.; Sardesai, N. P.; Joshi, A. A.; Faria, R. C.; Lee, N. H.; Rusling, J. F. *Anal. Chem.* **2015,** *87*, 4472.

63. Zhang, S.; Zang, L.; Zhang, X.; Dai, H.; Xu, G.; Zhang, Q.; Yang, C.; Lin, Y. *Electrochim. Acta* **2016,** *196*, 67.

64. Mariani, S.; Scarano, S.; Spadavecchia, J.; Minunni, M. *Biosens. Bioelectron.* **2015,** *74*, 981.

65. Tran, H. V.; Piro, B.; Reisberg, S.; Huy Nguyen, L.; Dung Nguyen, T.; Duc, H. T.; Pham, M. C. *Biosens. Bioelectron.* **2014,** *62*, 25.
66. Lee, J.; Park, I.-S.; Kim, H.; Woo, J.-S.; Choi, B.-S.; Min, D.-H. *Biosens. Bioelectron.* **2015,** *69*, 167.

67. Liu, R.; Yang, Z.; Guo, Q.; Zhao, J.; Ma, J.; Kang, Q.; Tang, Y.; Xue, Y.; Lou, X.; He, M. *Electrochim. Acta* **2015,** *182*, 516.

68. Rodríguez-Hernández, J.; Cortajarena, L. A., Selective Biorecognition on Polymer Surfaces: General Issues. In *Design of Polymeric Platforms for Selective Biorecognition*, Rodríguez-Hernández, J.; Cortajarena, L. A., Eds. Springer International Publishing: Cham, 2015; pp 1.

69. Li, J.; Chang, K.-W.; Wang, C.-H.; Yang, C.-H.; Shiesh, S.-C.; Lee, G.-B. *Biosens. Bioelectron.* **2016,** *79*, 887.

70. Zhang, L.; Li, L.; Ma, C.; Ge, S.; Yan, M.; Bian, C. *Sens. Actuators, B* **2015,** *221*, 799.

71. Kassal, P.; Steinberg, I. M.; Steinberg, M. D. *Sens. Actuators, B* **2013,** *184*, 254.

72. De Marcellis, A.; Depari, A.; Ferri, G.; Flammini, A.; Sisinni, E. *Sens. Actuators, B* **2013,** *179*, 313.

73. Zi, Y.; Lin, L.; Wang, J.; Wang, S.; Chen, J.; Fan, X.; Yang, P.-K.; Yi, F.; Wang, Z. L. *Adv. Mater.* **2015,** *27*, 2340.

74. Zhang, Y.; Zhao, Y.; Cheng, X.; Weng, W.; Ren, J.; Fang, X.; Jiang, Y.; Chen, P.; Zhang, Z.; Wang, Y.; Peng, H. *Angew. Chem. Int. Ed.* **2015,** *54*, 11177.

75. Kannan, R.; Garg, A. In *Adaptive sensor fusion technology for mobile and wearable applications*, SENSORS, 2015 IEEE, 1-4 Nov. 2015; 2015; pp 1.

76. Sarpeshkar, R. *IEEE Transactions on Circuits and Systems II: Express Briefs* **2012,** *59*, 193.

77. Xu, S.; Zhang, Y.; Cho, J.; Lee, J.; Huang, X.; Jia, L.; Fan, J. A.; Su, Y.; Su, J.; Zhang, H.; Cheng, H.; Lu, B.; Yu, C.; Chuang, C.; Kim, T.-i.; Song, T.; Shigeta, K.; Kang, S.; Dagdeviren, C.; Petrov, I.; Braun, P. V.; Huang, Y.; Paik, U.; Rogers, J. A. *Nat Commun* **2013,** *4*, 1543.

78. Berchmans, S.; Bandodkar, A. J.; Jia, W.; Ramirez, J.; Meng, Y. S.; Wang, J. *J. Mater. Chem. A* **2014,** *2*, 15788.

79. Dong, L.; Xu, C.; Li, Y.; Wu, C.; Jiang, B.; Yang, Q.; Zhou, E.; Kang, F.; Yang, Q.-H. *Adv. Mater.* **2016,** *28*, 1675.

80. O'Connor, T. F.; Zaretski, A. V.; Savagatrup, S.; Printz, A. D.; Wilkes, C. D.; Diaz, M. I.; Sawyer, E. J.; Lipomi, D. J. *Sol. Energy Mater. Sol. Cells* **2016,** *144*, 438.

81. Jia, W.; Valdés-Ramírez, G.; Bandodkar, A. J.; Windmiller, J. R.; Wang, J. *Angew. Chem. Int. Ed.* **2013,** *52*, 7233.

82. Jia, W.; Wang, X.; Imani, S.; Bandodkar, A. J.; Ramirez, J.; Mercier, P. P.; Wang, J. *J. Mater. Chem. A* **2014,** *2*, 18184.

83. Oh, J. Y.; Lee, J. H.; Han, S. W.; Chae, S. S.; Bae, E. J.; Kang, Y. H.; Choi, W. J.; Cho, S. Y.; Lee, J.-O.; Baik, H. K.; Lee, T. I. *Energy Environ. Sci.* **2016**.

84. Jin-Hee, Y.; Hyun-Seung, C.; Seon-Hyung, P.; Seung-Hwan, S.; Kwang-Seok, Y.; Joo Hyeon, L. *Smart Mater. Struct.* **2016,** *25*, 035012.

85. Bandodkar, A. J.; Molinnus, D.; Mirza, O.; Guinovart, T.; Windmiller, J. R.; Valdes-Ramirez, G.; Andrade, F. J.; Schoning, M. J.; Wang, J. *Biosens. Bioelectron.* **2014,** *54*, 603.

86. Liu, G.; Ho, C.; Slappey, N.; Zhou, Z.; Snelgrove, S. E.; Brown, M.; Grabinski, A.; Guo, X.; Chen, Y.; Miller, K.; Edwards, J.; Kaya, T. *Sens. Actuators, B* **2016,** *227*, 35.

87. Jung, Y.; Park, H.; Park, J.-A.; Noh, J.; Choi, Y.; Jung, M.; Jung, K.; Pyo, M.; Chen, K.; Javey, A.; Cho, G. *Sci. Rep.* **2015,** *5*, 8105.

88. Kim, J.; Imani, S.; de Araujo, W. R.; Warchall, J.; Valdés-Ramírez, G.; Paixão, T. R. L. C.; Mercier, P. P.; Wang, J. *Biosens. Bioelectron.* **2015,** *74*, 1061.

89. Chen, F.; Deng, P.; Wan, J.; Zhang, D.; Vasilakos, A. V.; Rong, X. *Int. J. Distrib. Sen. Netw.* **2015,** *2015*, 12.

90. Chen, M.; Leung, V. C. M.; Mao, S. *Mobile Netw. Appl.* **2009,** *14*, 220.

91. Wu, X.; Zhu, X.; Wu, G. Q.; Ding, W. *IEEE Trans. Knowl. Data Eng.* **2014,** *26*, 97.

Chapter 2 All-Printed Stretchable Electrochemical Devices

2.1 Devices possessing intrinsic stretchability

2.1.1 Introduction

Soft stretchable devices have immense applications in various sensor,[1] wearable computer,[2] photovoltaic,[3] battery,[4] and optic[5] domains due to their intimate contact to curvilinear surfaces and ability to withstand high strain levels. Stretchable electronics thus belong to a unique section of conformal electronics. The last decade has witnessed major advances that have shaped the field of stretchable electronics.[6] Key to the success of such stretchable electronic devices is the judicious and specialized engineering of the fabrication materials and device designs. Various groups have achieved device stretchability by utilizing nanomaterials,[7] metal-based films,[1] serpentine lines, [8]or liquid metals.[9] Though these materials and layouts offer excellent stretchability, devices fabricated from these materials are commonly realized by lithographic or spin/spray coating techniques that are either expensive or incompatible with large-scale fabrication, thus leading to higher costs per device. Accordingly, there are pressing needs to develop large-scale low-cost fabrication routes of high-performance stretchable devices.

Extensive research in the field of stretchable devices has been devoted towards conformal devices for monitoring physical health parameters, such as body temperature, ECG, or body movements. Electrochemical sensors represent an important class of wearable sensors that provide important "*chemical information*" for various healthcare,[10] environmental[11] and defense[12] applications. Despite achieving major progress toward developing flexible and bendable tattoo,[13] textile[10] and plastic[14] based electrochemical devices, no effort has been

directed towards developing stretchable electrochemical devices that can withstand extreme tensile stress and meet the stretchability requirements of many applications. Stretchable printable electrically-conductive materials are highly desired for a variety of other next-generation surface-compliant electrochemical devices. Coupling these printable devices with other forms of stretchable electronics, will offer unprecedented opportunities in the energy, healthcare, defense and display fields where high-performance under severe mechanical strain is crucial.

The present study thus aims at filling this technological gap by demonstrating, for the first time, the use of screen printing to develop low-cost stretchable devices, in general, and conformal electrochemical electronics, in particular.[15] Here we demonstrate the realization of highly stretchable electrochemical devices based on screen printing of conducting inks judiciously tailored with elastomer and surfactant using custom-designed stencils (Figure 2.1.1 A). Screen printing technology offers large-scale low-cost production of variety of electrochemical devices and of flexible electronics systems, in general.[16] Considerable efforts have been devoted towards development of bendable screen printed electrochemical devices.[17, 18] However, the lack of stretchability of these devices seriously hinders their applications involving extreme tensile stress. Developing intrinsically stretchable inks is imperative for improving the performance and mechanical capabilities of printable electrochemical devices. Screen printing of specially synthesized stretch-enduring inks, as described here, can be easily utilized to fabricate variety of high-performance, yet inexpensive, stretchable devices for diverse applications that mandate mechanically resilient devices.

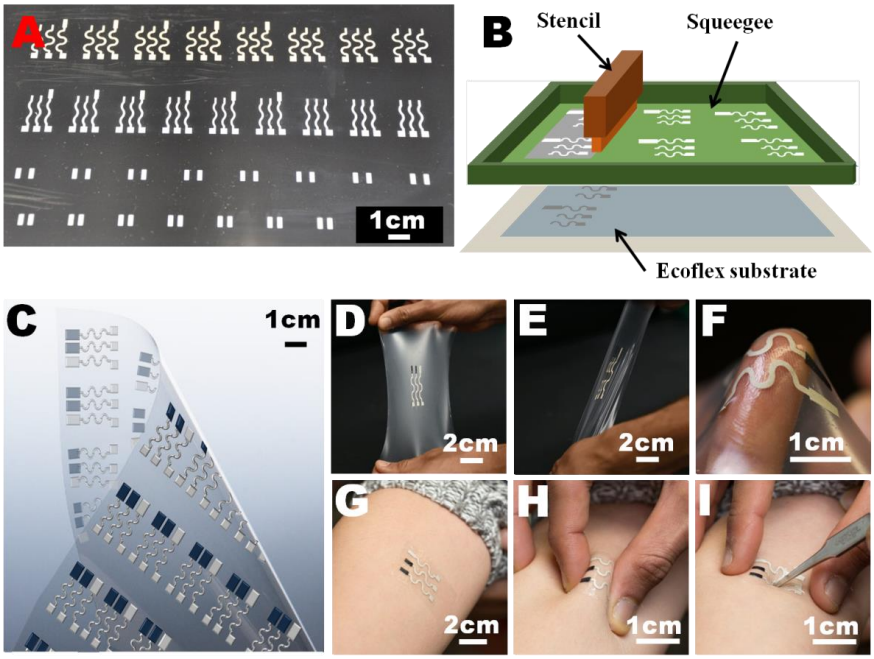


Figure 2.1.1. (A) Image of the printing stencil containing the different electrodes, contact pads and interconnect patterns. (B) Scheme depicting the screen printing of the stretchable device using tailor-made stretch-enduring inks. (C) Scheme depicting an array of all-printed stretchable electrochemical sensors. (D) Images illustrating application of stretching (E) torsional and (F) indentation strains to the printed sensor. (G) Conformal attachment of sensor to flexor carpi radialis of the forearm. Images of skin-mounted device during different deformations of the skin: application of (H) pinching and (I) indentation. (Reprinted with permission from ref. 15. Copyright 2015 Wiley.)

2.1.2 Experimental section

a. Stretchable electrochemical fabrication:

The fabrication process comprised of screen printing of ecoflex substrate and conductive inks using an MPM-SPM semi-automatic screen printer (Speedline Technologies, Franklin, MA). Sensor patterns were designed in AutoCAD (Autodesk, San Rafael, CA) and outsourced for fabrication on stainless steel through-hole 12” x 12” framed stencils (Metal Etch Services, San Marcos, CA). First, Ecoflex substrate was prepared by printing Ecoflex® 00-30 (Smooth-On, Inc., PA) on a supporting surface. Ecoflex® 00-30 was prepared by mixing equal volumes of pre-polymer A with pre-polymer B provided by the supplier.

Thereafter, the Ecoflex substrate was cured at ambient temperature for 1 hour. Subsequently, a sequence of Ag/AgCl (E2414, Ecron Inc., Wareham, MA), PEDOT:PSS (768650, Sigma-Aldrich, St. Louis, MO) and Ecoflex was printed to realize the complete electrochemical device. The Ag/AgCl pattern was cured at 120ºC for 3 min, while the PEDOT:PSS ink was cured at 65ºC for 10 min in a convection oven. The final Ecoflex layer, used to define the electrode area, was cured at room temperature for 1 hour.

Pristine electrochemical devices, used for preliminary studies, were realized by printing the inks and Ecoflex as received. In order to fabricate stretchable electrochemical devices, the substrate Ecoflex was prepared by screen printing Ecoflex polymer thoroughly mixed with 2 wt% Zonyl (Sigma-Aldrich, St. Louis, MO). Similarly, the pristine Ag/AgCl and PEDOT:PSS inks were first modified with 20% v/v Ecoflex containing 2 wt% Zonyl. The stretchable electrochemical devices were fabricated by printing the modified Ag/AgCl and PEDOT:PSS inks on the Zonyl-modified Ecoflex substrate.

b. Electrochemical studies:

i. Cyclic Voltammetric Studies:

Cyclic voltammetric (CV) studies were performed using a CH Instruments (Austin, TX) model 630C electrochemical analyzer. The electrolyte consisted of 1mM ferricyanide in 0.1M phosphate buffer (pH 7.0). CV plots were recorded in the -0.6V to 0.8V potential range with a scan rate of 0.1V/s.

ii. Electrochemical Impedance Spectroscopic Studies:

Electrochemical impedance spectroscopic studies were performed using a CH Instruments (Austin, TX) model 660 D electrochemical analyzer. The impedance data was recorded in the frequency range of 100 Hz to 0.01Hz with amplitude of 5mV using 1mM ferricyanide in 0.1M phosphate buffer (pH 7.0). The printed PEDOT:PSS electrode acted as

the working electrode, while external reference and counter electrode comprised of Ag/AgCl electrode (CH Instruments, Austin, TX) and platinum wire respectively.

c. Mechanical deformation studies:

The linear stretching study consisted of stretching the electrochemical device by 100% its initial length at a speed of 2mm/s followed by holding it at the 100% stretched state for 2s before releasing the external strain at a speed of 2mm/s. CV plots were recorded before and after application of 10 such stress cycles for a total of 50 iterations. The study aimed at studying the electrochemical properties of the device when under continuous linear tensile load comprised of stretching the device by 25% at a speed of 2mm/s. Thereafter, CV measurements were recorded every 15 min for a total of 60 min. In radial stretching study, the device was mounted on a customized radial stretcher and subjected to increasing levels of radial stretching (0%, 30%, 65%, 100% and 150% areal stretching). CV plots were recorded after every radial stretch cycle. While studying the effect of continuous radial stretching, the electrochemical device was stretched and maintained at 65% areal stretch for 150 min while its electrochemical properties were probed every 15 min via CV. The lateral bending experiment consisted of repeatedly sidewise bending of the sensor for 50 times. CV plots were logged after every 10 bending iterations.

2.1.3 Results and discussion

The highly stretchable electrochemical devices have been realized by printing specially engineered poly(3,4-ethylenedioxythiophene)-poly(styrenesulfonate) (PEDOT:PSS) and silver/silver chloride (Ag/AgCl) inks, containing silicone-based elastomeric polymer - Ecoflex and a non-ionic surfactant - Zonyl, on stretchable elastomeric substrate (Figure 2.1.1 B). PEDOT:PSS ink was used to realize the working and counter electrodes due to its electrochemical inertness, while the reference electrode was fabricated using Ag/AgCl ink

since it provides a constant electrochemical potential. By leveraging screen printing technology, large-scale fabrication of stretchable devices is thus feasible (Figure 2.1.1 C). The stretchable device has been designed to have 2D serpentine interconnects with turns of 180^0 angle between the electrode areas and contact pads. Such interconnect designs can endure high levels of strain without failure.[19]

As illustrated in Figure 2.1.1 (D-F) and Supporting Information Video S1, the new all-printed stretchable electrochemical devices can easily withstand repeated stretching up to 100% (D), extreme torsional stress (E) and indentations (F). Such attractive capabilities have not been reported earlier in connection to printable electrochemical devices. While there have been reports on stretchable PEDOT:PSS devices,[20] these are fabricated using spin-coating technique that cannot offer large-scale production or well-defined patterns mandated for advanced electrochemical devices. As illustrated in Figure 2.1.1 (G-I), the new printed stretchable devices can adhere firmly to complex non planar surfaces, such as the human skin. The resulting skin-mounted devices can withstand different mechanical deformations of the epidermis, including repeated pinching stress (Figure 2.1.1 H) and indentations using sharp objects (Figure 2.1.1 I). These images illustrate that the sensor remains intact and mated to the forearm even under such high stress levels.

A crucial step towards obtaining these all-printed stretchable electrochemical devices was the development of specially modified inks that offer printed electrodes having intrinsic stretchability, combined with favorable electrochemical performance, comparable to that of conventional printed rigid electrodes. Preliminary work aimed at printing pristine (unmodified) commercial PEDOT:PSS and Ag/AgCl inks on Ecoflex substrates followed by applying tensile stress to the printed device. As illustrated in Figure 2.1.2A, the printed Ag/AgCl and PEDOT:PSS layers started debonding and developed major cracks even when the underlying Ecoflex substrate was under 10% strain. Conductive and polymeric-binder

microparticles are the two major components of printable inks. The printed electrodes experience a shear stress when a tensile force is applied to the underlying stretchable substrate. Hence, the ink components must have strong adherence to the substrate and stretchable properties to endure such stress, to prevent abrupt peeling and cracking of the printed layer. The poor performance of the pristine ink-printed device can thus be attributed to the plastic nature of the ink components and their poor adherence to the Ecoflex substrate. The printed trace consists of multi-layers of randomly oriented conductive filler particulates, held together by the binder (Figure 2.1.2 A). Upon application of tensile force, the plastic nature of the components of the printed trace causes it to develop cracks at several locations in order to accommodate the external stress. Increasing the stress level further leads to peeling of the edges of the cracked pattern. When the external stress is withdrawn, the printed trace is unable to recover its electrical conductivity due to the major cracks and debonding that occur under mechanical deformation, thus leading to device failure.

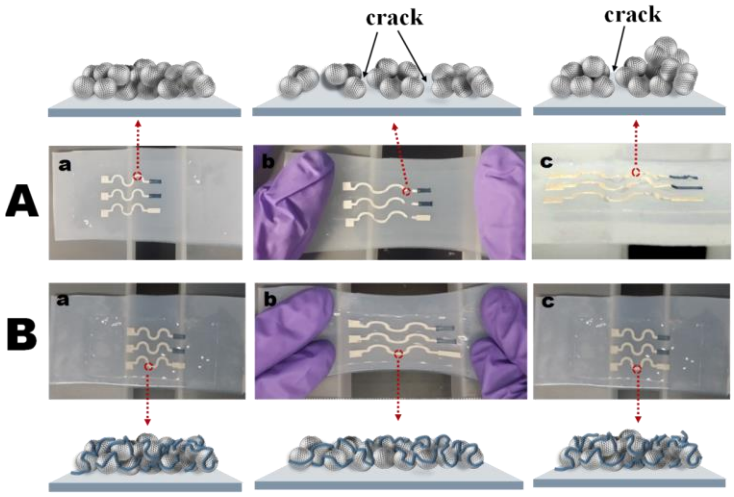


Figure 2.1.2. Mechanical (stretch-and-release) deformation study performed on the printable electrochemical device fabricated by pristine (A) and modified (B) Ag/AgCl and PEDOT:PSS inks. In each panel, the images show the device before (a), during (b) and after (c) application of a 100% tensile strain. The corresponding schemes depict the microscopic structure of these printed traces during steps a-c. (Reprinted with permission from ref. 15. Copyright 2015 Wiley.)

Thus, to develop highly stretchable all-printed electrochemical electronics, the inks were modified with materials that impart stretchabilty to the printed electrodes and improve their adhesion to the underlying stretchable substrate. Ecoflex, was therefeore selected as an additive to confer stretchability to the pristine inks. Preliminary optimization studies revealed that mixing the respective inks with 20% v/v of Ecoflex provided the optimal ink composition for obtaining electrodes with desired stretchability and electrical conductivity. In order to address the debonding challenge and the subsequent delamination of printed layers, the fluorosurfactant zonyl was first thoroughly mixed at 2 wt% with Ecoflex. Previous reports conclude that zonyl improves the wettability of the ink onto silicone-based substrates and also reduces the effect of strain on resistance of the conductive traces.[20] Control experiment studying the effect of stretching of traces printed using Ecoflex-modified Ag/AgCl ink (without zonyl) revealed debonding of traces for strains greater than 50%, while traces obtained using ink containing zonyl could easily be stretched beyond 50% without appreciable damage. Hence zonyl-modified Ecoflex was used to prepare the Ecoflex-modified PEDOT:PSS and Ag/AgCl inks, as well as the underlying stretchable Ecoflex substrate. The modified PEDOT:PSS ink was used for fabricating the stretchable working and counter electrodes while the tailored-made Ag/AgCl ink was used for fabricating the underlying stretchable conductive traces and the reference electrode. A final Ecoflex layer was printed to define the electrode and contacts areas. As clearly evident from Figure 2.1.2 B, the device prepared using these modified inks can easily withstand linear stretching up to 100%.

The excellent resiliency against mechanical deformations of devices prepared using modified inks can be explained by delving at the microscopic level of the printed traces (Figure 2.1.2 B, Scheme). The stretch-enduring inks are a composite of Ecoflex, conductive ink and zonyl. When an external tensile load is applied to the stretchable device, the stress generated within the printed trace is absorbed mostly by the stretchable Ecoflex component.

Under tensile stress, the interpenetrating Ecoflex polymer stretches while maintaining the physical contact between the randomly oriented multi-layers of printed conductive particles, thus imparting considerable stretchability (Figure 2.1.2 B, b). Zonyl, on the other hand, modulates the surface property of the inks to enhance the bonding of the printed trace to the substrate surface and avoid delamination during application of stress. Unlike the device printed using pristine inks, the device fabricated using modified inks returns to its original form upon release of the external load (Figure 2.1.2 B,C). DMSO improves the packing density and crystal size of PEDOT and causes clustering with reduced PSS content at the surface. This rearrangement suppresses defect generation at the interface and results in higher device performance.[21] Hence the PEDOT:PSS electrodes were treated with DMSO to enhance their electrical conductivity. Optimization studies revealed that 1 min incubation in DMSO was sufficient to enhance the conductivity by almost two orders. Apart from improving the conductivity, the DMSO treatment also augmented the mechanical resiliency of the electrodes.

The remarkable stretchability and attractive performance of the new printable electrochemical devices have been examined using cyclic voltammetry (CV) to probe potential changes in the electrochemical reactivity as a function of applied stress. The electrochemical behavior of the stretchable device was thus evaluated under linear (Figure 2.1.3A), radial (Figure 2.1.3 B) and bending (Figure 2.1.3 C) stresses to emulate diverse deformations expected in real-life applications. The first study analyzed the electrochemical performance of the stretchable devices when subjected to 100% linear stretching (Figure 2.1.3 A). CV was recorded before and after 10 such fatigue cycles for a total of 50 iterations. Figure 2.1.3 D clearly illustrates that such repeated extreme deformations have minimal effect on the ferricyanide peak current or potential. For most practical applications, stretchable devices must perform even while under tensile load. To emulate such harsh condition, a 25% linear strain was continuously applied to the stretchable device and CV measurements were

performed at 15 min intervals for a total of 60 min. As depicted in Figure 2.1.3E, the device performs desirably with no perceivable electrochemical failure under such stress. These CV results underscore the resiliency of the devices to endure extreme linear tensile.

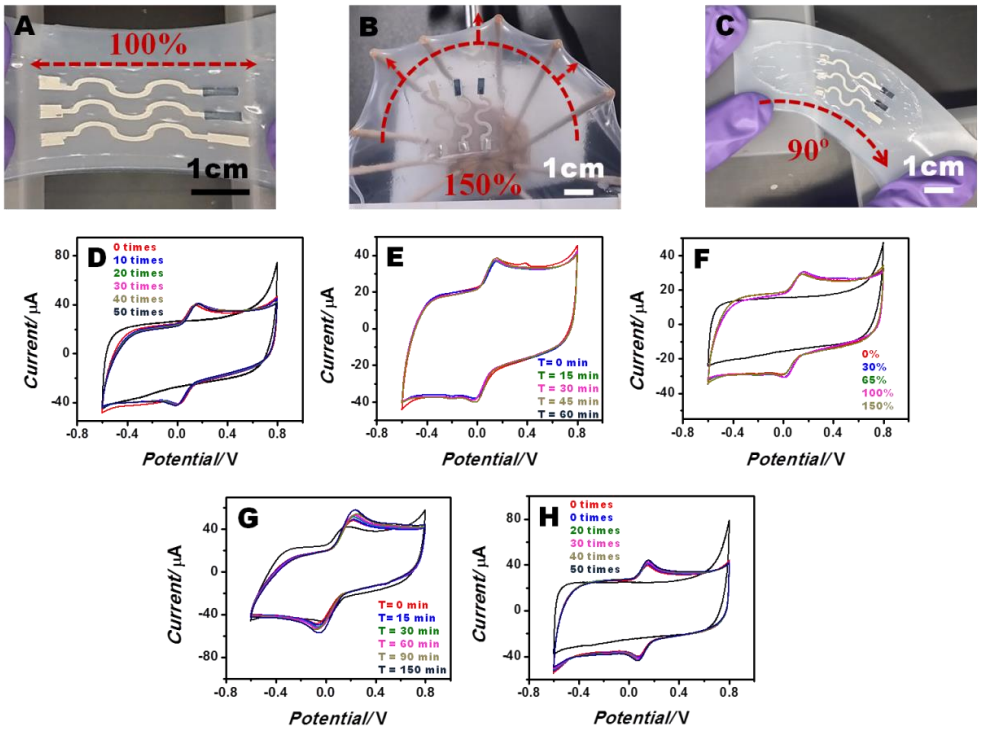


Figure 2.1.3. Images of the stretchable electrochemical sensor when (A) stretched linearly by 100%, (B) stretched radially by 150%, and (C) bent by 90^0. Cyclic voltammograms obtained by the stretchable electrochemical sensor (D) after every 10 cycles of 100% linear stretching for a total of 50 repetitions, (E) while under 25% linear stretching strain for a total of 60 min (CV recorded after every 15 min), (F) after every stepwise increment of radial stretching strain up to 150%, (G) while under 65% radial stretching strain for a total of 150 min (CV recorded after every 30 min), and (H) after every 10 cycles of 90^0 bending for a total of 50 repetitions. Medium, phosphate-buffer with 1mM ferricyanide redox probe (pH 7). (Reprinted with permission from ref. 15. Copyright 2015 Wiley.)

In real-life scenarios, the devices are expected to simultaneously experience tensile stress along multiple axes. To study the device under such conditions, it was subjected to increasing levels of radial deformation (Figure 2.1.3B). CV plots were recorded before and after application of increasing levels of radial strain up to 150% areal deformation (Figure 2.1.3F). Such multiple axes deformation of the device had minimal effect on its electrochemical behavior. Thereafter, the device was analyzed under continuous areal

deformation of 65% for a total of 150 min. It was noted that such a continuous stress had a small initial effect on the electrochemical properties (Figure 2.1.3G). The oxidation peak current varied with a R.S.D. of 10.18% for the entire study. Nonetheless, the effect is minimal while considering the extent of multiple axes stress experienced continuously by the device. Lateral bending by 90^0 was the another form of mechanical stress study performed on the device to study its compliance towards bending stress, commonly encountered in practical applications (Figure 2.1.3C). In this experiment, CVs were recorded after every 10 bending cycles for a total of 50 iterations. In agreement with the results of the above mentioned mechanical deformation studies, the device exhibits minimal deterioration of the electrochemical response (Figure 2.1.3H) as the oxidation peak current varied with a R.S.D. of 4.16% for the entire study. Overall, these studies indicate that the applied stress has a negligible effect on the electrochemical reactivity, irrespective of the type and extent of tensile stress applied. Such resiliency indicates no apparent change in the electrode morphology and the electrode-electrolyte interface, key characteristics of high-performance electrochemical devices.

The effect of linear stretching of the Ag/AgCl and PEDOT:PSS traces on their morphology and conductivity was also studied (Figure 2.1.4). SEM image of each ink trace taken before and after 100% stretching revealed no discernible cracks for the Ag/AgCl trace, while minor cracks were observed in case of the PEDOT:PSS trace. It was observed that the resistance for each ink trace followed a sigmoidal path under increasing levels of applied stress. Electrochemical impedance spectroscopy (EIS) is an attractive technique for monitoring electrode crack initiating and propagation.[22] Hence, EIS was utilized to closely examine the electrode surface and to study its variation under mechanical stress (Figure 2.1.5). The evolution of electrode cracking can be studied by monitoring the shift in the impedance phase as a function of frequency.[22] The phase shift versus frequency plots obtained for the

stretchable device revealed an increase in phase shift with increasing level of applied stress (Figure 2.1.5A, B). This implies that increasing level of external tensile force causes increase in crack size. The evolution of cracks under constant applied stress was also studied by subjecting the device to a constant strain of 25% over 60 min, while recording the EIS spectra every 15 min (Figure 2.1.5C). It was noted that the phase shifted in the first 15 min and then remained nearly stable thereafter (Figure 2.1.5D). This indicates that at a fixed level of strain, the cracks are generated and evolved within the first few minutes and then remain almost dormant as long as the strain level remains constant. It should be noted, however, that even though minor cracks may appear within the electrodes, they have negligible effect on the overall electrochemical behavior of the stretchable device, as indicated from the CV experiments.

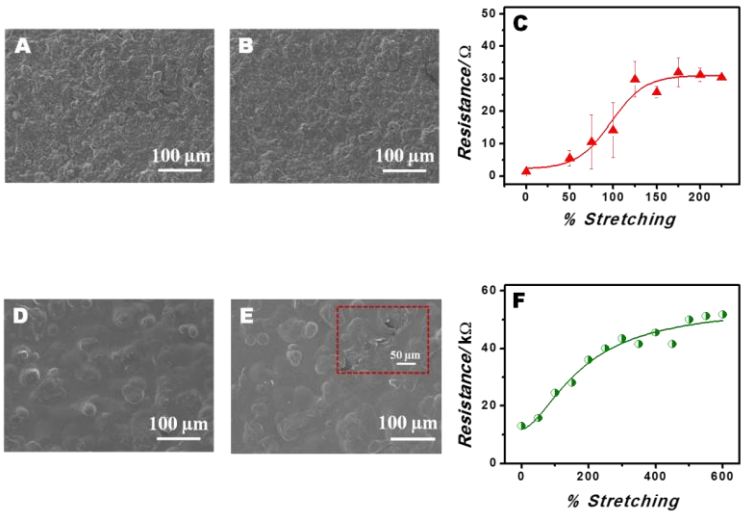


Figure 2.1.4. Scanning electron micrographs (A) before (B) after 100% linear stretching and (C) effect of stretching on the resistance of a printed stretchable Ag/AgCl trace. Scanning electron micrographs (A) before (B) after 100% linear stretching, and (C) effect of stretching on the resistance of a printed stretchable PEDOT:PSS trace. (Reprinted with permission from ref. 15. Copyright 2015 Wiley.)

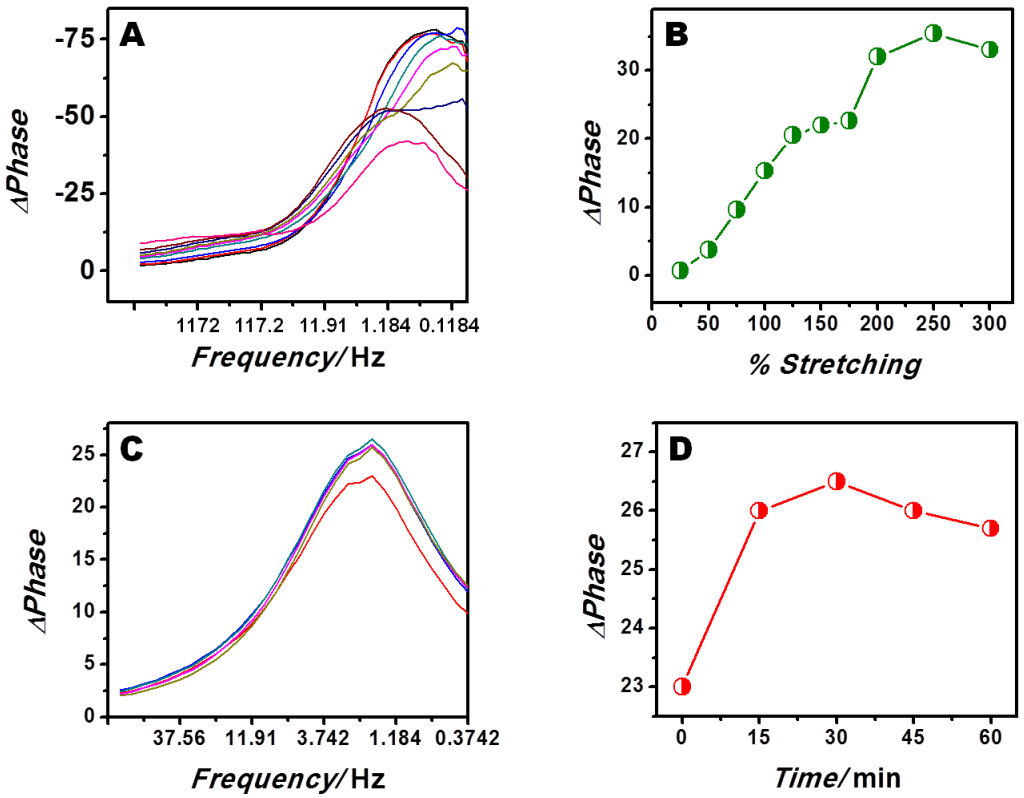


Figure 2.1.5. (A) Phase shift versus applied frequency data recorded for a stretchable sensor after successive increment of linear strain up to 200% (increment step = 25%) and (B) corresponding phase shift measured at 1Hz (obtained from A) with respect to an unstrained sensor as a function of applied linear stretching stress. (C) Phase shift versus applied frequency data recorded for a stretchable sensor under continuous linear strain of 25% for a total of 60 min (data recorded after every 15 min), and (D) corresponding phase shift measured at 1Hz (obtained from C) with respect to an unstrained sensor as a function of time. (Reprinted with permission from ref. 15. Copyright 2015 Wiley.)

2.1.4 Conclusions

In conclusion, we have demonstrated for the first time printable electrochemical devices that exhibit remarkable stretchability through the rationale synthesis of specially engineered screen printable inks. Stretchable low-cost devices were thus realized by transforming non-stretchable, pristine Ag/AgCl and PEDOT:PSS inks into stretch-enduring inks by judiciously tailoring them using Ecoflex and zonyl modifiers. By optimally formulating the inks, the printed device can withstand high tensile stress without incurring

major cracking or debonding. Mechanical deformation studies performed on the stretchable device reveal that linear stretching upto 100% and radial deformation upto 150% have negligible effect on its electrochemical properties. These results clearly highlight the conformal nature of the printed electrochemical device. Further improvements are expected by printing devices having hierarchical levels of stretchability that can endure even higher strain levels. The low-cost and scalability of the screen printing process is highly attractive in the field of stretchable devices which is presently dominated by expensive lithographic techniques. Similar ink modification procedures can be used for preparing other printable conducting inks (*e.g.*, based on carbon nanomaterials) to realize stretchable devices for specific electrochemical applications. Furthermore, functionalization of the stretchable electrodes with additional materials (*e.g.*, biomolecules, polymers) could lead to a wide range of inexpensive stretchable devices for variety of applications. This could be achieved by entrapping the biomolecules in stretchable biocompatible matrices, for example, hydrogels synthesized onto the stretchable electrodes. Apart from providing biocompatible environment to the biomolecules, such matrices will also absorb the extrenal mechanical stress and avoid any damage to the biomolecules. The method of synthesizing and tailoring inks for large-scale printing of stretchable devices holds great promise in the field of compliant electronics. The new highly stretchable electrochemical devices should enable new sensing, energy and display applications that require extreme tensile stress, and hold a considerable potential for next-generation wearable systems.

2.2 Devices possessing combined intrinsic and design-induced stretchability

2.2.1 Introduction

The past decade has witnessed an exponential increase in research activities related to soft, stretchable electronics.[23, 24] These devices readily yield to external stress and thus survive mechanical deformations with minimal effect on their performance. This remarkable behavior has led to a foray of stretchable electronics in diverse fields that were originally untouched by conventional rigid electronics, for example, wearable devices,[25, 26] robotics,[27, 28] or bionics,[29, 30] which demand electronics that can endure external strain. Diligent engineering of fabrication materials and of the device design is an indispensable requisite for achieving devices that are compliant towards extreme stress.[31] Keeping cognizance of this critical requirement, researchers have developed stretchable devices that rely on serpentine metallic structures,[32] nanomaterials,[33] conductive polymers,[34] or liquid metals.[35] Although such ingenious approaches have led to compliant soft electronics, they rely on expensive lithographic techniques[36] or small-scale spin/spray coating methods[37] that lead to high manufacturing costs. Alternatively, screen printing techniques offer low-cost and large-scale fabrication of reproducible printed devices.[38] The present work leverages screen printing process coupling specially engineered stretchable inks and a careful device design pattern to realize highly stretchable carbon nanotube (CNT)-based electrochemical devices that can withstand extreme strains up to 500% with minimal effect on their performance.

Printed electronics has acquired tremendous attention and its market size is expected to reach $300 billion over the next two decades.[20] Printed electrochemical devices, in particular, are an important section of printed electronics that plays a pivotal role in healthcare,[39] energy[40] and security[41] domains. However, majority of these printed electrochemical high-performance devices are mechanically fragile. In many of these

applications, the printed electrochemical devices experience harsh mechanical deformations that hamper full realization of their potential. In order to address this drawback, researchers have introduced printed electrochemical devices based on flexible paper,[42] plastic[43] or textiles.[44] Recently, we demonstrated a stretchable PEDOT:PSS-based printed electrochemical device.[45] However, PEDOT:PSS is expensive, finds limited use as an electrode material in electrochemical devices, and could withstand strain of up to 100%. In the present work, we leverage low-cost screen printing technology (Figure 2.2.1A) for large-scale fabrication of printable CNT-based electrochemical array devices that offer the highest stretchability reported to date by a printed device (Figure 2.2.1B).[46] An important novel aspect of the present work is the judicious preparation of a highly stretchable CNT-based ink and its combination with judiciously designed device pattern that provides the device with two degrees of stretchability to accommodate extreme strains of upto 500%.

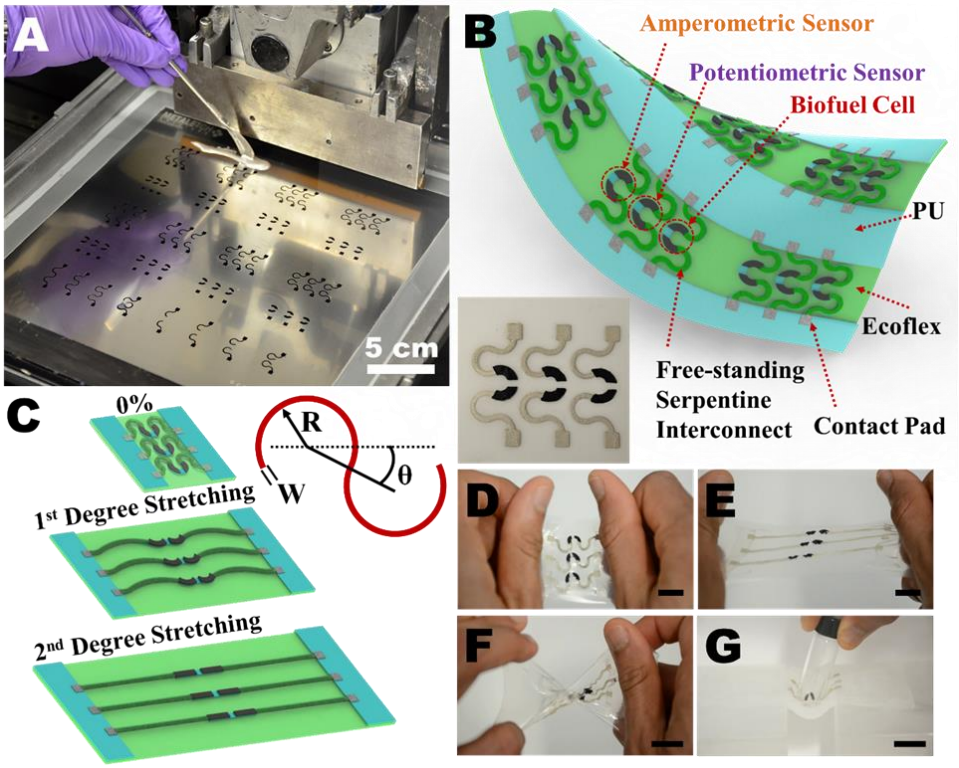


Figure 2.2.1: (A) Image of the stencil employed for printing the stress-enduring stretchable devices. Schematics showing (B) large-scale printed stretchable device arrays along with their various applications (Inset shows an image of a printed CNT-based array device) and (C) the two degrees of stretching – design-induced (1st Stretching) and intrinsic stretchability (2nd Stretching) – enabling the printed arrays to accommodate high levels of strains along with parameters defining the curvature of a free-standing serpentine interconnect (top right). Photographs of stretchable array under (D) 0% and (E) 175% linear (F) 180^0 torsional and (G) 5 mm indention strains. Scale bar for images D-G, 1cm. (Reprinted with permission from ref. 46. Copyright 2016 American Chemical Society.)

2.2.2 Experimental section

a. Chemicals and reagents:

Carboxylic acid functionalized multi-walled carbon nanotubes (CNTs) (purity >95%, diameter = 10-20 nm, length = 10-30 µm), polyurethane (PU) (Tecoflex SG-80A), Ecoflex® 00-30 (Smooth-On, Inc., PA), ferricyanide, mineral oil, tetrahydrofuran (THF), polyvinyl butyral (PVB), NaCl, methanol, nonactin (NAT), 2-nitrophenyl octyl ether (*o*-NPOE), potassium tetrakis(4-chlorophenyl)borate (KTClPB), chitosan, glucose oxidase (GOx) from

Aspergillus niger, Type X-S (EC 1.1.3.4), 1, 4-naphthoquinone (NQ), D (+)-glucose, bovine serum albumin (BSA), glutaraldehyde, potassium phosphate dibasic (K_2HPO_4), potassium phosphate monobasic (KH_2PO_4), and Nafion®, ethanol, and tetrathiafulvalene (TTF) were purchased from Sigma-Aldrich. All other chemicals were of analytical grade and were used without further purification. Ultra-pure deionized water was used in the preparation of the aqueous electrolyte solutions. Ecoflex® 00-30 was prepared in-house by mixing equal volumes of pre-polymer A with pre-polymer B provided by the supplier.

b. Synthesis of stretchable CNT and Ag/AgCl inks:

Stretchable CNT ink was prepared by mixing 100mg of CNTs with 70mg of mineral oil. This composition was dispersed in THF for 1 h in an ultrasonic bath and then homogenized in a shaker for 5h. Thereafter, 113mg of PU was added and the resulting mixture was shaken overnight. A solid-to-solvent ratio of 1mg: 9µL was maintained for printing purpose. The stretchable Ag/AgCl ink was prepared by thoroughly mixing 177.2mg Ag/AgCl ink (E2414, Ecron Inc., Wareham, MA) with 26.5mg Ecoflex.

c. Fabrication of stretchable electrochemical device array:

The fabrication process employed an MPM-SPM semi-automatic screen printer (Speedline Technologies, Franklin, MA). Sensor patterns were designed in AutoCAD (Autodesk, San Rafael, CA) and outsourced for fabrication on stainless steel through-hole 12” x 12” framed stencils of 125µm thickness (Metal Etch Services, San Marcos, CA). The printing process comprised of first screen printing a 75µm thick layer of Ecoflex on a supporting surface (Laser temporary transfer tattoo paper kits from HPS Papilio, Rhome, TX). While the Ecoflex layer was still uncured, it was carefully placed on a 26µm thick PU sheet (DelStar Technologies Inc., Middletown, DE) and allowed to bond with the PU layer while curing overnight at ambient room temperature. Precaution was taken to avoid entrapment of air bubbles while placing the Ecoflex layer onto the PU sheet. Thereafter, the protective paper

on top of the PU sheet was gradually peeled off to expose the PU layer. Subsequently, a sequence of stretchable Ag/AgCl, stretchable CNT and Ecoflex ink was printed to realize the complete electrochemical device array. The printed stretchable Ag/AgCl and CNT patterns were cured at 120^{o}C for 6min, and 85^{o}C for 10min in a convection oven, respectively. The final Ecoflex layer, used to define the electrode area and contact pads, was cured at room temperature for 1h. Subsequently, the free-standing serpentine interconnects were realized by excising the printed pattern, followed by placing it on an Ecoflex supporting base (75µm thick). The contact pads of the printed device array were firmly adhered to the underlying Ecoflex base by using freshly prepared liquid Ecoflex as a glue. The step involving excising the printed pattern was avoided in order to obtain traces with surface-bound interconnects. The device array was subsequently modified with specific reagents and biomolecules for achieving electrochemical sensors and biofuel cells.

d. Fabrication of stretchable ion-selective potentiometic ammonium sensor:

The ammonium-selective membrane cocktail was prepared by mixing 2wt% NAT, 35wt% *o*-NPOE, 1wt% KTClPB and 27wt% PU. The membrane solution was prepared by dissolving 100 mg of the above mixture in THF (1 mL). The cocktail was vigorously shaken for 1.5 h in an ultrasonic bath. The cocktail for making reference membrane was prepared by dissolving PVB (78.1 mg) and NaCl (50 mg) in methanol (1 mL). The cocktail was then vigorously shaken for 1h in an ultrasonic bath.

To fabricate the stretchable ammonium-ion sensor, 1.5µL of the reference membrane cocktail was drop-casted twice onto the Ag/AgCl reference electrode, and the ammonium sensitive electrode was modified by dropping 1.5µL of the ammonium-selective membrane cocktail three times onto CNT indicator electrode. The sensor was left to dry overnight before use.

e. Fabrication of stretchable amperometric glucose sensor:

The stretchable glucose sensor was fabricated by functionalizing the CNT-based stretchable electrode with TTF mediator and GOx enzyme. This was achieved by first preparing a solution of 1% Nafion and TTF (50mM) in ethanol and a separate solution of GOx (40mg/ml) with BSA (10mg/ml) in 0.1M phosphate buffer (pH 7). The TTF solution and the GOx solution were then subsequently mixed in 1:1 v/v ratio and drop-casted onto the CNT-based stretchable electrode. The electrode was left to dry for at least 2h. Finally, 1μL of 3wt% PVC in THF was casted onto the electrode and dried at ambient temperature for at least 2h before use.

f. Fabrication of stretchable glucose biofuel cell:

The bioanode was realized by modifying the stretchable CNT-based electrode with NQ mediator and GOx enzyme. 0.2 M NQ was first dispersed in ethanol and acetone (9:1 v/v) solution and sonicated for 1h. After sonication, 5 μL of NQ solution was drop casted onto the electrode at room temperature. The enzyme solution was prepared by mixing GOx (40 mg/mL) with BSA (10 mg/mL) in 0.2 M phosphate buffer. Subsequently, a 6 μL aliquot of the enzyme solution and 1 μL glutaraldehyde (1%) were casted on the electrode and dried under ambient conditions, and then covered with 2 μL of a 1 wt% chitosan solution. The cathode was obtained by electrodepositing platinum (Pt) on the other CNT-based stretchable electrode from a commercial platinum plating solution (Platinum RTP; Technic Inc, Anaheim, CA) for 600 s at -0.65 V (vs Ag/AgCl, 3M KCl). Finally, the cathode was covered with 1 μL Nafion® (5 %). Each electrode had a surface area around of 0.04 cm^2.

g. Resistance studies:

The resistance studies comprised of connecting the free-standing and surface-bound stretchable Ag/AgCl and CNT-based serpentine traces to a multimeter interfaced with a personal computer with a computer for real-time data acquisition. The in-situ variation of the resistance was recorded as the traces were subjected to increasing levels of applied stress.

h. Electrochemical studies:

Electrochemical characterization of the printed device was performed using a CH Instruments (Austin, TX) model 630C electrochemical analyzer. The preliminary studies focusing on the effect of applied strain on the device's electrochemical properties were performed using an electrolyte consisting of 10mM ferricyanide in 0.1M phosphate buffer (pH 7.0). Cyclic voltammograms (CV) were recorded over the -0.45V to 0.45V voltage range with a scan rate of 0.1V/s. The ammonium ion potentiometric sensor studies were performed using an electrolyte comprising varying concentrations of NH_4Cl in deionized water. Glucose sensor and biofuel cell experiments employed 0.1M phosphate buffer (pH 7.0) containing varying glucose concentrations. The glucose concentration was measured by the stretchable sensor by applying a constant voltage of +0.05V and measuring the current for 50s after a 1min incubation. The electrocatalytic activity of the anode and cathode of the biofuel cell were examined with a platinum-wire counter electrode, and an Ag/AgCl (3.0 M KCl) reference electrode. Polarization curves were recorded by applying linear sweep voltammetry with a scan rate of 1 mV/s in 0.2M phosphate buffer solution (pH 7.0).

i. Mechanical resiliency studies:

The preliminary study aimed at studying the effect of mechanical stress on the stretchable device array was analyzed by recording variation in the resistance of Ag/AgCl and CNT-based free-standing and surface-bound serpentine traces. A typical test involved measuring the resistance of an un-stretched trace. Thereafter a desired level of external stress was applied followed by release of the applied stress and measurement of the resistance.

The subsequent electrochemical approach to study the effect of applied stress on the electrochemical properties of the printed device was performed in a fashion similar to the resistance study. Cyclic voltammograms (CV) was first obtained for an unstretched device followed by stretching it to a desired strain and then gradually bringing it back to its

unstretched position. Subsequently, CV was recorded to identify any variation in the electrochemical properties of the device. In case of the study for repeated 300% stretching study, the device was stretched for a total of 150 times and the CV was measured after every 30 cycles. In order to study the effect of applied stress in real-time, the printed device was maintained at a strain of 300% and CV were recorded after every 10 min for a total of 60 min. Throughout the entire study, the device was strained to 300%. The effect of mechanical stress on the stretchable potentiometric ammonium ion sensor, amperometric glucose sensor and glucose biofuel cell was also studied in a manner similar to the preliminary electrochemical studies (discussed above).

2.2.3 Results and discussion

In the present work, we leverage low-cost screen printing technology (Figure 2.2.1A) for large-scale fabrication of printable CNT-based electrochemical array devices that offer the highest stretchability reported to date by a printed device (Figure 2.2.1B). An important novel aspect of the present work is the judicious preparation of a highly stretchable CNT-based ink and its combination with judiciously designed device pattern that provides the device with two degrees of stretchability to accommodate extreme strains of upto 500%. Specifically, the device comprises of free-standing serpentine interconnects printed using stretchable CNT and Ag/AgCl inks (Figure 2.2.1B). Detailed experiments were performed to optimize the ink composition and connecting angle of the interconnects to obtain a printed device with highest stretchability. When an external strain is applied to the device, the serpentine structure unwinds to accommodate the stress (Figure 2.2.1C). Upon further increment of the applied load, the intrinsic stretchability of the printed ink – imparted by combining CNT with elastomeric polyurethane (PU) binder – offers additional stretchability to the device. Unlike their metallic counterparts,[32] the printed free-standing serpentine structures have two levels of

stretchability – due to unwinding of free-standing serpentine structure (1st degree stretchability) and due to intrinsic stretchability of printable inks based on ink formulation (2nd degree stretchability). This enables the CNT-based printed device to display remarkable stretchability compared to an earlier study.[45] CNT was selected as the electrode material since carbon is the most widely used electrode material due to its low background current, wide potential window, and electrochemical inertness. Additionally, the functional groups present on the CNTs can be used to tether biomolecules or chemical moieties for specific sensing[47] and energy[48] applications without compromising their inherent stretchability. Furthermore, the exceptional mechanical and electrical properties of CNTs combined with the elastomeric properties of PU offer an attractive nanomaterial-based system for achieving stretchable electronic devices. To demonstrate the viability of the new platform to realize wide range of highly stretchable electrochemical sensors and biofuel cells, the CNT-based printed device array was employed for developing amperometric glucose sensor, an ion-selective ammonium ion potentiometric sensor, and enzymatic glucose biofuel cell. Coverage of these printable devices with different reagent layers does not compromise their resistance to extreme mechanical strains.

Intrinsic stretchability was achieved by utilizing specially synthesized intrinsically stretchable inks. As reported in our earlier work, commercial screen printable inks cannot be utilized to obtain stretchable devices due to the rigid nature of the patterns printed using these inks.[45] Hence, our efforts were directed towards preparing customized stretchable CNT and Ag/AgCl-based screen printable inks. Initially, varying amounts of CNTs were directly dispersed in Ecoflex® to obtain a stretchable CNT ink. However, a stretchable CNT ink with optimal printability, stretchability and electrochemical properties could not be achieved. Homogenous dispersion of conductive fillers within the binder is an essential requirement to obtain printable inks that demonstrate excellent printability and electrochemical response.[38]

Keeping this in view, PU was considered as the stretchable binder due to its ability to form hydrogen bonds with the carboxyl groups of the CNTs, thus leading to improved dispersion of CNTs within the PU binder.[49] However, preliminary efforts of direct mixing of varying amounts of CNTs in PU led to inks possessing poor mechanical resiliency, high resistivity or sub-optimal electrochemical properties. This could be attributed to the unstable dispersion of CNTs in THF which affects the final dispersion of CNTs upon adding PU to obtain stretchable CNT ink. In order to address this challenge, suitable dispersing agents such as ionic liquid (1-ethyl-3-methylimidazolium tetrafluoroborate) and mineral oil were considered. Ultimately, mineral oil was chosen since it is inexpensive and led to homogenous dispersion of CNT in THF. PU was then dispersed in the CNT-mineral oil suspension to obtain stretchable CNT ink that could be printed easily to fabricate conductive electrodes possessing excellent electrochemical and mechanical properties. Figure 2.2.2 shows SEM images of a stretchable CNT ink-based printed trace. The images indicate homogeneous distribution of CNTs within the PU and mineral oil matrix and the uniformity of the printed trace. The stretchable Ag/AgCl ink was prepared based on our earlier work.[45]

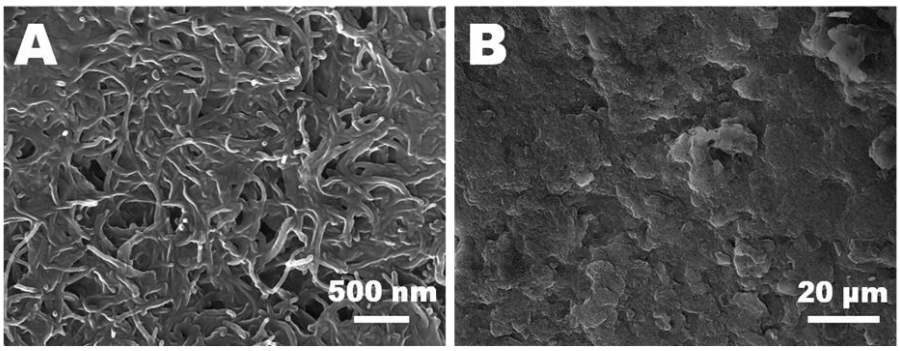


Figure 2.2.2: SEM images of printed stretchable CNT ink-based trace at different magnifications. (Reprinted with permission from ref. 46. Copyright 2016 American Chemical Society.)

In order to achieve the goal of highly stretchable devices, an approach that relies on the synergistic effect of combining intrinsically stretchable screen printable inks and distinct

design pattern that offers additional stretchability to the printed device was employed. The device-induced stretchability was achieved by designing interconnects between the active electrodes and contact pads in the form of free-standing serpentine structures with optimal connecting angle. Several groups have shown that serpentine interconnects offer high levels of stretchability.[50] As depicted in Figure 2.2.1C, when an external load is applied to the printed device array, the free-standing serpentine interconnects accommodate most of the stress by unwinding themselves (1^{st} degree stretching). This continues till the serpentine structures are almost straightened. Upon further increment of the applied strain, the intrinsic stretchability of the printed inks comes into play to offer further compliance to the applied stress (2^{nd} degree stretching). Thus, the synergistic effect of device design and stretchable inks provides the printed device array with high tolerance towards extreme levels of multi-dimensional complex strains. Images of the stretchable device array (Figure 2.2.1D) under various forms of mechanical deformations, including linear stretching, torsional twisting and indentation stress, are also shown in Figure 2.2.1E-G, respectively. The video and the images underscore the ability of the printed device array to endure extreme and complex multi-dimensional strains with minimal effect on its structural integrity.

Earlier reports on stretchable serpentine structures have revealed that parameters like inner radius (R), trace width (W) and connecting angle (θ) play an important role in dictating the extent of stretchability for the serpentine structures (Figure 2.2.1C, top right).[50] In order to obtain a compact device size, 'R' and 'W' were maintained at 2 mm and 1 mm, respectively, while 'θ' was varied between 0˚ to 45˚ to identify the best configuration that offers highest stretchability without compromising the structural integrity of the device. The extent of 1^{st} degree stretching (unwinding of serpentine trace till it straightens) could be increased from ~57% to ~233% by changing 'θ' between 0 and 45^0. Thus, geometrically, the stretchability of the device should increase with an increase in 'θ'. Single free-standing Ag/AgCl serpentine

traces of varying 'θ' were fabricated and changes in their resistance as a function of applied strain were recorded. As expected, serpentine structures with higher 'θ' values offer higher resiliency towards applied strain (Figure 2.2.3A). However, this was true only for 'θ' values from 0-30^0. The serpentine with θ = 45^0 displayed poorer compliance towards mechanical deformations as compared to that with θ = 30^0. This may be attributed to the fact that the serpentine structure with θ = 45^0 experiences complex out-of-plane bending and twisting while the external load is gradually removed. Out-of-plane bending and twisting of the serpentine structure leads to undesired strain at the microscopic level and thus causes an increase in resistance. Inferior resiliency of serpentine structures with θ = 45^0, compared to that with θ = 30^0 towards external load has also been reported earlier.[51]

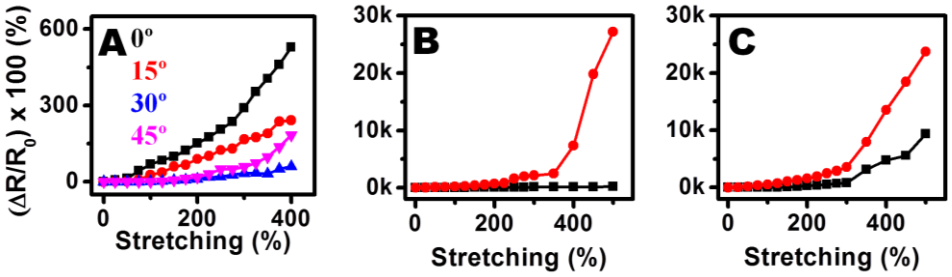


Figure 2.2.3: Comparison of the effect of applied strain on the resistance of printed (**A**) free-standing Ag/AgCl-based trace possessing different contacting angles (θ); (**B**) Ag/AgCl-based free-standing (black plot) and surface-bound (red plot) serpentine traces (θ = 30^0) and (**C**) CNT-based free-standing (black plot) and surface-bound (red plot) serpentine traces (θ = 30^0). (Reprinted with permission from ref. 46. Copyright 2016 American Chemical Society.)

We also carried out experiments comparing free-standing serpentine traces fabricated using stretchable Ag/AgCl (Figure 2.2.3B) and CNT (Figure 2.2.3C) inks with corresponding stretchable ink-based surface-bound serpentine traces and with free-standing traces fabricated using non-stretchable Ag/AgCl (without Ecoflex binder) and CNT (without PU binder) inks. Optical and electron microscopic analysis of the non-stretchable CNT-based trace clearly illustrate microscopic and macroscopic cracks throughout the trace immediately upon curing

(Figure 2.2.4) due to the absence of a binder to withhold the CNTs. Furthermore, SEM images reveal that the traces printed using non-stretchable CNT ink have a rough, non-uniform surface morphology (Figure 2.2.4C) as compared to the uniform printability offered by its stretchable counterpart (Figure 2.2.2B). The superior printability of the stretchable CNT ink, as compared to the non-stretchable ink, can be attributed to the presence of PU that acts as an efficient binder for uniform dispersion of the CNTs.

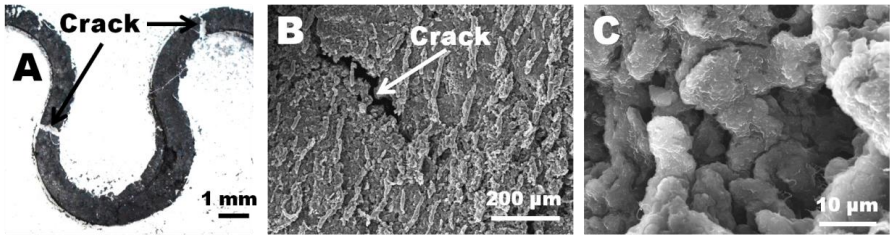


Figure 2.2.4: (A) Optical and (B, C) SEM images showing macroscopic and microscopic cracks and morphology of the printed trace fabricated using non-stretchable CNT ink. (Reprinted with permission from ref. 46. Copyright 2016 American Chemical Society.)

On the other hand, the non-stretchable Ag/AgCl-based free-standing trace could be stretched up to a strain of 200% due to the unwinding of the serpentine structure. However, application of additional stress led to immediate cracking of the trace due to the lack of intrinsic ink stretchability (Figure 2.2.5A) while no cracking was observed for the stretchable Ag/AgCl ink-based trace (Figure 2.2.5B). In the case of stretchable Ag/AgCl and CNT ink-based traces, stretched upto 500% strain, the resistance increased by ~800% and ~3500% for surface-bound Ag/AgCl and CNT-based devices, respectively, and by ~200% and ~ 300% for the free-standing Ag/AgCl and CNT-based free-standing traces. SEM studies analyzing the CNT-based free-standing trace before and after the 500% stretching reveal that initially the trace comprises of a crack-free homogenous morphology (Figure 2.2.6A). However, after application of 500% strain, microscopic cracks appear at some locations (Figure 2.2.6B).

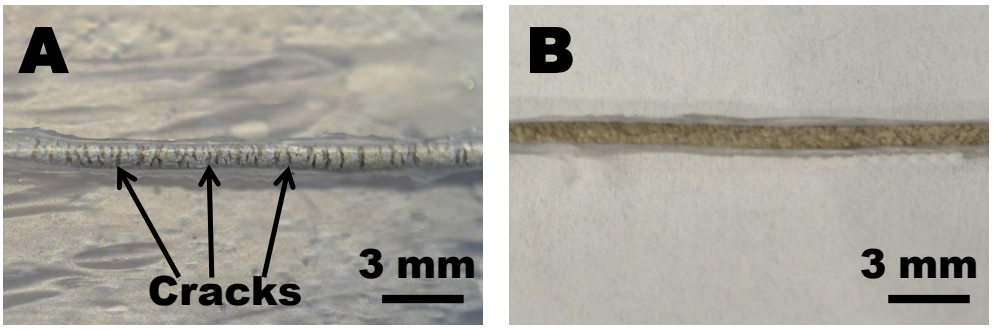


Figure 2.2.5: Images showing (A) non-stretchable and (B) stretchable Ag/AgCl ink-based trace under 200% strain. (Reprinted with permission from ref. 46. Copyright 2016 American Chemical Society.)

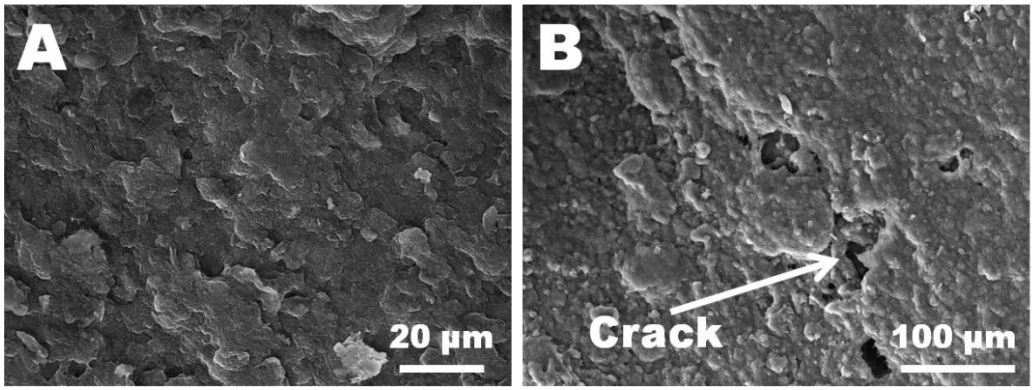


Figure 2.2.6: SEM image of stretchable CNT ink-based trace (A) before and (B) after being stretched by 500%. (Reprinted with permission from ref. 46. Copyright 2016 American Chemical Society.)

The microscopic cracks observed in the SEM images help explain the increased resistance of the printed traces upon undergoing mechanical deformations. It must be noted, however, that though the resistance increases, application of such extreme strains had a negligible impact on the electrochemical properties of the printed device. As clearly evidenced from Figures 2.2.3B and C, the traces possessing single degree of stretchability display inferior stretchable property as compared the corresponding ones that have two degrees of stretchability. These data support the significance of traces possessing two degrees of stretching over their counterparts having single degree stretching (intrinsic stretchability or

design stretchability), reflecting the former's ability to endure higher stretchability than that of the latter. Based upon these results, free-standing serpentine interconnects having $\theta = 30^0$ were selected to realize the stretchable electrochemical device array.

Cyclic voltammetry is widely used to study different electrode materials and analyze changes in the electrode-electrolyte interface. Hence, this technique was utilized to study the effect of applied strain on the electrochemical properties of the printed device array with ferricyanide as a redox probe. The first set of experiment comprised of studying the effect of increasing strain levels on cyclic voltammograms (CVs). The printed device was repeatedly stretched with increasing strains upto 500% (Figure 2.2.7A). The CV was first measured for an unstretched device (Figure 2.2.7B, black plot). It was later stretched to 100% of its length and then subsequently released to its initial position. This fatigue cycle was repeated 30 times and a CV was recorded. Similar fatigue cycles of increasing strains (upto 500%) were subsequently applied to the same device and the CV was measured at each step. The final CV recorded after 500% stretching is showing in Figure 2.2.7B (red plot). Stains >500% could not be applied since this pushed the underlying Ecoflex substrate (75 μm thickness) beyond its natural strain limits and led to its tearing. The device stretchability can be further improved by employing a thicker underlying substrate and by exploring other elastomers that offer stretchability greater than Ecoflex. As observed in Figure 2.2.7B, the redox peak separation (ΔE_p) as well as the peak heights of the ferricyanide probe remain nearly identical even when the device experiences such extreme levels of applied strains (R.S.D. for $\Delta E_p = 2.71\%$). These data indicate the minimal effect of severe mechanical deformations on the electrochemical properties of the printed device. The device can accommodate significantly higher levels of strains than the device reported in our previous work (maximum strain: 100%)[45] due to its synergistic effect of intrinsic and design-induced stretchability. Furthermore, unlike the PEDOT:PSS electrodes used earlier, the current device rely on commonly used CNTs. The

narrow peak separation and low background charging current, observed in the CVs of Figure 2.2.7, highlight the advantages of the CNT-based stretchable electrodes for electrochemical applications. Thereafter, the next study aimed at evaluating the effect of repeated stretching (300%) on the CVs obtained from the device. In this case, the device was stretched by 300% for total of 150 times and CVs were recorded after every 30 cycles. Figure 2.2.7C shows the initial (before stretching) and the final CV recorded at the end of the study The test again revealed that the device could easily withstand repeated stress cycles with negligible effect on its electrochemical properties (R.S.D. for ΔE_p = 2.30%).

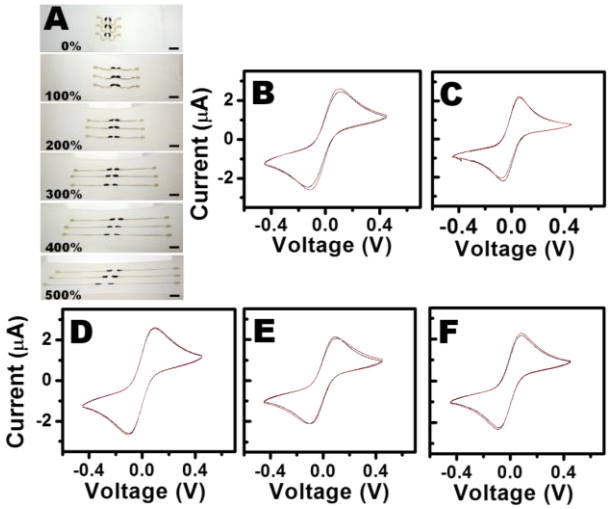


Figure 2.2.7: (A) Photographs of the printed stretchable array under increasing levels of applied strain (scale bar = 1cm). CVs recorded before (black plot) and after (red plot) applying (B) increasing levels of strain from 0 to 500% with increments of 100%, (C) repeated 300% stretching cycles for a total of 150 iterations, (D) a continuous strain of 300% for 60 min, and after applying (E) repeated indentations (5 mm) for a total of 50 repetitions and (F) repeated torsional twisting stress cycles for a total of 50 iterations. (B, C, E and F): The device was maintained at maximum strain for 2 s during each stress cycle. (Reprinted with permission from ref. 46. Copyright 2016 American Chemical Society.)

Numerous real-life applications of stretchable devices mandate flawless performance even when the devices are continuously strained for extended periods. To analyze the performance of the printed device under such conditions, it was continuously maintained at a strain of 300% and the CV was recorded every 10 min (initial and final CVs are shown in

Figure 2.2.7D). As evidenced from the figure, the CV shape remains almost similar over the entire test (R.S.D. for ΔE_p = 0.72%). Such real-time investigation of the device discloses its immaculate performance even when subjected to continuous stress of extreme levels. Again, it must be noted that the two levels of stretchability of the present device allow it to offer a superior performance under continuous strain as compared to our earlier reported device (that could be maintained at 25% strain for a similar study).[45] The device was also tested for its defiance against complex, multi-dimensional deformations, for example, repeated indentations of 5 mm depth (Figure 2.2.1G) and repeated torsional twisting (Figure 2.2.1F). The initial and final CVs obtained during these experiments are shown in Figure 2.2.7E and F. These plots reveal that such multi-dimensional deformations also have minimal effect on the device's electrochemical properties (R.S.D. for ΔE_p = 3.45% and 0.95% for Figures 2.2.7E and F, respectively).

Potentiometric ion-selective sensors and amperometric biosensors play a pivotal role in various healthcare[52] and environmental[53] applications. Several such applications mandate devices that can endure mechanical stress.[54] Hence, in such scenarios, the highly stretchable CNT-based device arrays can have immense use. Additionally, each CNT electrode of the array can be functionalized with specific receptor (e.g., ionophore or enzyme), thus offering multi-analyte detection. Considering such potential widespread applications, the CNT-based stretchable device was functionalized with an ammonium ion selective membrane as a proof-of-concept highlighting the utility of the new platform to realize highly stretchable potentiometric sensors (Figure 2.2.8A). The stretchable ammonium ion sensor displayed inconsequential effect of repeated 300% stretching on its potential response to varying ammonium concentrations (Figure 2.2.8B). During the entire mechanical resiliency study the sensor responded in a near-Nernstian fashion (67.5 mV/p[NH_4^+]) and its response fluctuated negligibly (RSD: 2.46 %), as observed in Figure 2.2.8C.

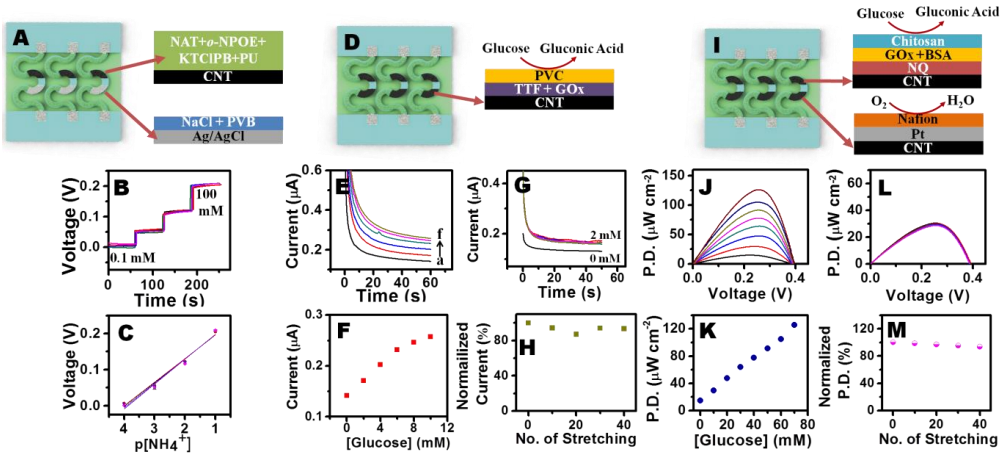


Figure 2.2.8: (A) Schematic of a stretchable ion-selective NH_4^+ sensor. (B) Voltage vs time data recorded for increasing NH_4^+ concentration (0.1 – 100 mM) and (C) Calibration plot recorded after application of 10 cycles of 300% strain for a total of 40 cycles. (D) Schematic of a stretchable amperometric glucose sensor. (E) Amperograms recorded for increasing glucose concentration (a –f: 0 – 10 mM). (F) Corresponding calibration plot. (G) Amperograms obtained for a glucose sensor after every 10 cycles of 300% stretching for a total of 40 iterations and (H) stability of the sensor response after each 300% stretching iterations. (I) Schematic of a stretchable glucose bio-fuel cell. (J) Power density vs voltage curves for the stretchable glucose bio-fuel cell and (K) maximum power density vs glucose concentration. (L) Power density vs voltage plots for a glucose bio-fuel cell after every 10 cycles of 300% stretching for a total of 40 iterations and (M) biofuel cell stability after each 300% stretching iterations. (B, G and L): The device was maintained at maximum strain for 2 s during each stress cycle. (Reprinted with permission from ref. 46. Copyright 2016 American Chemical Society.)

Similarly, the CNT-based device was functionalized with glucose oxidase (GOx) to demonstrate the ability of the stretchable platform in realizing highly stretchable amperometric biosensors. The glucose sensor was fabricated by functionalizing the CNT electrode with tetrathiafulvalene (TTF) as a mediator and GOx as the enzyme (Figure 2.2.8D). The resulting amperometric sensor displayed a linear response to increasing glucose levels (Figure 2.2.8E,F) along with negligible variance in its response when it was stretched repeatedly by 300% (Figure 2.2.8G,H, RSD: 4.98%).

Enzymatic biofuel cells, as energy harvesters and self-powered sensors, have garnered a tremendous recent attention for various invasive,[55] minimally invasive[56] and non-invasive,[57] applications. In such cases, the biofuel cells are intimately in contact with soft tissues that may undergo extreme mechanical deformations. The CNT-based stretchable device was thus modified to obtain a glucose biofuel cell. Specifically, the bioanode was functionalized with 1,4-naphthoquinone (NQ) as a mediator and GOx as the enzyme while the cathode comprised of electrodeposited platinum (Figure 2.2.8I). Figure 2.2.8J,K shows the power density (P.D.) curves obtained for increasing levels of glucose while Figure 2.2.8L,M shows the high stability of the power generated upon stretching the device repeatedly by 300% (RSD: 2.57%). The linear increase of the highest P.D. obtained from the stretchable biofuel cell with increasing glucose concentration (Figure 2.2.8K) reveals that the biofuel cell also behaves as a self-powered glucose sensor. Such self-powered sensors are quite attractive for decentralized applications where powering sensors is a challenge.

The results obtained from the potentiometric ammonium ion sensor, amperometric glucose sensor and enzymatic glucose biofuel cell and self-powered glucose sensor, underpins a compelling evidence of the ability of the stretchable CNT-based device array to be easily functionalized with a host of receptors and reagents to realize a wide range of highly stretchable electrochemical sensors and biofuel cells for diverse applications which demand intimate contact with surroundings and where extreme mechanical deformations are common. Furthermore, the results highlight that the device's mechanical resiliency remains uncompromised even after coating it with layers containing delicate chemical and biochemical reagents. The array system can thus be utilized to realize highly stretchable multi-analyte sensors, multi-fuel biofuel cells, or a combination of sensors and biofuel cells.

2.2.4 Conclusions

In conclusion, the present work demonstrates the first example of a highly stretchable all-printed CNT-based electrochemical sensors and biofuel cells that can withstand strains as high as 500% with negligible effect on their structural integrity and electrochemical performance. The device thus offers the highest stretchability among all the reported screen printed devices. The printed device can endure such extreme stress due to the synergistic effects of its design pattern and use of specially engineered stretchable inks that offer stretchability at two levels – unwinding of the free-standing serpentine interconnects and intrinsic stretchability of custom-designed inks which rely on the exceptional mechanical and electrical properties of CNTs and elastomeric properties of PU binder. The device has been characterized using resistance and various electroanalytical techniques for studying its mechanical deformation resiliency. Preliminary resistance studies reveal the pivotal role played by free-standing serpentine interconnects and control of their connecting angle in realizing the high stretchability. Subsequent CV studies indicate that the device shows negligible variation in its electrochemical response even when repeatedly stretched (up to 500%), twisted and indented. The device also performed flawlessly when continuously stretched by 300% for 1h. As compared to previous work on PEDOT:PSS based printed stretchable device,[29] the present device relies on commonly used CNT electrodes and demonstrates superior stretchability. Ultimately, the CNT-based device was functionalized with reagent layers containing ionophores or enzymes to realize highly stretchable ammonium ion-selective potentiometric sensor, amperometric glucose biosensor and enzymatic glucose biofuel cell and self-powered biosensor. The sensors and biofuel cells displayed remarkable endurance towards repeated strains of 300%, indicating minimal effect of applied stress on the electrode material and also on delicate enzymes and other reagents immobilized onto the

electrodes. Furthermore, CNT-based electrodes represent a common platform that allows wide range of strategies to immobilize receptors and other reagents into highly bio-compatible three dimensional micro-environments to realize sensors and biofuel cells with improved characteristics.[50,51] The array system thus offers the opportunity to fabricate multi-analyte sensors, multi-fuel biofuel cells and a combination of sensors and biofuel cells, thus providing a multi-functional platform for sensing and energy harvesting. Future work will focus on further characterizing the inks' rheological properties, studying the tensile properties of the printed traces and the performance of the device while undergoing dynamic repeated large strain, and on improving further the stretchability (beyond 500%) by employing thicker substrates and exploring other highly stretchable elastomers. The present work therefore has the promise to lay the foundation for scalable, low-cost fabrication of fully-printed highly stretchable and high-performance electrochemical devices for diverse applications in healthcare, defense, consumer electronics and energy domains.

This chapter is based, in part, on the material as it appears in Advanced Materials, 2015, by Amay J. Bandodkar, Rogelio Nuñez-Flores, Wenzhao Jia, and Joseph Wang; in part on the material as it appears in Nano Letters, 2016, by Amay J. Bandodkar, Itthipon Jeerapan, Jung-Min You, Rogelio Nuñez-Flores, and Joseph Wang. The dissertation author was the primary investigator and corresponding author of these papers.

2.3 References

1. Cotton, D. P. J.; Graz, I. M.; Lacour, S. P. *IEEE Sens. J.* **2009,** *9*, 2008.

2. Kim, J.; Banks, A.; Cheng, H.; Xie, Z.; Xu, S.; Jang, K.-I.; Lee, J. W.; Liu, Z.; Gutruf, P.; Huang, X.; Wei, P.; Liu, F.; Li, K.; Dalal, M.; Ghaffari, R.; Feng, X.; Huang, Y.; Gupta, S.; Paik, U.; Rogers, J. A. *Small* **2015,** *11*, 906.

3. Yang, Z.; Deng, J.; Sun, X.; Li, H.; Peng, H. *Adv. Mater.* **2014,** *26*, 2643.

4. Yan, C.; Wang, X.; Cui, M.; Wang, J.; Kang, W.; Foo, C. Y.; Lee, P. S. *Adv. Energy Mater.* **2014,** *4*, 1301396.

5. Ghisleri, C.; Siano, M.; Ravagnan, L.; Potenza, M. A. C.; Milani, P. *Laser Photon. Rev.* **2013,** *7*, 1020.

6. Lipomi, D. J.; Tee, B. C. K.; Vosgueritchian, M.; Bao, Z. *Adv. Mater.* **2011,** *23*, 1771.

7. Yamada, T.; Hayamizu, Y.; Yamamoto, Y.; Yomogida, Y.; Izadi-Najafabadi, A.; Futaba, D. N.; Hata, K. *Nat. Nano.* **2011,** *6*, 296.

8. Kim, D.-H.; Lu, N.; Ma, R.; Kim, Y.-S.; Kim, R.-H.; Wang, S.; Wu, J.; Won, S. M.; Tao, H.; Islam, A.; Yu, K. J.; Kim, T.-i.; Chowdhury, R.; Ying, M.; Xu, L.; Li, M.; Chung, H.-J.; Keum, H.; McCormick, M.; Liu, P.; Zhang, Y.-W.; Omenetto, F. G.; Huang, Y.; Coleman, T.; Rogers, J. A. *Science* **2011,** *333*, 838.

9. Yoon, J.; Hong, S. Y.; Lim, Y.; Lee, S.-J.; Zi, G.; Ha, J. S. *Adv. Mater.* **2014,** *26*, 6580.

10. Windmiller, J. R.; Wang, J. *Electroanalysis* **2013,** *25*, 29.

11. Li, M.; Li, Y.-T.; Li, D.-W.; Long, Y.-T. *Anal. Chim. Acta* **2012,** *734*, 31.

12. Bandodkar, A. J.; O'Mahony, A. M.; Ramirez, J.; Samek, I. A.; Anderson, S. M.; Windmiller, J. R.; Wang, J. *Analyst* **2013,** *138*, 5288.

13. Bandodkar, A. J.; Jia, W.; Wang, J. *Electroanalysis* **2015,** *27*, 562.

14. Cai, J.; Cizek, K.; Long, B.; McAferty, K.; Campbell, C. G.; Allee, D. R.; Vogt, B. D.; La Belle, J.; Wang, J. *Sens. Actuators, B* **2009,** *137*, 379.

15. Bandodkar, A. J.; Nuñez-Flores, R.; Jia, W.; Wang, J. *Adv. Mater.* **2015,** *27*, 3060.

16. Metters, J. P.; Kadara, R. O.; Banks, C. E. *Analyst* **2011,** *136*, 1067.

17. Liao, C.; Mak, C.; Zhang, M.; Chan, H. L. W.; Yan, F. *Adv. Mater.* **2015,** *27*, 676.

18. VanDersarl, J. J.; Mercanzini, A.; Renaud, P. *Adv. Funct. Mater.* **2015,** *25*, 78.

19. Gonzalez, M.; Axisa, F.; Bulcke, M. V.; Brosteaux, D.; Vandevelde, B.; Vanfleteren, J. *Microelectron. Reliab.* **2008,** *48*, 825.

20. Lipomi, D. J.; Lee, J. A.; Vosgueritchian, M.; Tee, B. C. K.; Bolander, J. A.; Bao, Z. *Chem. Mater.* **2012,** *24*, 373.

21. Thomas, J. P.; Zhao, L.; McGillivray, D.; Leung, K. T. *J. Mater. Chem. A* **2014,** *2*, 2383.

22. Bosch, R.-W. *Corros. Sci.* **2005,** *47*, 125.

23. Kim, D. H.; Ghaffari, R.; Lu, N. S.; Rogers, J. A. *Annu. Rev. Biomed. Eng.* **2012,** *14*, 113.

24. Lipomi, D. J.; Bao, Z. A. *Energy Environ. Sci.* **2011,** *4*, 3314.

25. Ramuz, M.; Tee, B. C. K.; Tok, J. B. H.; Bao, Z. N. *Adv. Mater.* **2012,** *24*, 3223.

26. Cotton, D. P. J.; Graz, I. M.; Lacour, S. P. *IEEE Sens. J.* **2009,** *9*, 2008.

27. Lu, N.; Kim, D. H. *Soft Robotics. March* **2014,** *1*, 53.

28. Majidi, C. *Soft Robotics. March* **2014,** *1*, 5.

29. Someya, T. *IEEE Spectrum* **2013,** *50*, 50.

30. Kim, J.; Lee, M.; Shim, H. J.; Ghaffari, R.; Cho, H. R.; Son, D.; Jung, Y. H.; Soh, M.; Choi, C.; Jung, S.; Chu, K.; Jeon, D.; Lee, S. T.; Kim, J. H.; Choi, S. H.; Hyeon, T.; Kim, D. H. *Nat. Commun.* **2014,** *5*, 5747.

31. Rogers, J. A.; Someya, T.; Huang, Y. G. *Science* **2010,** *327*, 1603.

32. Xu, S.; Zhang, Y. H.; Cho, J.; Lee, J.; Huang, X.; Jia, L.; Fan, J. A.; Su, Y. W.; Su, J.; Zhang, H. G.; Cheng, H. Y.; Lu, B. W.; Yu, C. J.; Chuang, C.; Kim, T. I.; Song, T.; Shigeta, K.; Kang, S.; Dagdeviren, C.; Petrov, I.; Braun, P. V.; Huang, Y. G.; Paik, U.; Rogers, J. A. *Nat. Commun.* **2013,** *4*, 1543.

33. Takahashi, T.; Takei, K.; Gillies, A. G.; Fearing, R. S.; Javey, A. *Nano Lett.* **2011,** *11*, 5408.

34. Savagatrup, S.; Printz, A. D.; Rodriquez, D.; Lipomi, D. J. *Macromolecules* **2014,** *47*, 1981.

35. Kubo, M.; Li, X. F.; Kim, C.; Hashimoto, M.; Wiley, B. J.; Ham, D.; Whitesides, G. M. *Adv. Mater.* **2010,** *22*, 2749.

36. Kim, D. H.; Lu, N. S.; Ma, R.; Kim, Y. S.; Kim, R. H.; Wang, S. D.; Wu, J.; Won, S. M.; Tao, H.; Islam, A.; Yu, K. J.; Kim, T. I.; Chowdhury, R.; Ying, M.; Xu, L. Z.; Li, M.; Chung, H. J.; Keum, H.; McCormick, M.; Liu, P.; Zhang, Y. W.; Omenetto, F. G.; Huang, Y. G.; Coleman, T.; Rogers, J. A. *Science* **2011,** *333*, 838.

37. Akter, T.; Kim, W. S. *ACS Appl. Mater. Interfaces* **2012,** *4*, 1855.

38. Metters, J. P.; Kadara, R. O.; Banks, C. E. *Analyst* **2011,** *136*, 1067.

39. Carrilho, E.; Martinez, A. W.; Whitesides, G. M. *Anal. Chem.* **2009,** *81*, 7091.

40. Chen, P. C.; Chen, H. T.; Qiu, J.; Zhou, C. W. *Nano Res.* **2010,** *3*, 594.

41. Bandodkar, A. J.; O'Mahony, A. M.; Ramirez, J.; Samek, I. A.; Anderson, S. M.; Windmiller, J. R.; Wang, J. *Analyst* **2013,** *138*, 5288.

42. Cunningham, J. C.; Brenes, N. J.; Crooks, R. M. *Anal. Chem.* **2014,** *86*, 6166.

43. Kim, J.; Valdes-Ramirez, G.; Bandodkar, A. J.; Jia, W. Z.; Martinez, A. G.; Ramirez, J.; Mercier, P.; Wang, J. *Analyst* **2014,** *139*, 1632.

44. Schazmann, B.; Morris, D.; Slater, C.; Beirne, S.; Fay, C.; Reuveny, R.; Moyna, N.; Diamond, D. *Anal. Methods* **2010,** *2*, 342.

45. Bandodkar, A. J.; Nunez-Flores, R.; Jia, W. Z.; Wang, n. *Adv. Mater.* **2015,** *27*, 3060.

46. Bandodkar, A. J.; Jeerapan, I.; You, J.-M.; Nuñez-Flores, R.; Wang, J. *Nano Lett.* **2016,** *16*, 721.

47. Merkoci, A.; Pumera, M.; Llopis, X.; Perez, B.; del Valle, M.; Alegret, S. *TrAC, Trends Anal. Chem.* **2005,** *24*, 826.

48. Zhou, M.; Deng, L.; Wen, D.; Shang, L.; Jin, L. H.; Dong, S. J. *Biosens. Bioelectron.* **2009,** *24*, 2904.

49. Sahoo, N. G.; Jung, Y. C.; Yoo, H. J.; Cho, J. W. *Macromol. Chem. Phys.* **2006,** *207*, 1773.

50. Gonzalez, M.; Axisa, F.; Bulcke, M. V.; Brosteaux, D.; Vandevelde, B.; Vanfleteren, n. *Microelectron. Reliab.* **2008,** *48*, 825.

51. Carta, R.; Jourand, P.; Hermans, B.; Thoné, J.; Brosteaux, D.; Vervust, T.; Bossuyt, F.; Axisa, F.; Vanfleteren, J.; Puers, R. *Sens. Actuators, A* **2009,** *156*, 79.

52. Miller, P. R.; Xiao, X. Y.; Brener, I.; Burckel, D. B.; Narayan, R.; Polsky, R. *Adv. Healthc. Mater.* **2014,** *3*, 876.

53. Hart, J. P.; Wring, S. A. *TrAC, Trends Anal. Chem.* **1997,** *16*, 89.

54. Bandodkar, A. J.; Molinnus, D.; Mirza, O.; Guinovart, T.; Windmiller, J. R.; Valdes-Ramirez, G.; Andrade, F. J.; Schoning, M. J.; Wang, J. *Biosens. Bioelectron.* **2014,** *54*, 603.

55. Halamkova, L.; Halamek, J.; Bocharova, V.; Szczupak, A.; Alfonta, L.; Katz, E. *J. Am. Chem. Soc.* **2012,** *134*, 5040.

56. Valdes-Ramirez, G.; Li, Y. C.; Kim, J.; Jia, W. Z.; Bandodkar, A. J.; Nunez-Flores, R.; Miller, P. R.; Wu, S. Y.; Narayan, R.; Windmiller, J. R.; Polsky, R.; Wang, J. *Electrochem. Commun.* **2014,** *47*, 58.

57. Jia, W.; Valdés-Ramírez, G.; Bandodkar, A. J.; Windmiller, J. R.; Wang, J. *Angew. Chem., Int. Ed.* **2013,** *52*, 7233.

Chapter 3 All-Printed Self-healing Electrochemical Devices

3.1 Microcapsules-based devices

3.1.1 Introduction

Device failure incurred due to mechanical fatigue and excessive strain is a major cause of concern in the field of electronics as this shortens a device's lifespan and increases maintenance costs.[1, 2] Additionally, in some scenarios, replacing dysfunctional devices may become complicated[3, 4] and can have high environmental price tag.[5] Biological systems overcome this challenge of mechanical damage by utilizing unique self-healing processes that enable them to augment their lifespan.[6, 7] Taking cues from Nature, several groups have developed biomimetic materials that autonomously repair themselves when mechanically damaged.[8] Such self-healing materials rely on either capsule, vascular or intrinsic methods, and have been developed for applications in construction,[9, 10] corrosion,[11, 12] prosthetics,[13, 14] tissue engineering[15] and electronics.[16-18]

Printed electronics has garnered tremendous attention and its market size is expected to reach $300 billion over the next two decades.[19] Mechanical damage induced device failure represents a major challenge hampering the progress of this growing field due to the fragile nature of the printed devices. Yet, little attention has been given to the preparation of self-healing inks for realizing smart printed electronics that will self-repair when damaged.[16-18] The reported conductive self-healing materials either require heat to initiate the healing process,[16] or rely on healing agent-filled capsules loaded in a separate non-conductive, elastomeric coating overlaying the conductive printed circuit.[18, 20] In the former case, additional apparatus is mandated to initiate the healing process and thus such materials are less attractive when

autonomous self-healing is required. In the latter case, the capsules may fail to release the healing agent (in response to mechanically-induced cracks in the printed conductive trace) due to mismatch between the elastic properties of the rigid conductive circuit and the overlaying self-healing agent-loaded coating.

Over the past two decades printed electrochemical devices have acquired remarkable importance in healthcare,[21] energy[22, 23] and security[24, 25] domains. In several practical situations, electrochemical devices, such as wearables[26, 27] or batteries,[28, 29] face mechanical deformations that could potentially reduce their lifespan. In order to address this issue, researchers have fabricated devices on plastic,[30, 31] paper,[32, 33] and textile[34, 35] substrates that can be easily bent and even stretched.[36] However, any strain beyond the limits of these devices' resiliency leads to permanent failure. Therefore, it is critical to develop self-healing conductive inks for fabricating intelligent all-printed electrochemical devices that autonomously restore the lost electrical conductivity caused by mechanical damage, degradation and failure.

In the present work we report, for the first time, the synthesis of printable inks containing self-healing microcapsules for fabricating self-repairable inexpensive electrochemical devices.[37] Unlike previous work,[18] the new tailor-made conductive inks contain the self-healing capsules and do not require a separate coating of the microcapsules over the printed structure. By judiciously identifying the binder and thinner we were able to synthesize conductive inks that could be easily loaded with the healing capsules while enabling convenient printing (Figure 3.1.1A). When the printed device is damaged, the capsules release the hexyl-acetate healing solvent to restore the mechanical and electrical contacts. Since the capsules are loaded directly in the inks, the entire footprint of the printed electrochemical devices has the ability to self-heal upon mechanical damage. By leveraging printing technology and the self-healing inks, we demonstrate smart electrochemical devices

that rapidly self-repair mechanical damage at ambient temperature, and restore electrochemical performance.

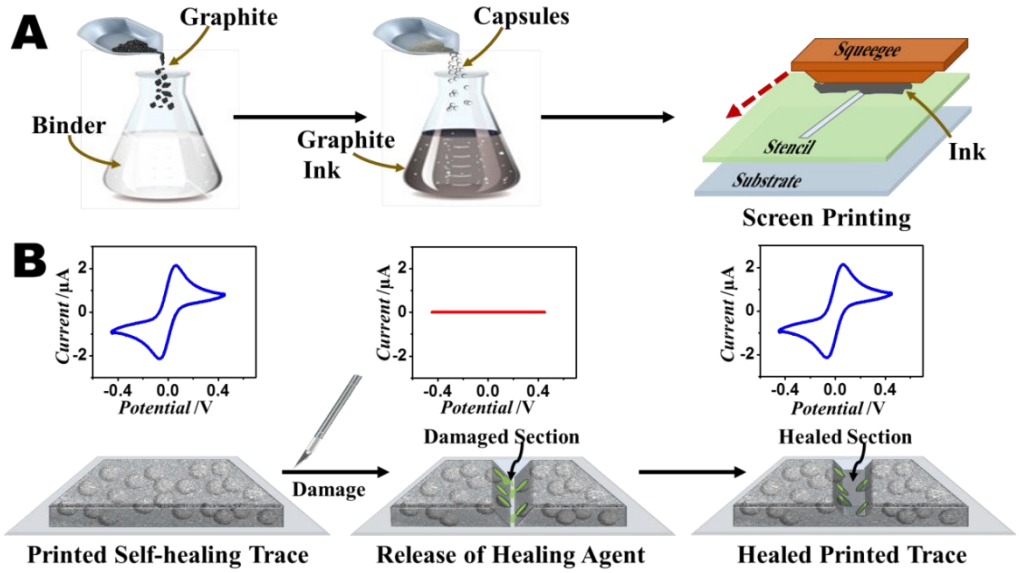


Figure 3.1.1: Printed electrochemical devices with a built-in healing function. Schematic showing the (A) preparation of the self-healing carbon ink and screen printing procedure and (B) self-repairable process occurring when a self-healing printed electrode is mechanically damaged, along with a typical voltammetric response at the various stages. (Reprinted with permission from ref. 37. Wiley.)

3.1.2 Experimental section

a. Chemicals and reagents:

Potassium ferricyanide, hexyl acetate, urea, formalin, resorcinol, Selectophore™ grade sodium ionophore X, bis(2-ethylhexyl) sebacate (DOS), sodium tetrakis[3,5-bis(trifluoromethyl)phenyl] borate (Na-TFPB), polyvinyl chloride (PVC), tetrahydrofuran (THF), and sodium chloride (NaCl) were purchased from Sigma Aldrich (St. Louis, MO). Graphite powder (synthetic microcrystals grade APS, 2–15 µm, 99.999%) was obtained from Alfa Aesar (Ward Hill, MA). Acrylic varnish binder (5008, Gloss medium varnish) and thinner (5620, Flow-Aid) were purchased from Liquitex (Piscataway, NJ). Polyurethane pre-polymer (Desmodur L75) was generously provided by Bayer MaterialScience LLC

(Pittsburgh, PA). Ethylene co-maleic anhydride (Zemac-400) was generously provided by Vertellus Health & Specialty Products LLC (Zeeland, MI).

b. Capsule synthesis:

Briefly, 6.66 mL of distilled water was placed in a 20 mL beaker, along with 1.66 mL of 2.5 wt% ethylene co-maleic anhydride as a surfactant. Thereafter, urea (166.6 mg), ammonium chloride (16.6 mg), and resorcinol (16.6 mg) were added and thoroughly mixed to obtain the wall-forming solution. The pH was then adjusted to 3.5 by using 20wt% NaOH solution. Separately, Desmodur L75 (266.6 mg) was dissolved in hexyl acetate (4 mL) and then added drop-wise to the wall-forming solution which was constantly stirred (500 rpm) in a water bath maintained at ambient temperature. After 10 min of stirring, formalin solution (422 mg) was added, and the temperature was increased to 55 ºC. The reaction was allowed to be carried out for the next 4 h at this temperature under continuous stirring. Thereafter, the beaker was cooled to room temperature and the capsules were filtered and allowed to dry at room temperature for at least 24 h before use.

c. Ink synthesis:

A typical synthesis of carbon self-healing ink comprised of first thoroughly mixing graphite (572.7 mg) in acrylic varnish binder (700mg), followed by adding the thinner (200 µl). Immediately, capsules (67 mg) were mixed in the resulting carbon ink with gentle strokes for one minute till capsules were well dispersed. Care was taken to avoid any damage to the capsules while mixing them into the ink. The normal carbon ink was prepared similar to the self-healing carbon ink but without the capsules. The self-healing Ag/AgCl ink was prepared by directly mixing 10wt% capsules in the commercial Ag/AgCl ink (E2414, Ecron Inc., Wareham, MA).

d. Fabrication of self-healing electrochemical devices:

The fabrication process comprised of screen printing of the self-healing conductive inks using an MPM-SPM semi-automatic screen printer (Speedline Technologies, Franklin, MA) on a flexible polyethylene terephthalate (PET) substrate. Device patterns were designed in AutoCAD (Autodesk, San Rafael, CA) and outsourced for fabrication on stainless steel through-hole 12" x 12" framed stencils (Metal Etch Services, San Marcos, CA). A typical fabrication process consisted of first thoroughly cleaning the PET substrate with acetone for removing contaminants. Thereafter, the self-healing Ag/AgCl and carbon inks were screen printed on the PET substrate. The inks were cured at 65^0C for 10 min in a convection oven. The complete self-healing electrochemical devices were fabricated by printing the working and counter electrodes using the self-healing carbon ink, while the self-healing Ag/AgCl ink was used to realize the reference electrode, underlying connectors and contact pads of the working and counter electrodes. The device pattern was similar to our earlier work. The self-healing ion-selective potentiometric sodium sensor was fabricated by drop-casting 3 µl of the sodium ionophore cocktail on a 3 x 1mm area carbon electrode. The sodium selective membrane cocktail composition consisted of 1 mg sodium ionophore X, 0.55 mg Na-TFPB, 33 mg PVC, and 65.45 mg DOS dissolved in 660mL of nitrogen-purged THF. The cocktail was thoroughly mixed to dissolve all the components. The reference cocktail was prepared by dissolving 78.1 mg PVB and 50 mg NaCl in 1 mL methanol.

e. Electrical conductivity and optical studies:

The electrical conductivity measurements were performed using a digital multimeter (Radioshack) interfaced with a computer for real-time data acquisition. Optical images and videos were captured using an optical microscope (Motic SMZ-168 Series) coupled with a digital camera (Nikon, D7000). Electrical and optical studies were carried out for electrodes printed using self-healing carbon and Ag/AgCl inks and normal carbon and Ag/AgCl inks

(without microcapsules). All mechanical damages of the device were achieved by slicing the printed electrodes by an incision blade to completely sever the electrical connection.

f. Electrochemical studies:

Cyclic voltammetric (CV) studies were performed using a CH Instruments (Austin, TX) model 630C electrochemical analyzer. Voltammograms were recorded in solution consisting of 10mM ferricyanide prepared in 1M phosphate buffer (pH 7.0). CV plots were recorded over the -0.2V to 0.8V potential range with a scan rate of 0.1V/s. A different scan rate of 0.3V/s was used in studies where CV technique was utilized for *in-situ* monitoring of the self-healing process.

3.1.3 Results and discussion

A typical screen-printed conductive ink is composed of the conductor particles, polymeric binder and other additives.[38] Several binders and solvents were evaluated towards successful preparation of capsule-loaded self-healing carbon ink. Initially, capsules were directly loaded in commercial carbon inks obtained from different sources (Ercon Inc., Gwent Group and Henkel Inc.). However, either these inks could not be printed efficiently or the healing solvent failed to restore the mechanical damage. Attempts were also made by dispersing the capsules and graphite powder in commercial insulating ink (DuPont 5036). In this case, the conductivity was restored only after several minutes and the process was irreproducible. Subsequently, self-healing carbon inks based on polystyrene (poly(styrene-co-methyl methacrylate)) and acrylic (Speedball®, Art Products Inc.) binders were also explored. Printing of the polystyrene-based carbon ink was a major hurdle. In contrast, capsule-loaded acrylic-based carbon inks printed readily but displayed an unstable electrochemical behavior.

The study revealed that absorption of water by the acrylic binder led to its poor electrochemical stability. Therefore, a water-resistant acrylic varnish binder (Liquitex Inc.) was used to synthesize the self-healing carbon ink.

Inks with varying carbon and capsule loadings were prepared to optimize the ink composition. Low loading of the capsules led to their spare distribution within the ink and hence healing could occur only at locations where the capsules were present. Alternatively, high loading of capsules led to highly viscous inks that could not be printed efficiently. Ultimately, an ink containing 45wt% carbon and 5wt% capsule in acrylic varnish binder was selected, as this composition provided the best printability coupled with a favorable electrochemical performance. For preparing self-healing Ag/AgCl ink, inks from different vendors (Ercon Inc. and Gwent Group) were tested for successful dispersion of capsules. Of these, 10wt% capsules directly dispersed in Ag/AgCl Ercon ink possessed the most favorable printability, healing ability and electrochemical performance. The mechanism for self-healing process occurring when a printed trace is damaged is shown in Figure 3.3.1B. Upon mechanical damage, the capsules get ruptured causing the release of the healing agent around the crack. The released agent locally dissolves the binder which leads to redistribution of the filler particles and restoration of the conductive pathway. The optimal conductive ink formulation thus allows self-healing capability without the need for a separate capsule-containing layer.

Preliminary experiments examined the real-time restoration of electrical and mechanical contacts for self-healing carbon and Ag/AgCl traces (Figure 3.1.2). Printed carbon and Ag/AgCl traces fabricated using the self-healing and unmodified inks were coupled to a multimeter while placed under a microscope. Upon recording the initial conductivity, the traces were damaged by an incision knife. As seen in Figure 3.1.2, the trace obtained using self-healing carbon (Figure 3.1.2A) and Ag/AgCl (Figure 3.1.2A') ink readily self-restores its

electrical conductivity within few seconds even when completely damaged multiple times. These videos clearly illustrate the redistribution of the conductive particles (carbon or Ag/AgCl) immediately after the incision, due to the local dissolution of the binder by the released healing solvent, to recover the mechanical and electrical connections. Figure 3.1.2 also shows the snapshots before mechanical damage (Figure 3.1.2B and B') and after complete healing (Figure 3.1.2C and C') of the self-healing carbon and Ag/AgCl traces, respectively. On the other hand, trace fabricated using normal carbon or Ag/AgCl (no capsules) inks showed no restoration of the electrical conductivity upon damage (Figure 3.1.2A'' and A'''). Snapshots of showing the pristine carbon and Ag/AgCl trace before (Figure 3.1.2B'' and B''') and after (Figure 3.1.2C'' and C''') complete damage support the electrical study conclusion of failure of normal inks to restore electrical contact.

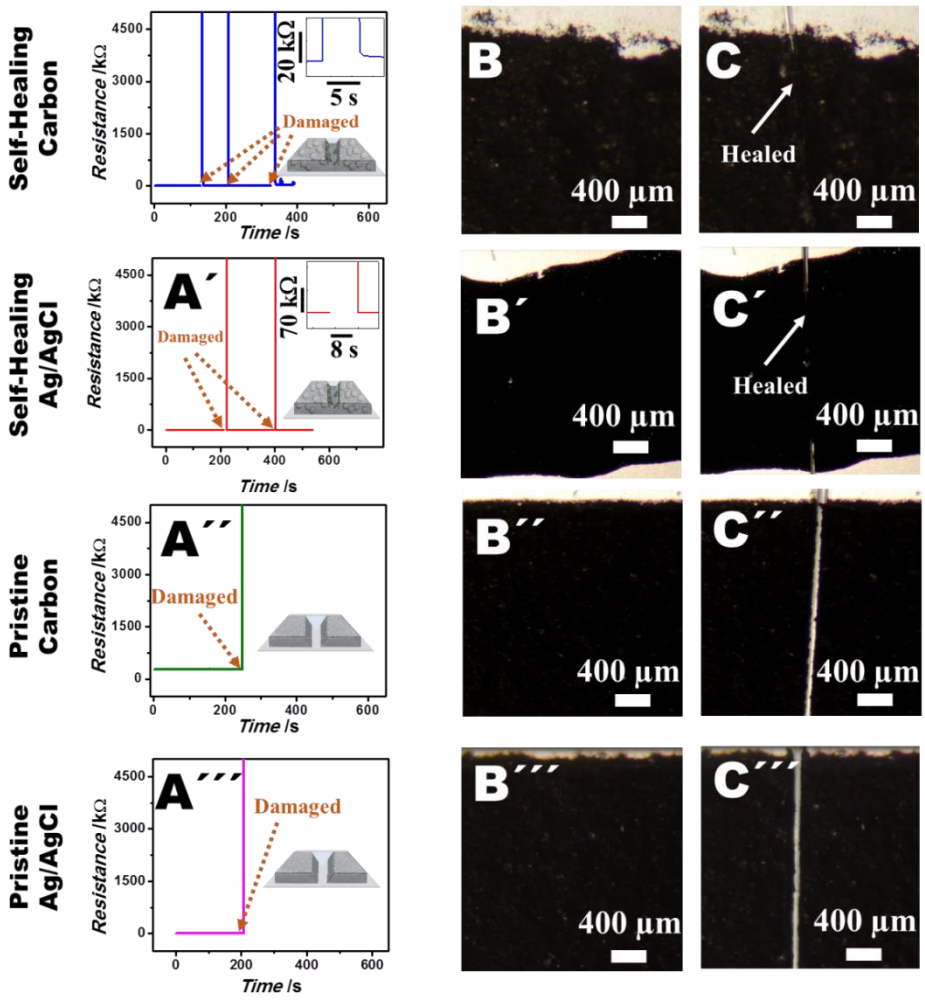


Figure 3.1.2: Real-time resistance study examining the conductivity restoration ability of a self-healing (A) carbon, (A') Ag/AgCl and pristine (A'') carbon and (A''') Ag/AgCl electrode respectively. Respective insets show schematics of the self-healed carbon (A), Ag/AgCl (A') and unhealed pristine carbon (A''), Ag/AgCl (A''') electrode, along with zoomed-in image showing the recovery of electrical connectivity (A, A'). Microscopic images taken (B, B') before damaging and (C, C') after complete repair of a self-healing carbon and Ag/AgCl electrode respectively. Microscopic images taken (B'', B''') before and (C'', C''') after damaging a pristine carbon and Ag/AgCl electrode printed using normal carbon and Ag/AgCl ink respectively. Snapshots were taken from the respective videos at t =~ 0s and t =~20s. (Reprinted with permission from ref. 37. Wiley.)

Cyclic voltammetry (CV) is widely used for studying electrode processes and characterizing the electrochemical performance of different electrode materials. It provides real-time information about the properties of the electrode-electrolyte interface.[39] Hence, CV was leveraged for in-situ investigation of the self-healing process occurring in the printed

electrochemical devices. The initial study aimed at examining the self-healing carbon electrodes. In these experiments, a printed carbon working electrode was coupled to an external Ag/AgCl reference and platinum wire counter electrode. The earlier electrical and optical studies concluded that the healing process is fast (~ seconds); hence, in order to observe such fast healing process in real-time, CVs were recorded at a scan rate of 0.3V/s. Upon obtaining a stable CV, the connector part of the self-healing electrode was incised. The flat CV observed in Figure 3.1.3A immediately after the incision reflects the complete loss of the electrical connectivity. However, self-restoration was initiated within ~1s, as indicated by the fluctuating current, and the electrode regained its original voltammetric behavior within 3s. Such experiments were performed several times to identify the approximate time for self-recovery of electrochemical properties. The individual CV plots obtained before, during damage and after healing are shown separately in the inset of Figure 3.1.3A. A similar experiment was also performed for a carbon electrode fabricated using normal carbon ink (Figure 3.1.3A'). As expected, the damaged electrode fails to recover, as noticed from the flat CV recorded after the damage. It should be noted that the CVs displayed in Figure 3.1.3A and A', of the two (modified and unmodified) electrodes before damaging are quite similar, indicating that introducing the capsules within the carbon ink has negligible impact on the electrochemical properties of the printed electrodes.

The next set of experiments, aimed at observing possible changes in the CVs before and after damaging the electrodes, was carried out using a scan rate of 0.1V/s. The carbon electrodes were damaged at two locations – the connector region and the active electrode area – thus covering the entire device. Figure 3.1.3B and C depicts the CVs before and after damaging the connector region and the active area of the self-healing carbon electrodes, respectively. The figures evidently illustrate the complete recovery of electrochemical behavior of the self-healing electrodes, independent of the damage location, vis-à-vis, the

connector or active areas. Analogous experiments were conducted on carbon electrodes printed using normal carbon ink. This study reveals that the capsule-free electrode is dysfunctional if the connector part is damaged (Figure 3.1.3B'). It also indicates that damaging the active electrode area leads to suppressed signal due to decreased surface area (Figure 3.1.3C').

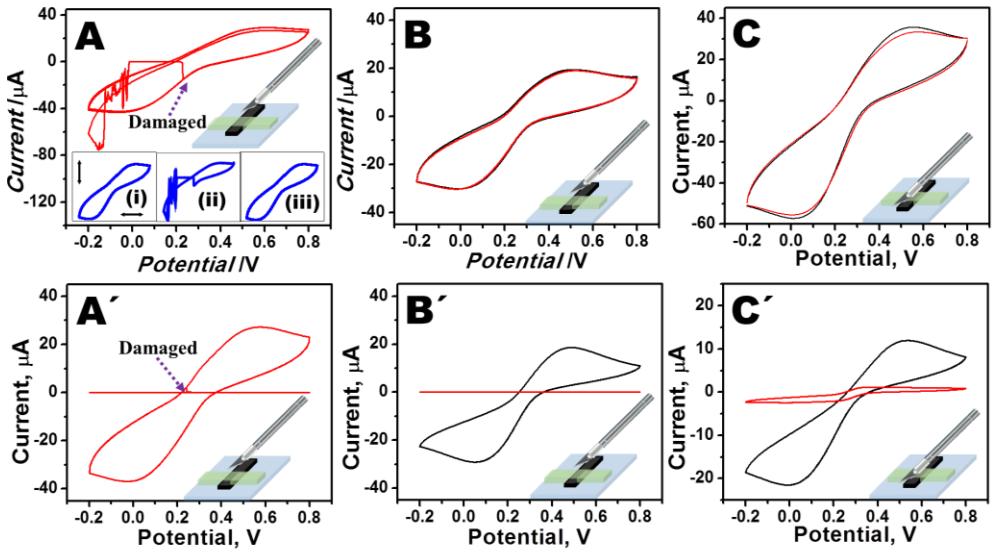


Figure 3.1.3: Self-restoring the electrochemical performance. In-situ CV study of the damage and healing processes for (A) self-healing and (A') normal carbon electrodes. Inset (A) shows individual CVs (i) before damage, (ii) during the damage, and (iii) after healing (vertical scale: 40µA; horizontal scale: 0.4V). CVs obtained for self-healing carbon electrode before damaging (black plot) and after complete healing (red plot) of the (B) connector and (C) active areas. CVs obtained for carbon electrodes printed using the normal ink before (black plot) and after (red plot) damaging of the (B') connector and (C') active areas. (Reprinted with permission from ref. 37. Wiley.)

The above experiments highlight the importance of the self-healing ink for developing smart electrochemical devices that can autonomously repair themselves, irrespective of the location of the damage. Subsequent experiments focused on fabricating and analyzing self-repair of complete electrochemical devices (consisted of working, counter and reference electrodes) printed using self-healing carbon and Ag/AgCl inks. In this evaluation, the reference (Figure 3.1.4A), counter (Figure 3.1.4B) and working (Figure 3.1.4C) electrodes

were separately damaged at their connector region. The individual CV plots obtained before and during the damage, and after the healing are shown separately in the respective insets along with a schematic of the printed device and the damage location. These CVs clearly indicate that, as expected, the device regained its electrochemical performance under all the three scenarios.

Real-time detection of electrolytes directly on the human body has gained tremendous attention for fitness monitoring.[40, 41] Such epidermal sensors commonly face the challenge of mechanical damage. Hence a self-repairable ion-selective potentiometric sodium sensor was fabricated. Figure 3.1.4D shows the response of such a sensor before and after damaging. The nearly identical data obtained corroborate the effective self-repair ability of the sensor. A similar experiment with a sodium sensor fabricated using the normal carbon electrode revealed that the mechanically-damaged sensor completely loses its sodium detection ability, displaying erratic signals characteristic of a failed potentiometric sensor (Figure 3.1.4E).

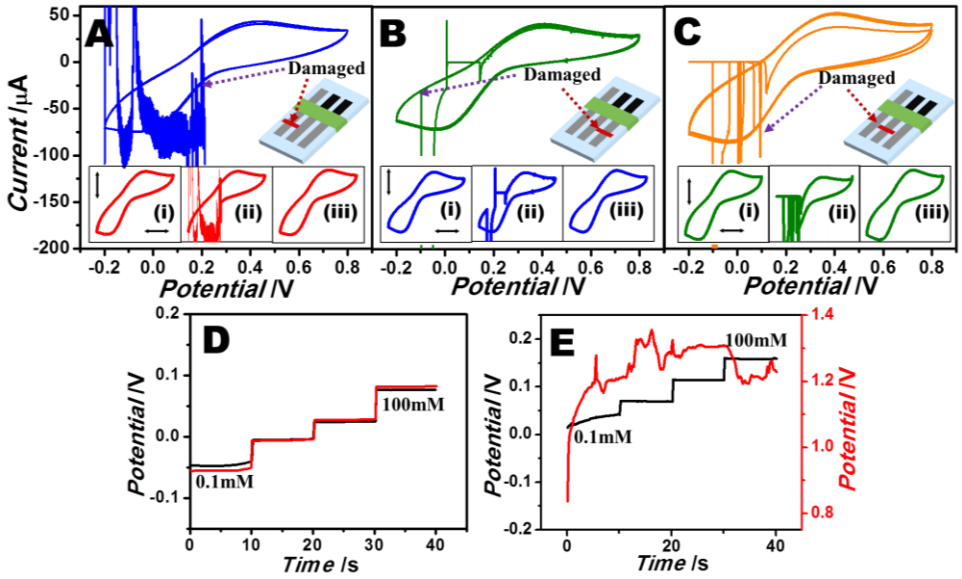


Figure 3.1.4: In-situ CV study of the repair process for a complete self-healing electrochemical device when the (A) reference (B) counter and (C) working electrodes are damaged in their respective Ag/AgCl connector region. Respective insets show schematic of the electrochemical device and individual CVs (i) before damaging, (ii) during damage, and (iii) after healing of the device (i-iii, vertical scale: 50μA; horizontal scale: 0.3V). Calibration plot for (D) a self-healing sodium electrode before its damage (black plot) and after complete self-healing (red plot); (E) potentiometric response of a sodium sensor fabricated on a carbon electrode printed with an normal ink before (black plot) and after (red plot) damage. (Reprinted with permission from ref. 37. Wiley.)

3.1.3 Conclusions

We have demonstrated the first example of a self-healing printed electrochemical device in which the ink material itself is used to repair the damage. Such all-printed electrochemical devices restore their initial electrochemical properties rapidly following complete mechanical damage. The self-healing inks have been carefully formulated to achieve suitable printability, favorable electrochemical behavior along with a rapid self-healing capacity. The autonomous healing ability is incorporated within the inks by adding healing-agent loaded microcapsules. Upon damage of the printed device, the ruptured capsules release the healing agent and initiate the recovery process involving local rearrangement of the conductive particles to restore the conductive pathway. Detailed electrical, optical and electrochemical studies performed on the printed devices reveal that the healing process

commences immediately after the device is damaged and that the electrochemical properties are recovered within a few seconds. Control studies concluded that addition of the self-healing capsules has negligible influence on the electrochemical properties of the printed electrodes. These studies emphasize the practical application of such bio-mimicking electrochemical devices in circumstances where mechanical damages are common. Such integration of self-healing materials into electrochemical devices thus prevents structural fractures and augments their longevity. A similar ink synthesis route can be followed to develop other inks for different forms of printed self-healing devices. Thus, the present work has tremendous scope towards diverse applications of printed devices, in general, and of printed electrochemical devices, in particular.

This chapter is based, in part, on the material as it appears in Advanced Electronic Materials, 2015, by Amay J. Bandodkar, Vinu Mohan, Cristian S. López, Julian Ramírez, and Joseph Wang. The dissertation author was the primary investigator and corresponding author of this paper.

3.2 References

1. Wang, Y.; Ma, E. W. M.; Chow, T. W. S.; Tsui, K. L. *IEEE Transactions on Industrial Informatics* **2014,** *10*, 419.

2. Lall, P.; Lowe, R.; Goebel, K. *IEEE Transactions on Reliability* **2012,** *61*, 858.

3. Halámková, L.; Halámek, J.; Bocharova, V.; Szczupak, A.; Alfonta, L.; Katz, E. *J. Am. Chem. Soc.* **2012,** *134*, 5040.

4. Szczupak, A.; Halamek, J.; Halamkova, L.; Bocharova, V.; Alfonta, L.; Katz, E. *Energy Environ. Sci.* **2012,** *5*, 8891.

5. de Ron, A.; Penev, K. *Technovation* **1995,** *15*, 363.

6. Martin, P. *Science* **1997,** *276*, 75.

7. Toback, F. G. *Kidney International* **1992,** *41*, 226.

8. Blaiszik, B. J.; Kramer, S. L. B.; Olugebefola, S. C.; Moore, J. S.; Sottos, N. R.; White, S. R. *Annual Review of Materials Research* **2010,** *40*, 179.

9. Jonkers, H. M.; Thijssen, A.; Muyzer, G.; Copuroglu, O.; Schlangen, E. *Ecol. Eng.* **2010,** *36*, 230.

10. Wang, J.; Van Tittelboom, K.; De Belie, N.; Verstraete, W. *Construction and Building Materials* **2012,** *26*, 532.

11. Shchukin, D. G.; Zheludkevich, M.; Yasakau, K.; Lamaka, S.; Ferreira, M. G. S.; Möhwald, H. *Adv. Mater.* **2006,** *18*, 1672.

12. Zheludkevich, M. L.; Shchukin, D. G.; Yasakau, K. A.; Möhwald, H.; Ferreira, M. G. S. *Chem. Mater.* **2007,** *19*, 402.

13. Kohl, S.; Evangelopoulos, D. S.; Kohlhof, H.; Hartel, M.; Bonel, H.; Henle, P.; Rechenberg, B.; Eggli, S. *Knee Surgery, Sports Traumatology, Arthroscopy* **2012,** *21*, 599.

14. Grill, W. M. *Expert Review of Medical Devices* **2007,** *4*, 107.

15. Juhas, M.; Bursac, N. *Curr. Opin. Biotechnol.* **2013,** *24*, 880.

16. Williams, K. A.; Boydston, A. J.; Bielawski, C. W. *J. Royal Soc. Inter.* **2007,** *4*, 359.

17. Tee, B. C. K.; Wang, C.; Allen, R.; Bao, Z. *Nat Nano* **2012,** *7*, 825.

18. Odom, S. A.; Chayanupatkul, S.; Blaiszik, B. J.; Zhao, O.; Jackson, A. C.; Braun, P. V.; Sottos, N. R.; White, S. R.; Moore, J. S. *Adv. Mater.* **2012,** *24*, 2578.

19. Kamyshny, A.; Magdassi, S. *Small* **2014,** *10*, 3515.

20. Blaiszik, B. J.; Kramer, S. L. B.; Grady, M. E.; McIlroy, D. A.; Moore, J. S.; Sottos, N. R.; White, S. R. *Adv. Mater.* **2012,** *24*, 398.

21. Carrilho, E.; Martinez, A. W.; Whitesides, G. M. *Anal. Chem.* **2009,** *81*, 7091.

22. Chen, P.; Chen, H.; Qiu, J.; Zhou, C. *Nano Research* **2010,** *3*, 594.

23. Jost, K.; Stenger, D.; Perez, C. R.; McDonough, J. K.; Lian, K.; Gogotsi, Y.; Dion, G. *Energy Environ. Sci.* **2013,** *6*, 2698.

24. Zhou, Y.; Yu, B.; Shiu, E.; Levon, K. *Anal. Chem.* **2004,** *76*, 2689.

25. O'Mahony, A. M.; Wang, J. *Electroanalysis* **2013,** *25*, 1341.

26. Bandodkar, A. J.; Wang, J. *Trends Biotechnol.* **2014,** *32*, 363.

27. Bandodkar, A. J.; Jia, W.; Wang, J. *Electroanalysis* **2015,** *27*, 562.

28. Cheng, Y.-T.; Verbrugge, M. W. *J. Electrochem. Soc.* **2010,** *157*, A508.

29. Zhao, K.; Pharr, M.; Vlassak, J. J.; Suo, Z. *J. Appl. Phys.* **2010,** *108*, 073517.

30. Windmiller, J. R.; Wang, J. *Electroanalysis* **2013,** *25*, 29.

31. Kim, J.; Valdes-Ramirez, G.; Bandodkar, A. J.; Jia, W.; Martinez, A. G.; Ramirez, J.; Mercier, P.; Wang, J. *Analyst* **2014,** *139*, 1632.

32. Cai, W.; Lai, T.; Du, H.; Ye, J. *Sens. Actuators, B* **2014,** *193*, 492.

33. Cunningham, J. C.; Brenes, N. J.; Crooks, R. M. *Anal. Chem.* **2014,** *86*, 6166.

34. Malzahn, K.; Windmiller, J. R.; Valdes-Ramirez, G.; Schoning, M. J.; Wang, J. *Analyst* **2011,** *136*, 2912.

35. Schazmann, B.; Morris, D.; Slater, C.; Beirne, S.; Fay, C.; Reuveny, R.; Moyna, N.; Diamond, D. *Anal. Methods* **2010,** *2*, 342.

36. Bandodkar, A. J.; Nuñez-Flores, R.; Jia, W.; Wang, J. *Adv. Mater.* **2015,** *27*, 3060.

37. Bandodkar, A. J.; Mohan, V.; López, C. S.; Ramírez, J.; Wang, J. *Adv. Electron. Mat.* **2015,** *1*, 1500289.

38. Wang, J.; Tian, B.; Nascimento, V. B.; Angnes, L. *Electrochim. Acta* **1998,** *43*, 3459.

39. Stamford, J. A. *Journal of Neuroscience Methods* **1990,** *34*, 67.

40. Rose, D. P.; Ratterman, M. E.; Griffin, D. K.; Hou, L.; Kelley-Loughnane, N.; Naik, R. R.; Hagen, J. A.; Papautsky, I.; Heikenfeld, J. C. *IEEE Transactions on Biomedical Engineering* **2015,** *62*, 1457.

41. Sonner, Z.; Wilder, E.; Heikenfeld, J.; Kasting, G.; Beyette, F.; Swaile, D.; Sherman, F.; Joyce, J.; Hagen, J.; Kelley-Loughnane, N.; Naik, R. *Biomicrofluidics* **2015,** *9*, 031301.

Chapter 4 Printed Wearable Pontentiometric Sensors

4.1 Wearable pH sensor

4.1.1 Introduction

Potentiometric ion selective electrodes (ISEs) have witnessed widespread use in various research, biomedical and industrial domains.[1, 2] Conventional ion-selective sensors consist of a membrane-based ion-selective electrode and a reference electrode, both of which require an internal solution to ensure a stable and sensitive response.[3] Although these sensors have been widely used in a plethora of practical applications, their intrinsic design imposes inherent limitations upon specific *in vivo* and *ex vivo* applications, particularly the internal solution complicates the fabrication process and limits their miniaturization. Furthermore, traditional ISEs are often fabricated by employing rigid materials (*e.g.*, glass), which hinder their integration on curvilinear surfaces. The challenges associated with the use of an internal solution were addressed by the development of solid-contact ISEs,[4] with the first example demonstrated almost 4 decades ago,[5] comprising of an ion-selective membrane casted on a solid metal wire. However, coated-wire sensors suffer from irreproducibility, albeit this issue was later solved by employing conducting polymers as ion-to-electron transducers.[6] Similar efforts have been pursued to eliminate the use of the internal solution required for the reference electrode.[7] Moreover, researchers have extended the capabilities of ion-selective sensors by fabricating all-plastic flexible ISEs,[8] including complete flexible solid-contact sensing devices using screen printing[9] and drop-casting techniques.[10] Yet, highly flexible and conformal integrated potentiometric sensors, compatible with the non-planarity and

irregularities of the human anatomy and enduring prolonged mechanical strain, are highly desired for the realization of epidermal chemical monitoring.

This work reports on the development and characterization of ion-selective potentiometric electrodes fabricated on temporary-transfer tattoo paper for direct epidermal pH measurements. An ideal wearable device mandates a conformal geometry that is compliant with skin and can withstand repeated mechanical stress while minimizing intrusion in the wearer's routine. Advances in textile-based sensors have offered considerable advantages in the field of on-body monitoring devices as they conform with the wearer's anatomy while enabling unobtrusive sensing. Recently, wearable devices have been developed for the detection of both physiological[11] and environmental[12] analytes. An optical device, reported by Curto *et al.*, describes a dermal microfluidic system that is able to respond to pH changes by employing a pH-sensitive dye.[13] A necessary requirement for effective real-time physiological monitoring is the continuous contact of the analyte with the sensor surface. We recently addressed this issue by developing electrochemical sensors that can be directly stamped onto the epidermis for on-body sensing.[14] We also newly introduced epidermal amperometric sensors based on the fabrication of temporary-transfer tattoo devices.[15] This was achieved by combining widely deployed screen printing and temporary transfer tattoo methodologies for the amperometric and voltammetric detection of electroactive molecules such as uric acid, ascorbic acid and TNT. The elasticity of the tattoo substrate, reinforced with addition of dispersed carbon fiber segments within the tattoo ink, allowed the amperometric sensor to attach firmly to the contours of the wearer, while possessing sufficient tensile strength to withstand repetitive mechanical deformation.

The current work builds on recent advances charted within the temporary-transfer tattoo electrochemical sensors domain toward the development of epidermal ion-selective potentiometric sensors.[16] To realize such tattoo-based potentiometric devices, we have

combined polyaniline-based solid-contact ISEs, commercially available temporary transfer tattoo paper and screen printing techniques using the hybrid fabrication protocol illustrated in Figure 4.1.1(i). The fabrication versatility offered by the screen printing methodology has allowed us to develop ISE tattoos in the form of a 'smiley face' with one eye acting as the pH-sensitive ISE while the second one serving as the reference electrode (Figure 4.1.1(ii)), thus concealing the complete sensor contingent in an artistic manner. The 'smiley face'-shaped tattoo sensors were readily printed on commercially available tattoo base paper using carbon, Ag/AgCl and insulator inks with a distinct stencil pattern employed for each layer. An adhesive sheet was later applied to the printed tattoo paper for subsequent transfer on various substrates. Further details of these steps are illustrated in Figure 4.1.1 and provided in the Experimental section.

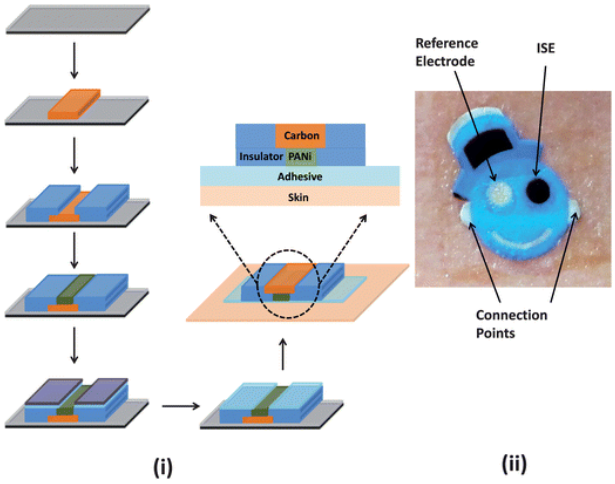


Figure 4.1.1 (i) Schematic representation of the fabrication protocol employed in the production of temporary transfer tattoo-based solid-contact ion-selective electrode (ISE) sensors. The sensor was prepared *via* a thick-film screen printing fabrication technique (only the carbon electrode (orange) and insulator (blue) are shown). The sensor is patterned onto a release agent-coated (grey layer) base paper (black). The carbon electrode is then modified with PANi followed by the application of the adhesive sheet. In order to transfer the tattoo, the protective sheet (purple) is removed from the adhesive layer (light blue) and then placed on the receiving substrate. (ii) Photograph of the tattoo ISE sensor illustrating the two electrodes and the connection points for the voltmeter. (Reprinted with permission from ref. 16. Copyright 2013 Royal Society of Chemistry).

The attractive pH-sensitive conductivity of poly(aniline) (PANi) associated with the reversible emeraldine salt (ES)–emeraldine base (EB) transition (acid–base reaction) has led to its widespread use in the fabrication of solid-state pH sensors.[17] Furthermore, PANi has minimal cytotoxicity and causes negligible skin irritation and sensitization.[18] Highly reproducible thin films of PANi can be easily obtained *via* electropolymerization, and PANi-based ISEs commonly do not require surface pretreatment. These characteristics along with their attractive performance (further discussed below) make PANi well-suited for developing biocompatible dermal tattoo-based potentiometric sensors. The resulting tattoo ISEs withstand repeated bending and stretching operations, which are of substantial relevance to wearable epidermal sensors. The new fabrication route thus yields body-worn potentiometric sensors that are compliant with the contours of the skin for the realization of non-invasive potentiometric monitoring. In the following sections, the development and characterization of tattoo-based ISE sensor devices for continuous epidermal pH monitoring is described and the performance of such devices under practical scenarios is provided.

3.1.2 Experimental section

a. Chemicals and reagents:

Potassium phosphate monobasic (KH_2PO_4), potassium phosphate dibasic (K_2HPO_4), hydrochloric acid (HCl), Nafion® 117 solution and aniline were obtained from Sigma Aldrich (St. Louis, MO) while citric acid was received from Fisher Chemical (Fair Lawn, NJ). Aniline was further purified by double distillation prior to use. Carbon fibers (8 μm diameter, 6.4 cm length, 93% purity) were procured from Alfa Aesar (Ward Hill, MA) and their length was reduced to ~0.5 mm (by cutting with a sharp blade) followed by thorough cleaning in acetone. All experiments were conducted at room temperature and all solutions were prepared using ultra-pure deionized water (18.2 MΩ·cm).

b. Instrumentation:

Electrochemical cleaning, deposition, and potentiometric analysis were performed using a CH Instrument (Austin, TX) model 630C electrochemical analyzer. A Mettler Toledo (Columbus, OH) S20 SevenEasy glass-electrode digital pH meter was employed for pH measurements. A miniaturized multimeter (Sinometer MS8216 DMM) was used for on-body measurements.

c. Fabrication of temporary tattoo sensors:

The ISE tattoo was designed to conceal the electrodes in a 'smiley face'. One eye (green) functioned as the pH-sensitive ISE while the other (silver) acted as the reference electrode (Figure 4.1.1(ii)). As illustrated in Figure 4.1.1(ii), the two ears were employed as connectors for the attachment of the digital multimeter. Design of the sensor pattern was performed in AutoCAD (Autodesk, San Rafael, CA) and fabricated on 75 μm thick stainless steel and mesh stencils (Metal Etch Services, San Marcos, CA). A unique stencil pattern was used for each electrode layer (*i.e.*carbon, Ag/AgCl, insulator). Conductive Ag/AgCl (E2414), carbon (E3449), and insulator inks (E6165) were procured from Ercon Inc. (Wareham, MA) and a transparent dielectric ink (5036) was obtained from DuPont Inc. (Wilmington, DE). Carbon fiber segments were dispersed within the conductive carbon ink matrix to increase the tensile strength of the electrode. Printing was accomplished *via* an MPM SPM semi-automatic screen printer (Speedline Technologies, Franklin, MA). Blank temporary transfer tattoo paper and the accompanying adhesive substrate (Papilio, HPS LLC, Rhome, TX) were used without further derivatization.

The fabrication process first involved printing the blue insulator ink, followed by the Ag/AgCl and the carbon inks, and finally, by another blue insulator layer. Following each routine, the ink was cured at 90 °C for 15 min. Subsequently, a 30 wt% KCl-doped transparent insulator was screen printed only on the surface of the reference electrode and then cured for 6

min at 90 °C. Finally, a total of 6 μL of the 5% Nafion solution was drop-casted on the Ag/AgCl reference electrode and left to dry overnight. These steps were imperative in order to obtain a stable reference potential; it was observed that, without these additional processing steps, the potential of the reference electrode drifted as a function of the pH of the solution, possibly due to leaching of chloride ions.

Prior to the electropolymerization of aniline, the working electrode was electrochemically cleaned by five cyclic voltammetric scans in 0.5 M HCl over the potential range of −0.3 V to 1.1 V (an external Ag/AgCl reference electrode and an external Pt wire auxiliary electrode were used in this processing step). Surface modification with PANi was performed in a 0.1 M aniline/1 M HCl solution by cyclic voltammetry from −0.2 V to 1.0 V (*vs.* Ag/AgCl) at 0.1 V s^{-1}. First, electropolymerization was performed for 12 cycles, then a fresh solution was dispensed on the surface, followed by additional 13 cycles. A total of 25 cycles were thus executed for the complete polymerization of the working electrode surface. During the cleaning and polymerization steps, the screen printed Ag/AgCl electrode was protected from the electrolyte solution to avoid its damage by highly acidic solutions and aniline. After air-drying the PANi film, the adhesive sheet was applied to the tattoo. For proper contact between the two electrodes and analyte solution, this adhesive sheet was excised to remove a rectangular-shaped region around the two electrodes (the two eyes). The as-prepared ISE tattoos were then ready for transfer and evaluation.

In order to apply the tattoos, the protective layer from the transparent adhesive sheet was first removed to expose the adhesive. To ensure proper adhesion between the tattoo and substrate, an extra adhesive layer was applied to the substrate. (Note: for applying the adhesive sheet to soft substrates, the adhesive sheet was first applied to a blank tattoo base paper, followed by removal of the protective sheet and attaching it to the substrate. The base paper was subsequently removed by gently applying water and peeling it off.) Later, the sticky

adhesive side of the tattoo was placed on the adhesive layer already applied to the substrate. This step was followed by applying water to the base paper and gently peeling it off. The total time for this transfer step was less than 3 min. The entire fabrication and transfer processes are shown in Figure 4.1.1(i).

4.1.2 Experimental section

a. *In vitro* characterization:

The ISE tattoos were firstly examined *in vitro* by applying them onto hard plastic substrates prior to on-body epidermal studies. The tattoo sensors were analyzed within the pH range of human sweat (pH 3–7, with a mean around pH 5)[19] using standard McIlvaine's buffers. Owing to the continuous fluctuations of the pH of the human perspiration, it is imperative that the ISE tattoos encompass a rapid and near-instantaneous response to pH modulations over this range. Figure 4.1.2(i) displays a characteristic potential-time recording at the tattoo-based potentiometric sensor for decreasing pH levels between 7 and 3 (in one-unit decrements). This real-time recording clearly illustrates that the tattoos exhibit a nearly instantaneous response to varying pH solutions, yielding 80% of their steady-state signal within the first 10 s while a completely stabilized signal was observed within 25 s. The resulting calibration plot (shown in the inset) displays a sub-Nernstian behaviour, with a mean slope (s_x) of 50.1 mV/pH and a relative standard deviation (RSD) of 3.72% (n = 4). The pH sensitivity (slope) and conductivity of PANi depend on orientation of the crystalline and amorphous phases of PANi.[20] The observed sub-Nernstian response of the PANi tattoo sensors is attributed to inferior orientation of these phases. As will be discussed later, mild mechanical deformations to the tattoos caused reorientation of the conducting and amorphous phases and improved the pH-sensitivity to a near-Nernst response. Batch-to-batch variations between the

tattoos also exhibited a low RSD of 4.63% (n = 4), hence indicating that the fabrication of reproducible devices is indeed feasible.

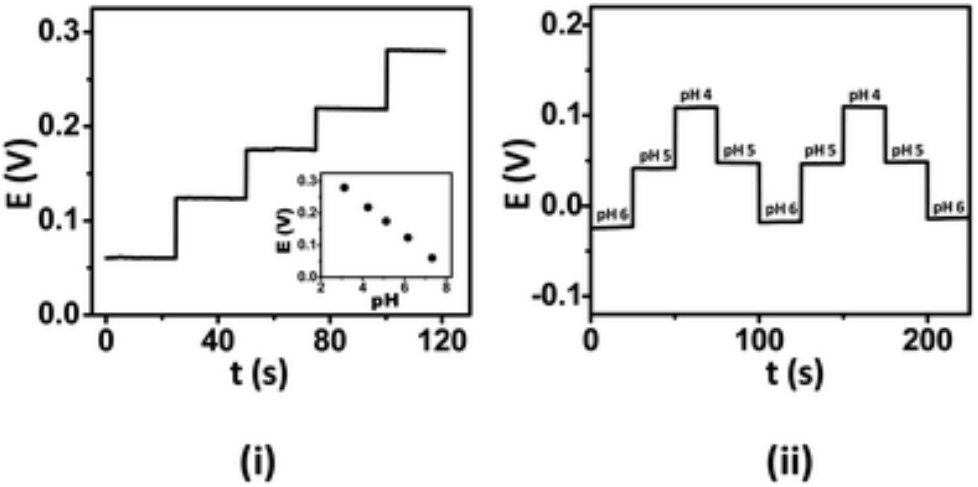


Figure 4.1.2: (i) Response of the ISE tattoo sensor, *in vitro*, upon calibration with unit decrease of pH using standard McIlvaine's buffers. (ii) Potential-time response of the ISE tattoo sensors,*in vitro*, demonstrates the reproducibility of the sensors in response to large pH fluctuations. (Reprinted with permission from ref.16. Copyright 2013 Royal Society of Chemistry).

It has been observed that the pH of human perspiration fluctuates according to the respiration rate.[21] As such, the tattoo sensors must also exhibit minimal carry-over in order to monitor such dynamically fluctuating pH environments. To investigate this parameter, the ISE tattoos were subjected to operation in varying pH solutions and consecutive measurements recorded without reconditioning or rinsing of the tattoo surface. Figure 4.1.2(ii) demonstrates the dynamic response of the tattoo ISE to alternate and multiple exposures to solutions of different pH. The device responds rapidly and favorably to these dynamic pH changes, rapidly regaining the same potentiometric signal for a given solution pH during this continuous operation. The negligible carry-over of the tattoo-ISE response reflects the fact that the emeraldine salt (ES)–emeraldine base (EB) transition of PANi is fast and reversible. Thus, the

tattoo sensors have the capability to perform effectively under continuously varying pH milieu, *viz.*, *in situ* pH measurement of human perspiration with low carry-over.

A distinctive feature of wearable sensors is their ability to endure prolonged mechanical strain, which is a key requirement of wearable and epidermal sensors. This is especially true in the athletics, fitness and military domains. It is thus essential to examine the influence of relevant mechanical stress upon the sensor performance prior to their integration with the epidermis. For this reason, the influence of mechanical strain permutations, including repeated bending and stretching, upon the potentiometric response were examined. The ISE tattoo sensors were subjected to a total of 50 bending and 40 stretching applications. For these studies, the tattoos were transferred onto GORE-TEX as its viscoelastic behaviour mimics that of skin. In the bending study, the tattoo was bent to 180° and maintained at that position for 5 s prior to release. The response of the tattoo was measured subsequent to 10 bending iterations from pH 7 to 3. In order to analyze the effect of stretching upon the electrochemical performance of the tattoos, the sensors were stretched an additional 10% in lateral extent and maintained at that position for 5 s followed by release and investigation of the response. In case of stretching deformation, the response was measured at an interval of 5 consecutive stretching operations. The deformation created during these studies actually yielded a beneficial effect upon the response of the tattoos. Specifically, in the absence of applied deformation, the tattoos yielded a sub-Nernstian response (52.8 mV/pH), as observed with plastic substrates. The response of the tattoos improved to 59.6 mV/pH within the first 10 bending iterations (Figure 4.1.3(i)). Thereafter, the response stabilized to yield a final slope of 57.5 mV/pH following the 50^{th} bending iteration. The RSD for the entire experiment was 5.71%. A similar trend was observed for the stretching study, where an initial slope of 53.0 mV/pH increased to 58.2 mV/pH following the 10^{th} stretching iteration and finally stabilized at 57.54 mV/pH after the 40^{th} stretch (Figure 4.1.4(i)). A 4.72% RSD was obtained. The

sensitivity enhancement observed is hypothesized to originate from the uncoiling and reorientation of the crystal and amorphous phases of PANi and the subsequent improvement in its conductivity owing to mechanical deformation.[20] Visual analysis of the tattoo sensors under bending and stretching was performed on human skin. For the bending studies, the tattoo was applied to the *cubital fossa* and the arm was bent completely until the fingers touched the *scapula acromion*, thus simulating the extreme deformation expected under heavy epidermal wear (Figure 4.1.3(ii)). In the stretching scenario, the tattoo was applied to the forearm and then stretched repeatedly to the maximum extent (Fig. 4.1.4(ii)). The photographs reveal that the potentiometric sensors are quite resilient and that their structural integrity does not easily degrade. Accordingly, the sensors are well-suited for applications involving continuous motion of the substrate, as experienced by the human body. These results thus substantiate that the presented tattoo ISE sensor design is well-positioned for migration towards evaluation on the human epidermis.

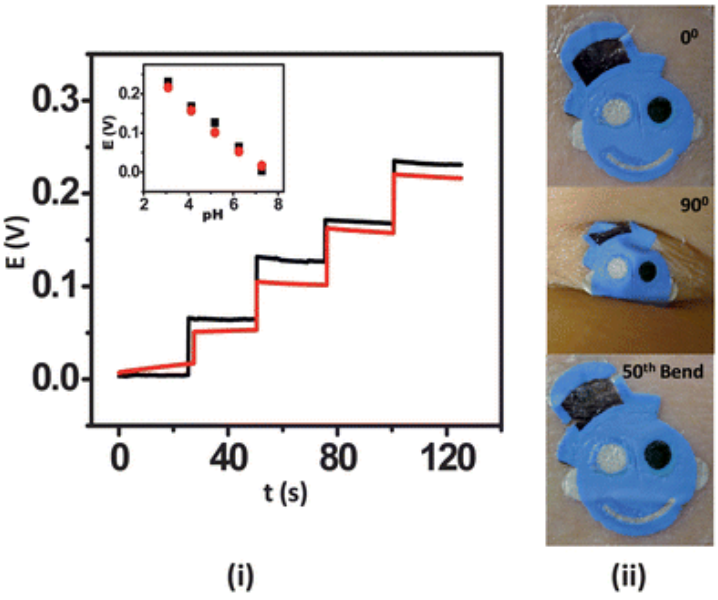


Figure 4.1.3: Influence of repeated mechanical strain (bending) upon the response of the tattoo ISE: (i) pH-responsive behavior of the ISE tattoo sensor over the 3–7 pH range prior to stretching (black) and following the 50th (red) bending on GORE-TEX; one unit pH decrement per addition. (ii) Images of the tattoo applied to *cubital fossa* at 0° bending, 90° bending, and after the 50th bending. (Reprinted with permission from ref. 16. Copyright 2013 Royal Society of Chemistry).

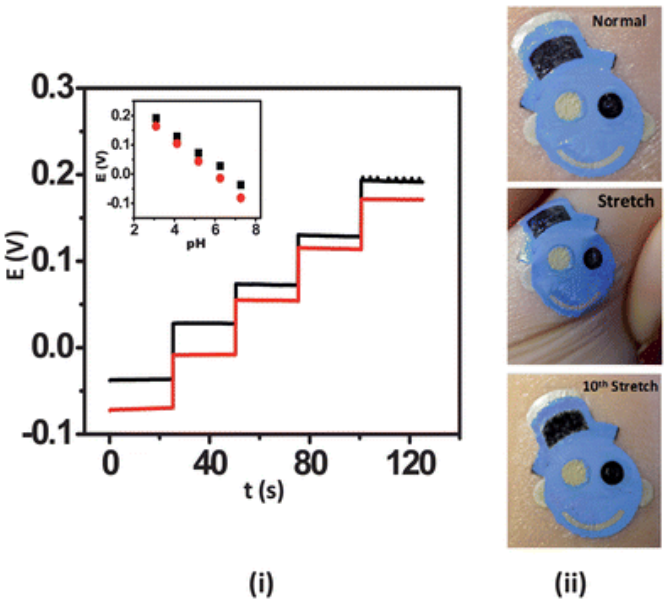


Figure 4.1.4: Influence of repeated mechanical strain (stretching) upon the response of the tattoo ISE: (i) pH-responsive behavior of the ISE tattoo sensor prior to stretching (black) and following the 40th (red) stretch on GORE-TEX; one unit pH decrement per addition. (ii) Images of the tattoo applied to the forearm at normal, during stretching, and after the 10thstretch. (Reprinted with permission from ref. 16. Copyright 2013 Royal Society of Chemistry).

b. Epidermal studies:

There are growing demands for ion-selective sensors in the medical, sports, athletics, and fitness fields where point-of-care devices for the monitoring of physiological conditions are required. Electrolyte (*i.e.* Na, Cl and K) and pH levels of perspiration can readily yield information regarding the metabolic state of an individual as well as their respiration dynamics during a fitness routine.[22] Thus, continuous pH analysis of human perspiration is of great importance in the areas of clinical diagnostics and sports medicine.

Following their *in vitro* characterization, the tattoo ISEs were thus applied to different locations throughout the body (neck, wrist and lower back) of an active, consenting volunteer (sex: male; age: 27; weight: 70 kg; height: 186 cm) while the multimeter readout unit was attached to the body using a commercially available arm-band (Figure 4.1.5). The multimeter leads were attached firmly to the connection points (ears) of the tattoo ISE sensor using

transparent polystyrene tape. The elasticity of the tattoo substrate allows the new potentiometric sensor to attach firmly to these different body locations. These areas were selected in order to vary operational conditions experienced by the sensors, as mechanical stress and local pH are expected to vary among these locations.[23] As illustrated in Figure 4.1.5, the complete device can be easily mounted on the epidermis without much hindrance to the wearer. The ISE application process and the subsequent mating of the sensor with the readout instrument required less than 5 min and was readily performed by the volunteer. During the experiment the volunteer used a stationary cycle in a gymnasium for a total of 40 min followed by a 10 min gradual cool down. The volunteer ingested no fluid (dehydrated state) during the entire exercise. Heart rate and cadence were maintained around 165 and 130 RPM, respectively. pH sensing of the subject's perspiration was performed by the ISE tattoos and the data were collected at regular intervals using the miniaturized multimeter. To confirm that the tattoos yielded accurate readings, the regional pH was verified using a conventional pH meter and glass electrode.

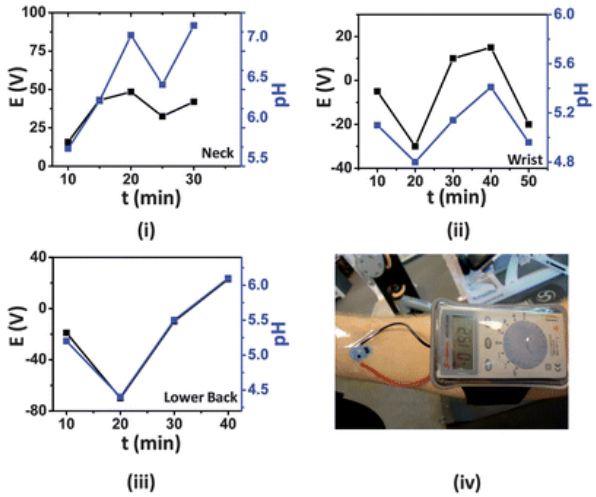


Figure 4.1.5: Real-time response (black) of the ISE tattoos applied to (i) neck, (ii) wrist and (iii) lower back. The plot in blue represents the pH measured by the conventional pH meter. (iv) Photograph showing the entire device (tattoo and digital multimeter) attached to the wrist for such epidermal measurements of pH in human perspiration. (Reprinted with permission from ref. 16. Copyright 2013 Royal Society of Chemistry).

Although an athlete initially perspires at a low rate, this is soon followed by heavier perspiration as physical activity continues. Thus, an important requirement for the tattoos is their ability to yield precise readings during a wide range of sweat flow rates. It was observed that during the first 10 min of exercise, the tattoos provided no response as the amount of perspiration generated was not sufficient to record a consistent open circuit potential. This was also true for the pH glass electrode. However, at the 10 min mark, sweat excretion became sufficient for the tattoo sensors to yield a stable reading. Initially, the pH measured at the three positions by the tattoo ISE sensors were nearly equivalent (∼pH 5.3) (Figure 4.1.5). The real-time sweat pH data obtained from the ISE sensors can be explained based on varying sweat rate at the respective body parts. The volunteer perspired most profusely in the vicinity of the neck, followed by the lower back and the wrists. As the sweat excretion rate increases, the relative concentration of lactate and pyruvate decreases due to dilution, and the pH concomitantly increases.[21]Figure 4.15(i–iii) clearly illustrate that the tattoo ISE sensors performed favorably with a mean slope of ∼54 mV/pH and their potentiometric response at the different body locations followed closely the pH values recorded with the glass electrode.

During the entire course of the experiment, it was observed that the tattoo ISEs performed well during both moderate and profuse perspiration. However, owing to the combination of excessive sweating and the highly curvilinear morphology of the skin on the neck, the neck-based tattoo ISE sensor functioned reliably for about 30 min. It is also important to note that the tattoos functioned satisfactorily even when minor cracks were observed (as long as connection to the multimeter was maintained). This is attributed to the fact that the potentiometric response is independent of electrode area, in contrast to area-dependent voltammetric and amperometric measurements. This represents an inherent merit of potentiometric measurements over alternative electrochemical techniques toward potential epidermal monitoring. Thus, the ISE tattoo sensors are attractive for measuring the pH of

human perspiration under practical scenarios, including complex body motions typically experienced during fitness and athletic routines.

4.1.3 Conclusions

We have successfully demonstrated the fabrication of tattoo-based solid-contact ISEs for epidermal pH monitoring by combining commercially available temporary transfer tattoo paper with conventional screen printing and solid-contact polymer ISE methodologies. The new fabrication route yields highly flexible body-worn potentiometric sensors that are compliant with the skin and concealed in an artistic tattoo pattern. Repeated bending and stretching of the tattoos exhibited minimal effect on their mechanical integrity and potentiometric behavior. In addition, the sensors exhibited no apparent carry-over effects, as is desired for successful monitoring of dynamic events. The devices were later applied to the lower back, neck and wrist of the human body and evaluated for real-time measurement of the pH levels of human perspiration during exercise. Advantageously, the tattoos performed in a near-Nernstian manner under such practical scenarios and provided stable signals even when operating under profuse perspiration. Furthermore, the tattoo ISE sensors were able to tolerate the complex mechanical deformations experienced by the human skin during exercise. The tattoo ISE sensors thus exhibit substantial potential as practical, body-worn devices for continuous physiological monitoring. The new potentiometric sensing concept can be readily expanded towards epidermal monitoring of other clinically relevant sweat electrolytes such as sodium, potassium, calcium, or magnesium.

4.2 Wearable sodium sensor

4.2.1 Introduction

Wearable chemical sensors, capable of real-time on-body monitoring of chemical constituents, can yield significant additional insights into the overall health status and performance of individuals, compared to that obtained by monitoring physical variables alone.[24] Roger's group introduced epidermal sensors for measuring physical physiological parameters.[25] Electrochemical devices offer considerable promise for such continuous non-invasive on-body monitoring.[15] Particular attention has been given recently to printed electrochemical sensors on flexible substrates and textiles.[12] Recently our group introduced the first tattoo-like electrochemical sensors, capable of adhering and conforming to the epidermis, for amperometric biosensing of lactate in human perspiration[26] or potentiometric sensing of sweat pH[16] and ammonium.[27] Continuous monitoring of sweat lactate and pH dynamic during exercise events has thus been demonstrated. Extending this attractive platform towards continuous non-invasive monitoring of key sweat electrolytes should benefit diverse healthcare, fitness, and military applications.

The present article describes the design and analytical performance of a temporary-transfer tattoo solid-contact ion-selective electrode (ISE) for the continuous non-invasive monitoring of sweat sodium concentration directly on the human epidermis.[28] Sodium is the most abundant electrolyte present in human sweat.[29] It is an excellent marker for electrolyte imbalance and provides valuable information regarding an individual's physical and mental wellbeing. Replenishing the sodium level in the body is important since it is essential for regulating water balance, pH, and osmotic pressure. This is especially true for athletes,[30] people working in hot and humid environments[31] and patients suffering from Cystic Fibrosis,[32] since, in these cases, the amount of sodium lost via sweating can reach dangerously high

levels causing hyponatremia, leading to deleterious physiological conditions. Monitoring the amount of sodium loss during sweating is thus extremely important.[11] A wearable device quantifying in real-time the transient sweat sodium concentrations could alert the wearer regarding his electrolyte loss and the concomitant need for electrolyte replenishment. Such device must be compact, easily worn, autonomous, and able to generate, display or store the results in a continuous fashion.

The current methodology for estimating sodium in the perspiration relies on collecting sweat via Macroduct® sweat collection systems followed by lab-based analysis of the collected fluid.[33] However, such a protocol has several shortcomings for routine operation. These include (i) A large sweat collection system that is uncomfortable to wear thus hindering the wearer's routine. (ii) Bulky centralized expensive instrumentation for sweat analysis that is incompatible with on-body testing. (iii) Compromised accuracy due to evaporation of the sweat samples during their transport. Such drawbacks can be addressed using wearable sensors. Diamond's team demonstrated a wearable waistband sodium sensor for on-body potentiometric monitoring of sodium.[11] Additional efforts aimed at on-body monitoring of other electrolytes included measurements of sweat chloride,[34] ammonium,[27] potassium[35] and pH[16] in human perspiration using disposable strip, textile-based, and tattoo-like ISE, respectively. Parallel activity has been devoted lately towards the development of portable wireless transceivers for potentiometric sensors.[36] However these devices have not been applied for on-body electrolyte monitoring.

In the following sections we will describe the design and fabrication of the new epidermal tattoo sodium ISE sensor, along with detailed *in-vitro* characterization of the analytical behavior and mechanical resiliency, followed by on-body testing using healthy individuals during exercise activity in conjunction with the wireless signal transduction. The new skin-worn sodium sensing system has been fabricated by combining thick film, laser

printing, solid state potentiometry, fluidics and tattoo-transfer technologies (Figure 4.2.1). In accordance to the phase-boundary potential theory,[37] the response of the new tattoo sodium sensor depends on the charge separations between the organic phase (membrane) and the aqueous phase (sample). The ionophore-based flexible solid-state Na ISE has been paired with a custom-designed Bluetooth-enabled wireless wearable transceiver, embedded in an adjustable armband, for continuous monitoring of sweat sodium levels directly on the human epidermis. The attractive performance and features of the new sodium tattoo-ISE indicate considerable promise for diverse real-life on-body monitoring applications.

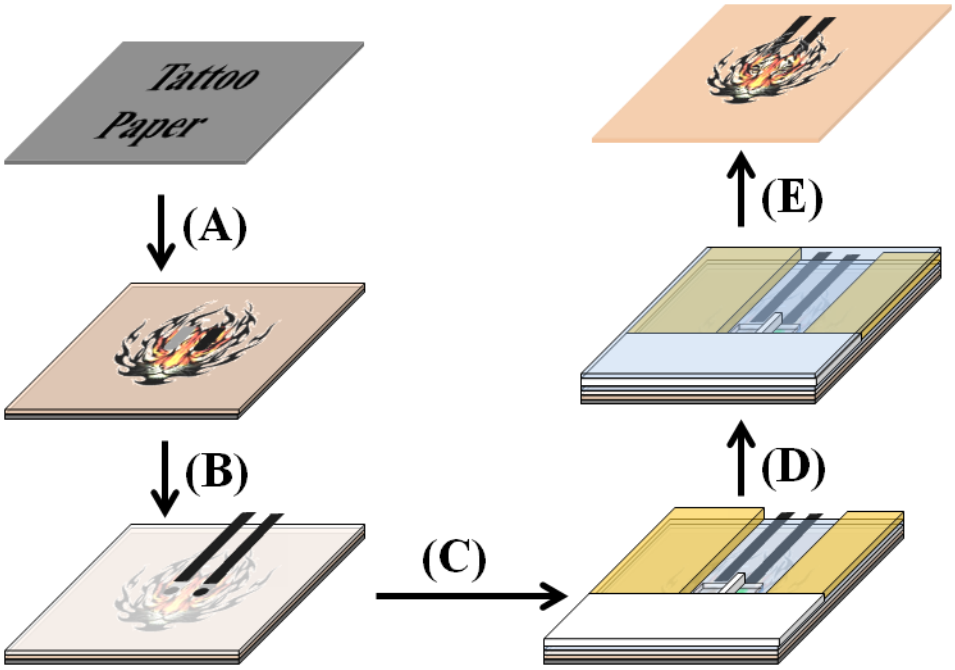


Figure 4.2.1: Schematic showing the fabrication and transfer process for the Na-tattoo sensor. The first step involves (A) screen printing an insulator coating (light gray) on the tattoo paper (dark gray) followed by laser printing the "Tiger Face". (B) Subsequently, a layer of skin color ink is coated and the two electrodes are screen printed. (C) Thereafter another layer of insulator (light gray) is printed to define the electrode area and contact points. For coupling the sensor to the wireless transceiver, flexible carbon coated PET connectors are attached to the printed contact points. (D) The two electrodes are then modified with respective membrane cocktails. Later the "stick-on fluidic channel" (details of fabrication in Fig. S1) is affixed to the Na-tattoo. (E) Finally the Na-tattoo sensor can be applied to the skin similar to any commercial temporary transfer tattoo. (Reprinted with permission from ref. 28. Copyright 2014 Elsevier).

4.2.2 Experimental section

a. Chemicals and reagents:

Selectophore™ grade sodium ionophore X, Bis(2-ethylhexyl) sebacate (DOS), sodium tetrakis[3,5-bis(trifluoromethyl)phenyl]borate (Na-TFPB), polyvinyl chloride (PVC), tetrahydrofuran (THF), and sodium chloride (NaCl), sodium sulfate (Na_2SO_4), sodium bicarbonate ($NaHCO_3$), potassium chloride (KCl), magnesium chloride ($MgCl_2 \cdot 6H_2O$), sodium phosphate anhydrous monobasic (NaH_2PO_4), calcium carbonate ($CaCO_3$) and ammonium hydroxide (NH_4OH) were procured from Sigma Aldrich (St. Louis, MO). Polyvinyl butyral resin BUTVAR® B-98 (PVB) was obtained from Quimidroga (Spain). All reagents were used without further purification. Carbon fibers (8 µm diameter, 6.4 mm length, 93% purity) were purchased from Alfa Aesar (Ward Hill, MA) and further processing was performed to reduce their length to approximately 2 mm; subsequent cleaning in acetone was performed. Ultrapure water was employed in all of the investigations. Chopped carbon fibers were dispersed within both conductive carbon (E3449) and silver/silver chloride (Ag/AgCl) (E2414) inks (Ercon, Inc, Wareham, MA). The carbon fibers were added to these inks, at 1.5% w/w and 1.2% w/w, respectively, to increase the tensile strength of the printed electrodes. Transparent insulator ink (DuPont 5036) was purchased from DuPont (Wilmington, DE). The stencil patterns were designed in AutoCAD (Autodesk, San Rafael, CA) and outsourced for fabrication (Metal Etch Services, San Marcos, CA). Laser temporary transfer tattoo paper kits were obtained from HPS Papilio (Rhome, TX). Artificial sweat comprised of various potential interfering electrolytes, including NaCl, Na_2SO_4, $NaHCO_3$, KCl, NaCl, $MgCl_2 \cdot 6H_2O$, NaH_2PO_4,, $CaCO_3$ and NH_4OH at physiological concentrations (Harvey et al., 2010).

b. Instruments:

Screen printing was performed using an MPM-SPM semi-automatic screen printer (Speedline Technologies, Franklin, MA). Electrochemical characterization was performed at

room temperature leveraging a CH Instruments (Austin, TX) model 630C electrochemical analyzer or a wireless transceiver. Mechanical stress studies were performed using a tensile test machine (Instron® 5900 Series Model 5982, Norwood, MA). The wireless transceiver was custom designed. Details on design and fabrication of wireless transceiver are given in Section S.1 of the Supplementary Data Section. Briefly, the transceiver consisted of an electrochemical analyzer-on-a-chip, an 8-bit low-power microcontroller (MCU, running custom scripts to perform the electrochemical measurements), a Bluetooth v2.1 + EDR 2.4GHz wireless module, voltage regulator, USB battery charger IC, and all associated passive components mounted on a 30 mm x 45 mm printed circuit board (PCB) and was powered by a rechargeable Li-ion 2032 button-cell battery (recharged via a micro-USB connector used for flashing the MCU). Data was relayed at one-second intervals to a Bluetooth-enabled PC via a serial data stream. A spring-loaded pressure connector was leveraged in order to interface with the Na-tattoo epidermal sensor.

c. Tattoo fabrication, modification and transfer process:

The Na-tattoo pattern was superimposed on a laser-printed color rendering of an artistic "*Tiger Face*". The first step consisted of screen printing of a layer of the transparent insulator onto the entire tattoo base paper sheet. This was followed by laser printing a two dimensional array of the "*Tiger Face*" onto the insulator-coated tattoo base paper. Subsequently, a layer of commercial skin-color paint was printed over the entire tattoo sheet and was allowed to dry at room temperature for 2 h. The next steps involved printing the carbon indicator and Ag/AgCl reference electrodes, followed by printing a layer of transparent insulator ink to define the electrode area and contact pads. The contacts for interfacing the Na-tattoo sensor to either the electrochemical analyzer or the wireless transceiver were fabricated via screen printing carbon ink on a flexible polyethylene terephthalate (PET) substrate. The printing process for electrodes and PET contacts has been described earlier.[26] Thereafter, the

region of the PET in contact with the Na-tattoo sensor was completely sealed by a clear nail varnish. This was necessary to avoid the accumulation of sweat in the seams.

The sodium selective membrane cocktail composition consisted of 1 mg sodium ionophore X, 0.55 mg Na-TFPB, 33 mg PVC, and 65.45 mg DOS dissolved in 660 µL of nitrogen-purged THF. The cocktail was thoroughly mixed to dissolve all the components. The reference cocktail was prepared by dissolving 78.1 mg PVB and 50 mg NaCl in 1 mL methanol. The PVB membrane has been recently described.[27] Briefly, the polymeric PVB membrane, containing electrolytes forms a nanoporous structure that allows the exchange of electrolytes with the solution, providing a stable potential, insensitive to changes in the ion concentration over a large concentration range. To build the sensor, 10 µL of the sodium selective membrane cocktail was drop-casted onto the carbon indicator electrode and the reference electrode was modified by 4 µL of the reference cocktail. The modified Na-tattoos were left to dry overnight before their implementation in any of the studies.

During *in-vitro* studies, the Na-tattoo was applied to rigid and elastic substrates in a similar fashion as described earlier.[26] In case of epidermal evaluation of the Na-tattoos, a fluidic channel and sink (*stick-on fluidic channel*) was fabricated atop the Na-tattoo. The *stick-on fluidic channel* directed the sweat to first flow over the two electrodes and then to the sink. In order to apply the Na-tattoo to the epidermis, an inverted U-shaped adhesive layer was applied to the skin. The gap present in the U-shaped adhesive was included for facilitating the replenishment of perspiration over the two electrodes. Thereafter, the transparent protective film present on the *stick-on fluidic channel* (attached to the Na-tattoo) was gently peeled and applied to the aforementioned U-shaped adhesive layer. For continuous sodium monitoring, the user first applies the tattoo sensor, as was described earlier[26] followed by wearing of wireless transceiver such that its contact pads are aligned with that of the Na-tattoo. The data

is then wirelessly transmitted to a notebook for logging and display. The complete fabrication and application of the Na-tattoo ISE to the epidermis is shown in Figure 4.2.1.

d. In-vitro evaluation of the Na-tattoo sensors:

The preliminary in-vitro studies for the Na-tattoo sensors were carried out by using a CH Instruments electrochemical analyzer. The Na-ISE tattoos were applied to rigid plastic substrates to evaluate the change in electromotive force (EMF) across the two electrodes in the presence of different concentrations of NaCl solutions. A similar study was also performed using artificial sweat. Furthermore, a carry-over study was conducted to check reversibility of the Na-tattoo sensors. In this experiment, the Na-tattoo ISE was exposed to NaCl solutions whose concentration alternated between 0.1mM and 10mM. The long term storage stability of the Na-tattoo was examined for a period of 3 weeks using 6 different electrodes. During this period, the sensors were kept in ambient conditions and no special effort was taken to protect these devices from light, dust and other environmental conditions that could be detrimental to the sensor response. In a separate set of studies, Na-tattoo sensors were applied to a Gore-tex^{TM} fabric to analyze the effect of mechanical deformation on sensor response. Subsequently, they were subjected to various mechanical deformation permutations by repeatedly bending, stretching and poking the tattoos on a tensile test machine. During the bending/stretching studies, the Na-tattoo sensor was fixed between two vertical clamps that moved at a predefined speed of 2 mm/s. In the bending study, the Na-tattoo was bent repetitively by 180^0 for a total of 100 cycles and the potentiometric response was recorded after every 20^{th} bending iteration. In case of stretching studies, the Na-tattoo sensor was subject to increasing strain from 0 to a maximum of 26%. The strain was increased after every 20 fatigue cycles for a total of 80 cycles. Similar to the bending study, the Na-tattoo response was measured after every 20 cycles. The poking evaluation on the Na-tattoo sensor consisted of clamping the device to a horizontal mounting stage. The sensor was then repetitively

indented to a depth of 5 mm by a cylindrical probe. The sensor's response was recorded at an interval of 10 poking (indentation) iterations. The effect of temperature variation on tattoo response was also studied over the 30^0C - 40^0C range. The study was performed by incubating the tattoo sensors in varying NaCl solutions at various temperatures.

e. Epidermal Na-tattoo sensor studies:

Epidermal evaluation of the Na-tattoo sensor was performed on ten healthy consenting subjects (between the ages of 20 and 40 years) with no prior history of heart conditions, diabetes, or chronic skeletomuscular pain. The subjects were recruited in response to follow-up from flyers posted within the university. Prior to the study, the subjects were prescreened and a signed consent form was obtained from each individual. The study was performed in strict compliance with the protocol that was approved by the institutional review board (IRB) at the University of California, San Diego. The study was deemed by the IRB as posing "*no greater than minimal risk*". Preceding an on-body test, the Na-tattoo sensor was calibrated with standard NaCl solutions (1, 10 and 100 mM) at 37 ^{0}C. The exercise bout consisted of cycling on a stationary cycle for 30 min followed by a 3 min of cool-down session and another 3 min of complete rest while remaining on the stationary cycle. Ramp mode was selected to insure that subjects perspired during the study. In this mode, the resistance increased every 3 min for the first 21 min followed by a gradual decrease. The absolute resistance level was selected according to subject's fitness level while the same intensity profile was employed throughout the human studies. However, in some cases (involving subjects who took more time to perspire), the exercise bout was extended beyond 30 min. Firstly, the Na-tattoo was evaluated for its performance in real-life situation by applying the Na-tattoo to five random participants and interfacing it with the electrochemical analyzer. The real-time data was collected and logged using the CH instrument software. Upon validating the Na-tattoo response, the next sub-section of the epidermal study consisted of integration of the Na-tattoo

sensor with the wireless transceiver. Before using the wireless transceiver in any human trails, it was first characterized in-vitro for its ability to seamlessly transmit data from the Na-tattoo to a laptop. For this study, a Na-tattoo sensor was applied to a rigid plastic substrate followed by coupling it to the wireless transceiver. The device was tested by preforming calibration and hysteresis studies. During these studies the wireless transceiver transmitted real-time data from the Na-tattoo sensor to a laptop via Bluetooth. Upon completion of its in-vitro evaluation, the transceiver was used for on-body studies. This was achieved by applying the Na-tattoo sensor to the remaining five subjects along with the wireless transceiver. In these cases the data was seamlessly transmitted from the Na-tattoo sensor to a laptop by the wireless transceiver while the subjects perspired on the stationary cycle.

4.2.3 Results and discussion

a. In-vitro Na-tattoo sensor characterization studies:

The composition of the ion selective and reference membranes has been optimized to approach a Nernstian response towards the primary sodium ion while mitigating potential sources of interference. The optimized sodium selective membrane cocktail composition comprised of 1 mg sodium ionophore X, 0.55 mg Na-TFPB, 33 mg PVC, and 65.45 mg DOS dissolved in 660 µL of nitrogen-purged THF. Upon using this composition, the sensor responded instantaneously in a near-Nernstian fashion to varying sodium concentrations over the 0.1 to 100 mM range (slope: 63.75 mV/$\log_{10}[Na^+]$, R.S.D.: 5.77%, n = 6). Figure 4.2.2A displays a typical response of the Na-tattoo sensor obtained during this study. The EMF versus $\log_{10}[Na^+]$ plot reveals that the signal reaches steady-state within 10 s. Such a rapid response is essential for epidermal sensors, aimed at monitoring rapidly changing sodium sweat levels. The long term stability of the Na-tattoos was also studied over a period of three weeks using 6 different tattoo sensors. It was observed that the Na-tattoo maintained its fast response towards

sodium ions with minimal loss in its sensitivity (slope: 60.41 mV/$\log_{10}[Na^+]$; R.S.D.: 5.71%; n = 6) even when kept in the ambient conditions, without any protection from light, moisture and dust. This reflects the resiliency of the Na-tattoos sensor against degradation and indicates that the device requires no special storage conditions. While an offset was observed for all sensors after the three week study, this could be readily addressed by calibrating each sensor prior to its on-body testing, thus ensuring reliable data. Furthermore, a long-term drift of 2.8 mV/h was recorded for the Na-tattoos.

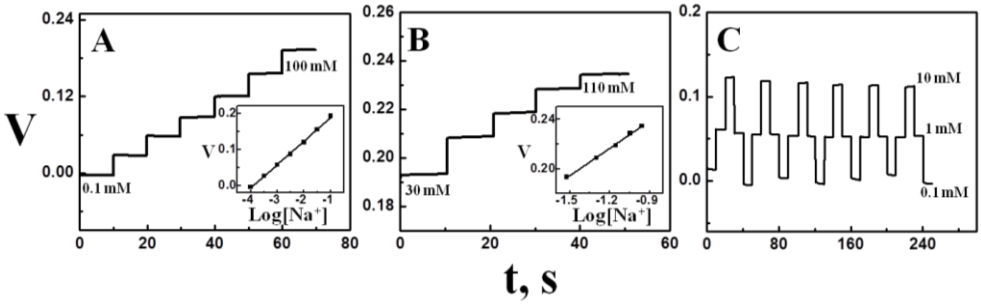


Figure 4.2.2: Response of the Na-tattoo sensor to (A) NaCl solutions (0.1–100 mM range), (B) artificial sweat with increasing sodium concentration (30–110 mM). Insets show the corresponding calibration plots. (C) Carry-over study examining the dynamic response of the Na-tattoo sensor to alternating 0.1, 1 and 10 mM NaCl solutions. (Reprinted with permission from ref. 28. Copyright 2014 Elsevier).

The human sweat contains several interfering electrolytes such as potassium, calcium, magnesium, and ammonium.[29] Thus, it is essential that epidermal sodium sensors perform desirably in the presence of these electrolytes. The selectivity of the Na-tattoo sensor was evaluated in artificial sweat containing physiological levels of potentially interfering electrolytes, while varying the sodium concentration over the physiological range (up to 110 mM).[38] The response displayed in Figure 4.2.2B, demonstrates the Na-tattoo sensor response in artificial sweat. The Na-tattoo sensor displayed a potential drift (in the artificial sweat) of 4.2 mV/min, which can be minimized by further surface modification of the electrode.[39]

Fast reversible interaction between the sensor and the analyte solution is mandatory for obtaining Nernstain response. The sweat sodium concentration commonly fluctuates with

sweat rate.[40] Hence, a reversible and rapid response is an essential requirement for a wearable device for monitoring the dynamics of sweat sodium levels. The reversibility of the Na-tattoo sensor was examined by measuring its response to alternating 0.1, 1 and 10 mM NaCl solutions, using 6 such carry-over cycles over a 4 min period. As illustrated in Figure 4.2.2C, the Na-tattoo sensor displays a nearly-reversible response in the millimolar range. The sensor requires a slightly longer response time for the 0.1mM concentration; this should not affect the sensor performance in real-life scenarios since sodium sweat concentrations are commonly in the millimolar range.

Apart from its ability to accurately detect sodium, the new epidermal ISE must also be able to withstand the rigors of daily human wear. Strain caused due to mechanical deformations, experienced by the epidermis during physical activity, can have deleterious effect on the sensor performance. Therefore the effect of such strains on the Na-tattoo response was evaluated. The sensor was bent repeatedly by 180^0 and its response was measured after every 20 fatigue cycles. Figure 4.2.3A displays the response of the sensor in connection to 100 such bending cycles, while the inset shows a photograph illustrating the extent of mechanical deformation witnessed by the tattoo during this study. Nearly identical calibration plots are observed after each 20 bending cycles (R.S.D.=6.83%), clearly demonstrating that the Na-tattoo ISE can withstand 180^0 repeated bending strain – the maximum a human body can withstand – with only negligible change in its response. Stretching is another strain that the epidermal sensor may experience. The human arm tissue can endure an ultimate failure strain of about 27%,[41] beyond which the tissue ruptures leading to injury. The Na-tattoo sensors were designed to survive such extreme conditions too. As illustrated in Figure 4.2.3B, the Na-tattoo signal is quite stable even when a stretching strain of 26% is applied to the underlying Gore-Tex® substrate. The R.S.D. value for the entire study of 80 stretching cycles was 9.35%. The inset of Figure 4.2.3B shows an image of a stretched Na-

tattoo sensor. It was noticed that when the underlying Gore-Tex® substrate is stretched, the Na-tattoo sensor first stretches with the substrate and on further increasing the strain, it generates corrugates within the tattoo structure to accommodate the excess stress. As a result, minimal tensile stress is experienced by the Na-tattoo sensor. The tattoo can thus withstand such high strains without compromising its sensing properties. Epidermal sensors can also experience mechanical deformations due indentations caused by poking. The response of the Na-tattoo sensor was evaluated against such deformations. The tattoo was thus repeatedly indented to a depth of 5mm with a cylindrical probe and the response was measured after every 10 indentations. As illustrated in Figure 4.2.3C, this study led to a relatively higher R.S.D. of 13%. Such behavior reflects the damage caused by the sharp edges of the cylindrical probe (used for inducing the dents) and not due to the dents themselves. It should be pointed out that such harsh indentations are rarely experienced by the epidermis. Overall, the mechanical deformation studies performed on the Na-tattoos sensor reveal that they maintain their favorable potentiometric response under extreme mechanical stress. We also evaluated the dependence of the Na-tattoo response on the temperature over the 30^0C - 40^0C range. Such range reflects the temperature variation of the human skin.[42] As illustrated in Figure 4.2.4, a small variation in slope of 0.1% was observed.

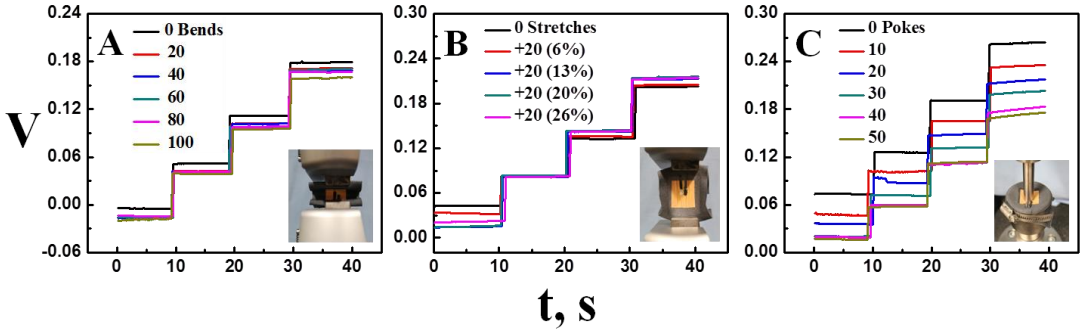


Figure 4.2.3: Effect of (A) bending, (B) stretching and (C) poking stress iterations on the Na-tattoo sensor response for NaCl solutions over the 0.1–100 mM range. Note: In the stretching study, an increasing strain from 0% to 26% was applied after every 20 stretching cycles. (Reprinted with permission from ref. 28. Copyright 2014 Elsevier).

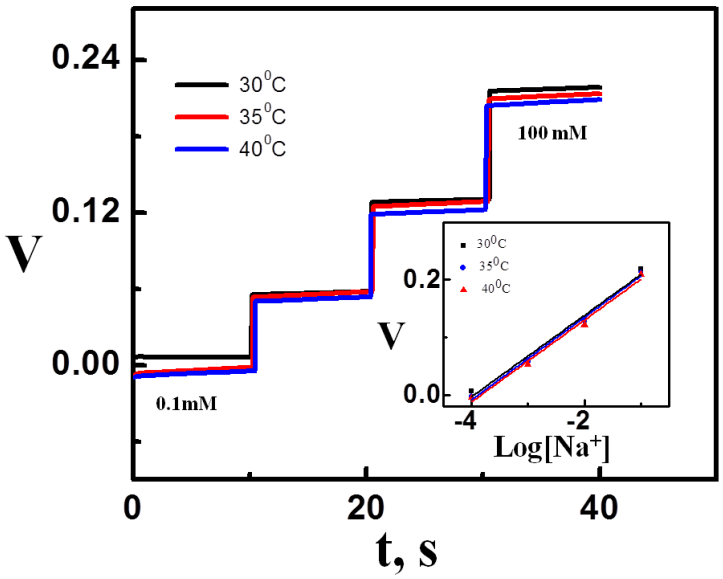


Figure 4.2.4: Effect of temperature on sensor response. (Reprinted with permission from ref. 28. Copyright 2014 Elsevier).

b. On-body characterization of the Na-tattoo sensor:

Preliminary epidermal evaluation of the Na-tattoo was performed by repeatedly pinching and poking the tattoo sensor applied to the deltoid of a human subject (Figure 4.2.5). Visual analysis showed that such deformations have negligible effect on its structural integrity. Subsequently, ten human subjects were recruited for evaluating the on-body performance of the new ISE device. During this study, the tattoo sensor was applied to the right deltoid of each participant. The ability of the sensor for real-time epidermal monitoring of sodium levels in sweat was first examined by interfacing the skin-worn Na-tattoo sensor with a conventional electrochemical analyzer, in a manner similar to our earlier work. Five subjects were randomly selected to participate in this sub-section of the epidermal study. For all subjects, the electrochemical analyzer recorded random fluctuating open circuit potentials till the participant began perspiring, as expected in the absence of sweat. However, sweat formation (and corresponding electrochemical cell completion) resulted in stabilizing the open circuit potential to allow convenient continuous sodium monitoring. Figure 4.2.6A and B

display representative real-time sodium concentration profiles obtained during this study for two different subjects. Note that these tracings do not show the initially recorded random physiologically-irrelevant values obtained before sweating. In most cases, the initial random fluctuating data was followed by a dip in the measured potential when the subject began perspiring (as observed in Figure 4.2.6A and more prominently in Figure 4.2.6B).

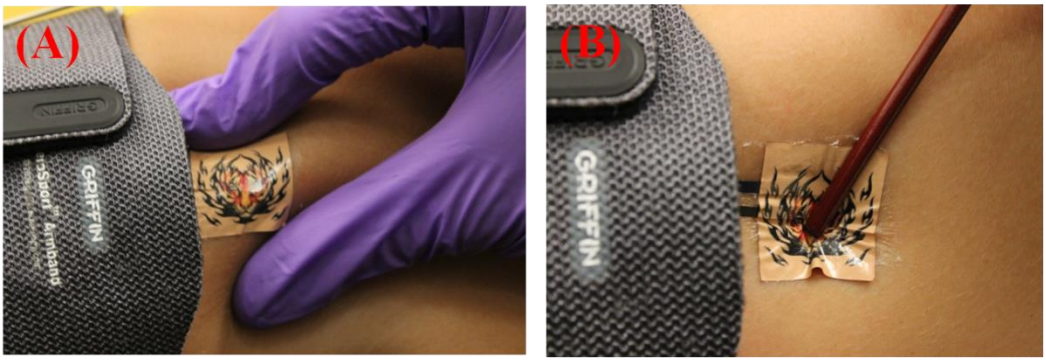


Figure 4.2.5: Photographs showing (A) pinching and (B) poking of the Na-tattoo sensor whist applied to the skin. (Reprinted with permission from ref. 28. Copyright 2014 Elsevier).

Physiologically relevant data was obtained after this point since the fluctuating data before this dip has no physiological relevance. In case of each subject, it was noticed that just the initial glazing of the skin due to sweat formation was sufficient to obtain physiologically relevant data. This can be attributed to the property of the *stick-on fluidic channel* to efficiently direct low amounts of sweat to the two electrodes and thus underscores the ability of the Na-tattoo sensor to detect sodium even during minimal sweating. This is an important feature of the Na-tattoo sensor, particularly for wearers with low sweat rate. As mentioned earlier, the exercise bout involved increasing the intensity level after every 3 min. Due to this incremental mode of workout, the perspiration rate increased with time. Several groups have shown that the sodium concentration in the perspiration increases with increasing sweat rate.[40] (Indeed, a similar trend was observed during the epidermal studies. Figure 4.2.6A and B clearly demonstrates the expected increasing sodium concentration with the course of the study. The study substantiated the ability of the Na-tattoo to respond to the temporal sodium

level in human perspiration. It should be noted that although the overall trend was similar for all the subjects, the exact real-time sweat sodium profile was unique for each subject. This could be because the extent of sodium excretion in perspiration is highly dependent on an individual's genetic predisposition, diet, environmental conditions and ability towards heat acclimatization. However, in all the cases the sodium concentration was within the physiological range.

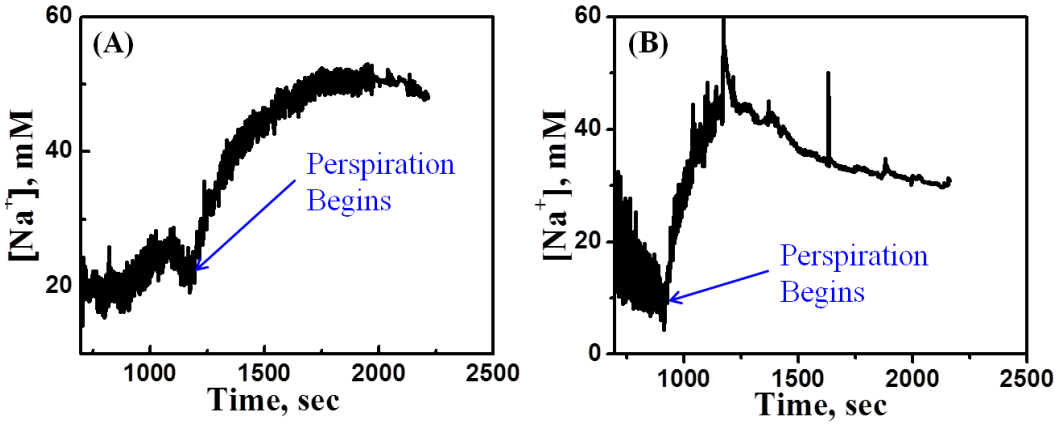


Figure 4.2.6: Real-time monitoring of sweat sodium levels for two subjects over a period of 36 min (30 min exercise activity (cycling) followed by 3 min of cool down and another 3 min of complete rest) by the skin-worn Na-tattoo sensor coupled with an electrochemical analyzer. (Reprinted with permission from ref. 28. Copyright 2014 Elsevier).

The subsequent phase of the epidermal study involved implementing a custom-designed wireless transceiver to relay the real-time potentiometric data generated at the Na-tattoo sensor to a personal computer. Briefly, it consisted of an electrochemical analyzer-on-a-chip, a low-power microcontroller, a Bluetooth wireless module, voltage regulator, USB battery charger IC, on a 30 mm x 45 mm printed circuit board, and was powered by a rechargeable button-cell battery. The wireless transceiver was first evaluated in-vitro by coupling it with a Na-tattoo sensor. Its transduction characteristics were evaluated by performing calibration and carry-over studies (Figure 4.2.7). During these studies, it was noted that the wireless device seamlessly transmitted the analytical data over a distance of 10 m

from the Na-tattoo sensor to a notebook for over an hour of use. Well defined calibration plot (slope: 64.1 mV/$\log_{10}[Na^+]$) with minimal carry over effects are indicated from Figure 4.2.7A and B, respectively. Furthermore, the response of the Na-tattoo sensor was similar to that obtained from the desktop electrochemical analyzer, substantiating the analytical fidelity of the wireless transceiver.

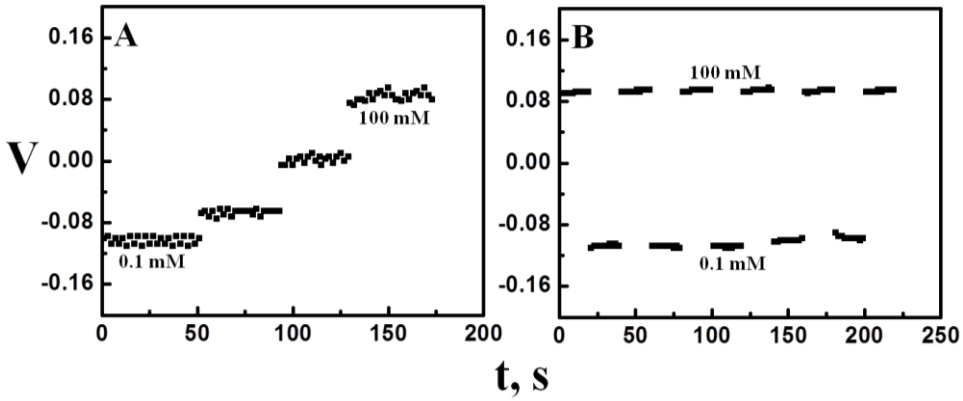


Figure 4.2.7: Wirelessly transmitted analytical sensor response (A) for NaCl solutions of varying concentrations (0.1–100 mM) and (B) during carry-over study using 0.1 and 100 mM NaCl solutions. (Reprinted with permission from ref. 28. Copyright 2014 Elsevier).

For its epidermal evaluation, the Na-tattoo sensor and the wireless device were adorned by each of the remaining five subjects, as shown in Figure 4.2.8A. The inset displays a close-up of the entire device. Figure 4.2.8B displays an image of the wireless transceiver encapsulated in the pocket of an armband while the inset shows the unpackaged system along with a US quarter dollar coin for size comparison. An identical workout regimen (as discussed above) was used in this phase of the epidermal study. Figure 4.2.8C and D displays the transient sweat sodium response for two subjects. Note that these tracings do not show the initially recorded physiologically-irrelevant random values obtained before sweating. An overall increment in the sodium concentration was recorded by the wireless transceiver during the entire course of the exercise bout. The overall trend was comparable to the profile obtained with the conventional electrochemical analyzer. However, as was discussed earlier, the exact

sweat sodium profile for each subject was unique. Furthermore, the wireless transceiver obviated the need for connectors and thus greatly reduced the intrusiveness of the analytical system. The wearable nature of the wireless transceiver makes the entire device quite user friendly without compromising the ability of the sensor to monitor the sodium dynamics, in real time, in the perspiration.

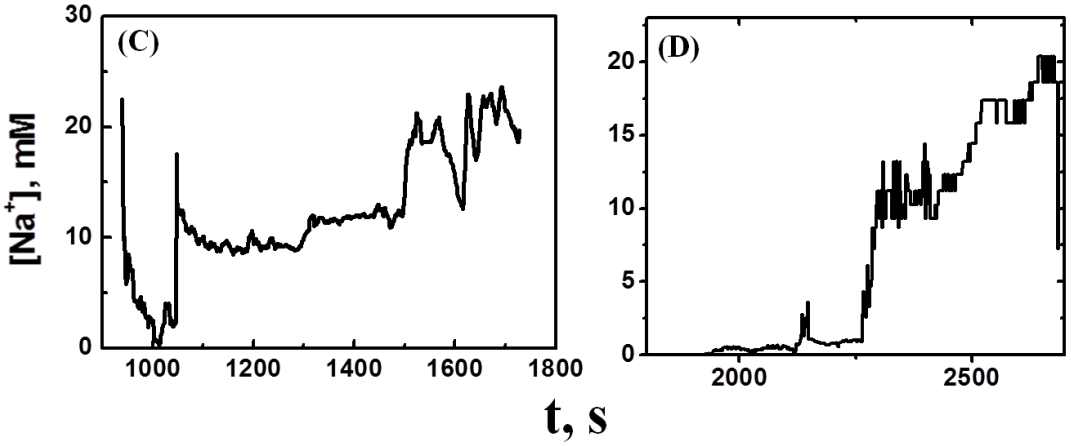


Figure 4.2.8: Photographs of wireless transceiver (A) worn by a subject along with the Na-tattoo (inset: a zoomed image of the entire device), (B) when encapsulated in an armband (inset: image showing a quarter dollar kept close to wireless transceiver for size comparison) and (C, D) Real-time sodium concentration monitoring in sweat by the Na-tattoo coupled with the wireless transceiver for two different subjects. (Reprinted with permission from ref. 28. Copyright 2014 Elsevier).

4.2.3 Conclusions

The work describes the fabrication, in-vitro and epidermal evaluation of a wearable tattoo sensor for continuous sodium monitoring in human perspiration. The tattoo ISE can be coupled with a Bluetooth capable wearable electronic transceiver making the entire device easily worn by an individual, obviating the need for wires for data recording. Extensive in-vitro characterization of the Na-tattoo sensor reveals that the device has a long shelf-life while maintaining its near-Nernstian response. Additionally, the Na-tattoo can survive extreme stress fatigues caused due to bending, stretching and poking. On-body testing during exercise

activity demonstrated the ability of the tattoo potentiometric sensor to monitor sweat sodium dynamics via a wearable wireless transceiver. The wireless nature of the device offers complete freedom to the wearer to perform the workout bout. The Na-tattoo sensing system thus holds considerable promise as a viable device for monitoring sodium in sweat and opens up new avenues in the field of wearable wireless non-invasive sensors and body sensor networks in connection to diverse fitness, military and medical applications. Yet, several challenges, such as minimizing potential drift, integrating temperature sensor (for addressing changes in body temperature), and further miniaturization of the transceiver, need to be met before the realization of such routine real-life applications.

This chapter is based, in part, on the material as it appears in Analyst, 2013, by Amay J. Bandodkar, Vinci W.S. Hung, Wenzhao Jia, Gabriela Valdés-Ramírez, Joshua R. Windmiller, Alexandra G. Martinez, Julian Ramírez, Garrett Chan, Kagan Kerman, and Joseph Wang; in part on the material as it appears in Biosensors and Bioelectronics, 2014, by Amay J. Bandodkar, Denise Molinnus, Omar Mirza, Tomás Guinovart, Joshua R. Windmiller, Gabriela Valdés-Ramírez, Francisco J. Andrade, Michael J. Schöning, and Joseph Wang. The dissertation author was the primary investigator and corresponding author of these papers.

4.3 References

1. Buck, R. P.; Lindner, E. *Anal. Chem.* **2001,** *73*, 88 A.
2. Durst, R. A. *Electroanalysis* **2012,** *24*, 15.
3. Michalska, A.; Maksymiuk, K. *Anal. Chim. Acta* **2004,** *523*, 97.
4. Cho, D.-H.; Chung, K.-C.; Park, M.-Y. *Talanta* **1998,** *47*, 815.
5. Cattrall, R. W.; Freiser, H. *Anal. Chem.* **1971,** *43*, 1905.
6. Bobacka, J. *Electroanalysis* **2006,** *18*, 7.

7. Tymecki, Ł.; Zwierkowska, E.; Koncki, R. *Anal. Chim. Acta* **2004,** *526*, 3.

8. Tymecki, Ł.; Zwierkowska, E.; Głb, S.; Koncki, R. *Sens. Actuators, B* **2003,** *96*, 482.

9. Wang, Y.; Xu, H.; Yang, X.; Luo, Z.; Zhang, J.; Li, G. *Sens. Actuators, B* **2012,** *173*, 630.

10. Novell, M.; Parrilla, M.; Crespo, G. A.; Rius, F. X.; Andrade, F. J. *Anal. Chem.* **2012,** *84*, 4695.

11. Schazmann, B.; Morris, D.; Slater, C.; Beirne, S.; Fay, C.; Reuveny, R.; Moyna, N.; Diamond, D. *Anal. Methods* **2010,** *2*, 342.

12. Windmiller, J. R.; Wang, J. *Electroanalysis* **2013,** *25*, 29.

13. Curto, V. F.; Fay, C.; Coyle, S.; Byrne, R.; O'Toole, C.; Barry, C.; Hughes, S.; Moyna, N.; Diamond, D.; Benito-Lopez, F. *Sens. Actuators, B* **2012,** *171–172*, 1327.

14. Windmiller, J. R.; Bandodkar, A. J.; Parkhomovsky, S.; Wang, J. *Analyst* **2012,** *137*, 1570.

15. Windmiller, J. R.; Bandodkar, A. J.; Valdes-Ramirez, G.; Parkhomovsky, S.; Martinez, A. G.; Wang, J. *Chem. Commun.* **2012,** *48*, 6794.

16. Bandodkar, A. J.; Hung, V. W. S.; Jia, W.; Valdes-Ramirez, G.; Windmiller, J. R.; Martinez, A. G.; Ramirez, J.; Chan, G.; Kerman, K.; Wang, J. *Analyst* **2013,** *138*, 123.

17. Zhang, X.; Ogorevc, B.; Wang, J. *Anal. Chim. Acta* **2002,** *452*, 1.

18. Humpolicek, P.; Kasparkova, V.; Saha, P.; Stejskal, J. *Synth. Met.* **2012,** *162*, 722.

19. Matousek, J. L.; Campbell, K. L. *Vet. Dermatol.* **2002,** *13*, 293.

20. Abell, L.; Adams, P. N.; Monkman, A. P. *Polymer* **1996,** *37*, 5927.

21. Kaiser, D.; Songo-Williams, R.; Drack, E. *Pflügers Archiv 349*, 63.

22. Latzka, W. A.; Montain, S. J. *Clin. Sports Med.* **1999,** *18*, 513.

23. Patterson, M. J.; Galloway, S. D. R.; Nimmo, M. A. *Exp. Physiol.* **2000,** *85*, 869.

24. Morris, D.; Schazmann, B.; Wu, Y.; Coyle, S.; Brady, S.; Fay, C.; Hayes, J.; Lau, K. T.; Wallace, G.; Diamond, D. *Conference proceedings : ... Annual International Conference of the IEEE Engineering in Medicine and Biology Society. IEEE Engineering in Medicine and Biology Society. Annual Conference* **2008,** *2008*, 5741.

25. Kim, D.-H.; Lu, N.; Ma, R.; Kim, Y.-S.; Kim, R.-H.; Wang, S.; Wu, J.; Won, S. M.; Tao, H.; Islam, A.; Yu, K. J.; Kim, T.-i.; Chowdhury, R.; Ying, M.; Xu, L.; Li, M.; Chung, H.-

J.; Keum, H.; McCormick, M.; Liu, P.; Zhang, Y.-W.; Omenetto, F. G.; Huang, Y.; Coleman, T.; Rogers, J. A. *Science* **2011,** *333*, 838.

26. Jia, W.; Bandodkar, A. J.; Valdés-Ramírez, G.; Windmiller, J. R.; Yang, Z.; Ramírez, J.; Chan, G.; Wang, J. *Anal. Chem.* **2013,** *85*, 6553.

27. Guinovart, T.; Bandodkar, A. J.; Windmiller, J. R.; Andrade, F. J.; Wang, J. *Analyst* **2013,** *138*, 7031.

28. Bandodkar, A. J.; Molinnus, D.; Mirza, O.; Guinovart, T.; Windmiller, J. R.; Valdés-Ramírez, G.; Andrade, F. J.; Schöning, M. J.; Wang, J. *Biosens. Bioelectron.* **2014,** *54*, 603.

29. Harvey, C. J.; LeBouf, R. F.; Stefaniak, A. B. *Toxicol. in Vitro* **2010,** *24*, 1790.

30. Rosner, M. H.; Kirven, J. *Clin. J. Am. Soc. Nephrol.* **2007,** *2*, 151.

31. Ladell, W. S. S. *J. Physiol.* **1955,** *127*, 11.

32. Stern , R. C. *New Eng. J. Med.* **1997,** *336*, 487.

33. Lee, N. V. L.; Miller, P. W.; Buono, M. J. *Clin. Physiol. Funct. Imaging* **2010,** *30*, 13.

34. Gonzalo-Ruiz, J.; Mas, R.; de Haro, C.; Cabruja, E.; Camero, R.; Alonso-Lomillo, M. A.; Muñoz, F. J. *Biosens. Bioelectron.* **2009,** *24*, 1788.

35. Guinovart, T.; Parrilla, M.; Crespo, G. A.; Rius, F. X.; Andrade, F. J. *Analyst* **2013,** *138*, 5208.

36. Novell, M.; Guinovart, T.; Steinberg, I. M.; Steinberg, M.; Rius, F. X.; Andrade, F. J. *Analyst* **2013,** *138*, 5250.

37. Bakker, E. *J. Electroanal. Chem.* **2010,** *639*, 1.

38. Bates, G. P.; Miller, V. S. *J. Occup. Med. Toxicol.* **2008,** *3*, 1.

39. Fibbioli, M.; Morf, W. E.; Badertscher, M.; de Rooij, N. F.; Pretsch, E. *Electroanalysis* **2000,** *12*, 1286.

40. Buono, M. J.; Ball, K. D.; Kolkhorst, F. W. *J. Appl. Physiol.* **2007,** *103*, 990.

41. Jacquemoud, C.; Bruyere-Garnier, K.; Coret, M. *J. Biomech.* **2007,** *40*, 468.

42. Rowell, L. B.; Murray, J. A.; Brengelmann, G. L.; Kraning, K. K. *Circ. Res.* **1969,** *24*, 711.

Chapter 5 Printed Wearable Amperometric Sensors

5.1 Wearable lactate sensor

5.1.1 Introduction

Wearable sensors have received considerable attention since they enable continuous physiological monitoring toward maintaining an optimal health status and assessing physical performance.[1] Recent research activity in this rapidly growing field has aimed at addressing the demands of epidermal sensing where durability, lightweight, and intimate skin conformance are core requirements.[2] These endeavors have resulted in a plethora of physical sensor devices for assessing vital signs such as heart rate, respiration rate, skin temperature, bodily motion, brain activity, and blood pressure.[3] However, further progress in this arena has been hindered by the lack of wearable and conformal chemical sensors and biosensors, able to monitor the chemical constituents residing on the epidermis of the wearer's body. Such wearable chemical (bio)sensors could lead to additional important insights into the overall health status than physical variables alone can provide.

The present work demonstrates a noninvasive enzymatic temporary-transfer tattoo biosensor for the continuous monitoring of lactate in human perspiration. Lactate is one of the most important biomarkers of tissue oxygenation, and thus it is of paramount importance for assessing physical performance for sports, military, and health care applications.[4] During intense physical activity, the usual aerobic metabolism is incapable of satisfying the energy demands of the human body. This is especially true in endurance-based activities such as the triathlon, cycling, or boxing. In such instances, the anaerobic process is invoked wherein the

stored glycogen is consumed to produce energy and lactate by muscle cells. This process is known as “glycolysis” or “lactate acidosis” and involves increased lactate levels in the blood.[5]

Lactate has thus been widely used by coaches, exercise physiologists, and sports physicians to monitor an athlete’s performance, particularly in connection to intensive and endurance-based activities.[6] Several lactate sensor strips, which rely on finger-stick blood draws, are commercially available. However, an inherent drawback of these sensors for sport and military applications is their intrusiveness and inconvenience, especially during physical activity/exercise. To obtain a temporal lactate profile, the subject’s blood is usually collected repetitively at brief time intervals while the athlete engages in rigorous training; this approach invariably hinders performance. This study seeks to tender useful information regarding an athlete’s metabolic response to controlled physical activity by offering useful insights into the temporal dynamics of lactate concentration in the perspiration in a completely noninvasive manner.

Sweat lactate is a function of eccrine gland energy metabolism; an increase in the exercise intensity leads to increased production of sweat lactate.[7] Perspiration may thus be conveniently utilized for the analysis of physical performance in individuals without the need for an invasive blood sampling approach.[8] Sweat lactate can also serve as a sensitive marker of tissue viability and may provide warning for pressure ischemia, reflecting the insufficient oxidative metabolism and a compromise of tissue viability.[9] Researchers have indeed made efforts to develop noninvasive systems for measuring lactate in perspiration.[10] However, these systems mandate the use of patches for sweat collection followed by laboratory analysis of the samples for lactate levels. Such processing is cumbersome and does not provide instantaneous feedback regarding dynamic fluctuations in lactate concentration. In the personalized healthcare field, especially in the sports/athletics/fitness domains, one requires a rapid and user-centric approach to analyze samples for efficient assessment. Hence, body-worn and

easy-to-use sensing devices are highly desired for the continuous assessment of lactate. Khodagholy et al. recently demonstrated an electrochemical transistor-based patch that could possibly be leveraged for sweat lactate sensing directly on the human epidermis.[11] However, no real-time, on-body perspiration lactate sensing study was conducted by the researchers.

In the present work, we demonstrate a noninvasive enzymatic temporary-transfer tattoo electrochemical biosensor for the continuous assessment of lactate levels in human perspiration.[12] In particular, the new device aims at yielding useful insight into the temporal dynamics of sweat lactate production during controlled physical activity. The development of epidermal biosensors for lactate monitoring builds on our promising recent introduction of temporary transfer tattoo-based electrochemical sensors.[13] These flexible tattoo sensors, fabricated via conventional screen printing methods, conform to the contours of the body and display resiliency toward extreme mechanical stresses expected from physical activity due to the presence of dispersed carbon fibers within the screen printed inks. The new epidermal lactate biosensor, displayed in Figure 5.1.1, consists of a mediated lactate oxidase (LOx) working electrode, prepared by functionalizing the surface of the printed tattoo electrode with tetrathiafulvalene (TTF) and multiwalled carbon nanotubes (CNT), followed by tethering the LOx enzyme, and a biocompatible chitosan overlayer. The latter prevents the efflux of the biochemical backbone from the reagent layer onto the underlying epidermis. The resulting tattoo lactate biosensor was evaluated extensively for its capability to withstand repeated iterations of mechanical deformations relevant to the wearer's daily activity. Additionally, its analytical figures of merit have been characterized. Finally, in order to validate the concept, the lactate biosensor was applied to the skin of human subjects, who were asked to endure prolonged physical exercise (cycling); the corresponding sweat lactate temporal profiles were recorded via amperometric methods. Simultaneous assessment using control epidermal tattoo sensors (lacking the LOx enzyme) confirmed the high specificity toward sweat lactate. The

temporal lactate profiles demonstrate that the new wearable lactate biosensor platform performs desirably under fitness routines, thereby substantiating its utility for the noninvasive assessment of lactate levels and degree of physical exertion. Such design, characterization, and in vivo evaluation of the new printed temporary transfer tattoo epidermal lactate biosensor are described in the following sections.

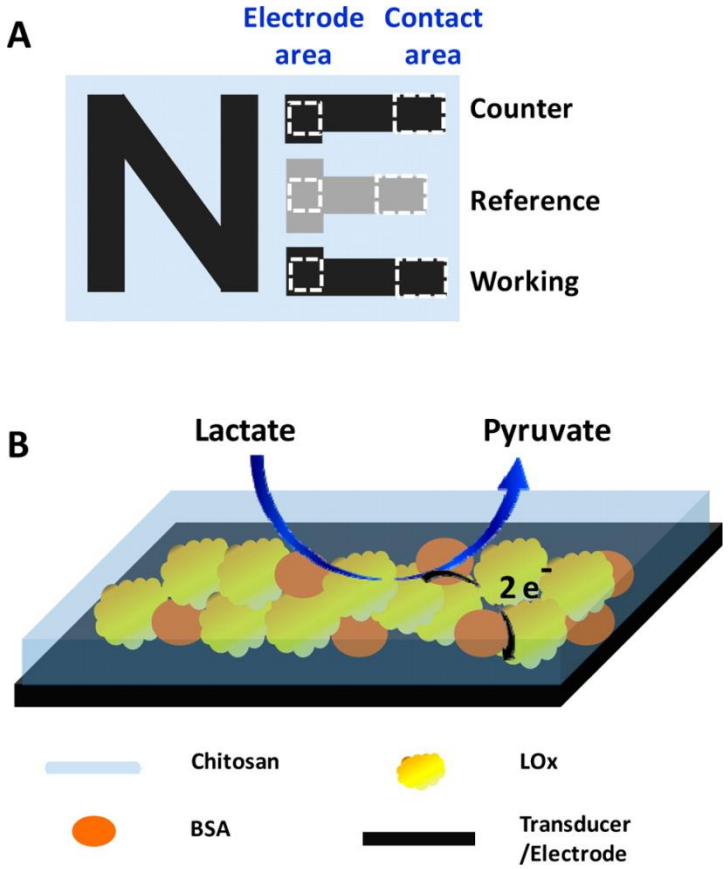


Figure 5.1.1: (A) Schematic illustration of a three-electrode "NE" tattoo biosensor for electrochemical epidermal monitoring of lactate. (B) Constituents of the reagent layer of the working electrode which is coated by biocompatible polymer (chitosan). See the text for further details. (Reprinted with permission from ref. 12. Copyright 2015 American Chemical Society.)

5.1.2 Experimental section

a. Reagents and instrumentation:

Glutaraldehyde solution (8%), tetrathiafulvalene (TTF), chitosan, acetic acid, bovine serum albumin (BSA), L-lactic acid, sodium phosphate monobasic (NaH_2PO_4), sodium phosphate dibasic (Na_2HPO_4), D(+)-glucose, L(+)-ascorbic acid, uric acid, and creatinine were obtained from Sigma-Aldrich (St. Louis, MO). L-Lactate oxidase (LOx) (activity, 101 U/mg) was procured from Toyobo Corp. (Osaka, Japan). Carboxy-functionalized multiwalled carbon nanotubes (CNT) were purchased from cheaptubes.com (Brattleboro, VT). All reagents were used without further purification. Carbon fibers (8 μm diameter, 6.4 mm length, 93% purity) were purchased from Alfa Aesar (Ward Hill, MA), and further processing was performed to reduce their length to approximately 2 mm; the carbon fibers were subsequently rinsed with acetone. Electrochemical characterization was performed at room temperature using a CH Instruments electrochemical analyzer (model 1232A, Austin, TX). The applied potentials in all measurements were versus the screen-printed pseudo Ag/AgCl reference electrode.

b. Temporary transfer tattoo fabrication, electrode modification and transfer process:

An "NE" logo, acronym for "NanoEngineering", was utilized for the design of the sensor (Figure 5.1.1A). The fabrication process of the tattoo is similar to our earlier work with slight modifications. Briefly, chopped carbon fibers were dispersed within both conductive carbon (E3449) and silver/silver chloride (E2414) inks (Ercon Inc., Wareham, MA) to 1.5 and 1.2 wt % levels, respectively, to increase the tensile strength of the electrodes. Sensor patterns were designed in AutoCAD[14] (Autodesk, San Rafael, CA) and outsourced for fabrication on stainless steel through-hole 12 in. × 12 in. framed stencils (Metal Etch Services, San Marcos, CA). Papilio temporary transfer tattoo base paper was purchased from HPS LLC (Rhome, TX). A sequence of the aforementioned carbon, silver, and insulator (Dupont 5036, Wilmington, DE) inks were patterned on the substrate employing an MPM-SPM semiautomatic screen printer (Speedline Technologies, Franklin, MA). As shown in Figure 5.1.1A, the "E" portion of the tattoo sensor design consists of a pseudoreference

(silver/silver chloride ink), counter and working electrodes (carbon ink). A transparent insulator was screen printed on the surface of the electrode pattern to confine the electrode and contact areas. Following every screen printing step, the printed pattern on the temporary transfer tattoo paper was cured at 90 °C for 15 min in a convection oven.

Following the printing of the tattoo electrode transducers, the working electrode was functionalized with the reagent layer. CNT were first suspended in ethanol (5 mg mL^{-1}) and sonicated for several hours until a uniform suspension was achieved. The suspension was subsequently mixed with a 0.1 M TTF ethanol/acetone (9:1 (v/v)) solution, using a volume ratio of 2:1 and sonicated for 1 h. A volume of 3 μL of the CNT/TTF suspension was subsequently cast onto the open area of the working electrode and was allowed to air-dry. Following this, 3 μL of LOx solution (40 mg mL^{-1} with 10 mg mL^{-1} of the BSA stabilizer) was cast on the electrode and dried under ambient conditions; this surface was later covered with 2 μL of a 1 wt % chitosan solution prepared in 1 wt % acetic acid. The electrodes were finally cross-linked with glutaraldehyde vapor in a sealed chamber and maintained at 4 °C overnight.

The temporary tattoo transfer process has been previously reported.[13] The one used in this study was identical with a minor modification made, a gap (12 mm × 3.5 mm) was included around the electrode area (between the tattoo and the skin) to facilitate the flux of fresh perspiration over the sensor for proper replenishment essential for continuous epidermal evaluation. With respect to in vitro amperometric measurements, the tattoos were applied to the substrate such that their functionalized side faced upward. In contrast, during epidermal evaluation, the functionalized side faced downward (making contact with the epidermis).

c. In vitro evaluation:

The electrochemical performance of the tattoo lactate sensor was evaluated in vitro by transferring it onto a rigid plastic substrate or onto a flexible GORE-TEX textile for

mechanical integrity studies. These studies were performed using a 0.1 M phosphate buffer (pH 7.0) solution. The operating potential for the tattoo lactate sensor was selected by using linear sweep voltammetry with a scan rate of 1 mV/s from −0.2 to 0.2 V using 8 mM lactate. The amperometric response was recorded after a 1 min incubation in the sample solution, using a potential step to +0.05 V (vs Ag/AgCl) for 60 s. Mechanical strain studies were performed with the transferred tattoo sensor on a GORE-TEX textile to emulate the viscoelastic properties of the skin. The biosensor was thus stretched ∼10% and bent at 90° for 5 s followed by subsequent relaxation for another 5 s. The bending/stretching and subsequent relaxation of the sensors was iterated 10 times after which the response to 8 mM lactate was measured. The sensor specificity was examined in the presence of physiological levels of the relevant constituents of human sweat, namely, 84 μM creatinine, 10 μM ascorbic acid, 0.17 mM glucose, and 59 μM uric acid.[15]

d. Epidermal lactate sensing:

The epidermal biosensor evaluation was performed in strict compliance with the protocol that was approved by the institutional review board (IRB) at the University of California, San Diego. The study was deemed by the IRB as posing “no greater than minimal risk” to the prescreened subjects who were recruited for the investigation. A total of 10 healthy volunteers (7 males and 3 females between the ages of 20 and 40, recruited in response to follow-up from flyers) with no prior medical history of heart conditions, diabetes, or chronic skeletomuscular pain were recruited for participation in the study, and informed, signed consent was obtained from each individual following a rigorous prescreening procedure. A tattoo lactate sensor was applied on the volunteer’s deltoid in order to assess the real-time lactate concentration profile. Rectangular sections of polyethylene terephthalate (PET) (3 mm × 18 mm), screen-printed with carbon ink, were attached to the tattoo contact pads (using conductive silver epoxy); this was used as a low-noise interface to the

electrochemical analyzer, in connection to fine stainless steel wires. The lactate response was recorded using amperometry at a low potential of +0.05 V (vs Ag/AgCl), which substantially reduces the possibility of electric shock due to the diminished electromotive force. Moreover, the potentiostat was configured with a current limit of 100 μA (the threshold for human perception and maximum safe level recommended by the U.S. National Electric Code) in order to diminish the chance of electric shock (Safety note: It is highly advised that the amperometric measurement apparatus bevoltage- and current-limited in order to reduce the likelihood of unintentional electric shock). In order to validate the selectivity of the biosensor to oxidize lactate, two temporary transfer tattoos were applied on the subjects' deltoid, one containing the LOx enzyme and the other absent of this enzyme.

Subjects were asked to mount a stationary cycle and begin cycling at a steady, comfortable cadence. Subjects were instructed to maintain their cadence while an increasing resistance was applied at 3 min intervals. The absolute resistance level was selected according to subject's fitness level while the same intensity profile was used throughout the human studies. This ensured that the anaerobic metabolism was invoked at similar time scales, hence augmenting the excretion of lactate in the perspiration in a controlled fashion. Following the intense fitness bout, the volunteers were asked to gradually reduce their cadence during a 3 min "cool-down" period whereby the resistance was reduced from maximal levels.

5.1.3 Results and discussion

a. Rationale for CNT/TTF/LOx/Chit surface functionalization:

The lactate concentration of the human sweat depends on a person's metabolism and physical performance and usually varies up to 25 mM.[16] Thus, a wide linear detection range coupled with a fast response time is essential for continuous epidermal monitoring of lactate. The tattoo sensors have been designed to meet these requirements, while eliminating the risk

of skin exposure to the constituents of the reagent layer (and potential toxic effects). Typical lactate biosensors utilize lactate dehydrogenase (LDH) or lactate oxidase (LOx). However, LDH requires the NAD^+ cofactor, which represents a noteworthy challenge for continuous noninvasive monitoring applications. LOx-based amperometric detection of lactate commonly requires a relatively high potential (>+0.65 V) in order to monitor the liberated peroxide product and is subject to potential electroactive interferences. Mediators, such as TTF, have been used to address such interferences by facilitating the low-potential electrocatalytic conversion of lactate by LOx.[17] TTF has been widely used as a mediator for biosensor applications and was shown not to cause skin irritation.[18] To improve the efficiency of the mediated tattoo lactate biosensor, CNT were dispersed together with TTF to serve as an effective electron transducer on the working electrode. The CNT/TTF complex was employed previously as an efficient electron shuttle.[19] Furthermore, given the goal of continuous epidermal usage of the tattoo sensor, the CNT/TTF/LOx reagent layer was coated with a biocompatible chitosan overlayer that functioned as a physical barrier and limited the efflux of the catalytic backbone from the tattoo onto the underlying epidermis.

b. In vitro evaluations:

To determine the operating potential of the tattoo sensor, linear sweep voltammetry was employed first in the presence and absence of lactate in buffer. The sensor displayed an onset potential of ∼−0.15 V with a peak around +0.05 V (vs Ag/AgCl) for the oxidation of lactate (not shown), indicating that the CNT/TTF/LOx/Chit reagent layer offers low potential lactate oxidation. Such low potential oxidation reflects the efficient electron donor–acceptor interaction of CNT/TTF,[20] which supports the shuttling of electrons between the redox center of the enzyme and the electrode surface. A potential step to +0.05 V (vs Ag/AgCl) was thus selected for all subsequent chronoamperometric measurements. The dynamic concentration range in response to increasing levels of lactate was subsequently investigated. Figure 5.1.2A

displays chronoamperograms obtained with the LOx-functionalized tattoo sensor for increasing lactate concentrations at 1 mM increments in 0.1 M phosphate buffer (pH 7.0). The tattoo sensor exhibits a well-defined lactate concentration dependence, with a highly linear response throughout the 1 mM to 20 mM range, beyond which a very slight curvature is observed (Figure 5.1.2B). Notice that the lactate concentration in human sweat usually varies to maximal levels of 25 mM.[16] The linear dynamic range is characterized with high sensitivity (slope, 644.2 nA/mM or 10.31 μA/mM cm^2; correlation coefficient, 0.996). Such high sensitivity is indicated also from the well-defined response to 1 mM lactate (Figure 5.1.2A) and the corresponding low noise level.

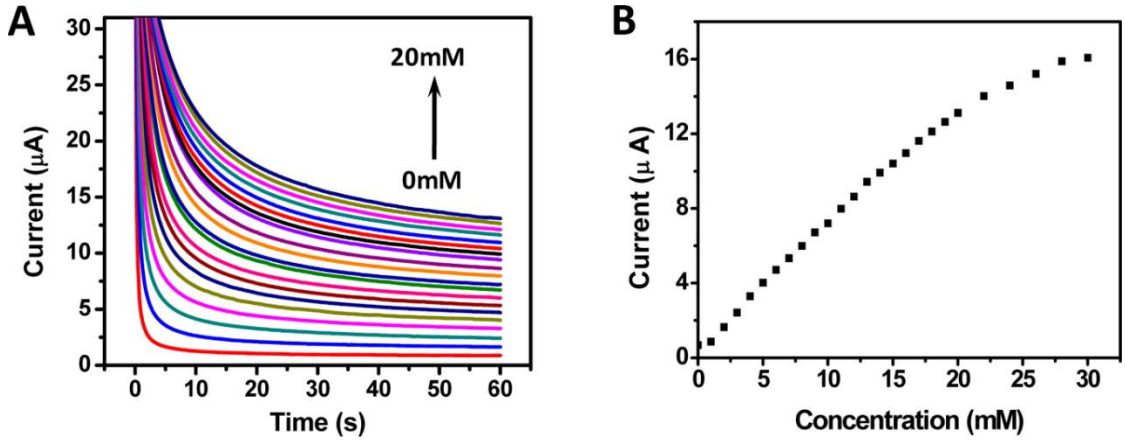


Figure 5.1.2: (A) Amperometric response for increasing concentrations of lactate (1 mM increments) over the 0–20 mM range; Eapplied = +0.05 V (vs Ag/AgCl). (B) Calibration plot up to 30 mM lactate, based on sampling the current at 60 s. (Reprinted with permission from ref. 12. Copyright 2015 American Chemical Society.)

Practical continuous monitoring applications of the new epidermal lactate biosensor paradigm require high operational stability during prolonged periods of operation. The stability of the tattoo biosensor was examined from the response to 8 mM lactate over an 8 h period, wherein the response of the tattoo sensor was recorded every 30 min. As illustrated from the repetitive chronoamperograms provided in Figure 5.1.3A, the lactate biosensor yields highly reproducible results (RSD = 3.60%), thus underscoring its applicability for long-term epidermal use. The highly stable response reflects the integrity of the tattoo biosensor and the

constituents of its reagent layers, benefit from the water-insoluble TTF mediator, the BSA enzyme stabilizer, a protective chitosan overcoating, and the glutaraldehyde cross-linker. Apparently, changes in the sweat pH and lactate levels have no apparent effect upon the enzyme activity, reflecting the "protective action" provided by the constituents of the reagent-layer. The shelf life of the biosensor was also examined for the ones stored at 4 °C for a period of 5 months. The responses of the biosensor remained stable during this prolonged storage period, with less than a 10% decay of the sensitivity.

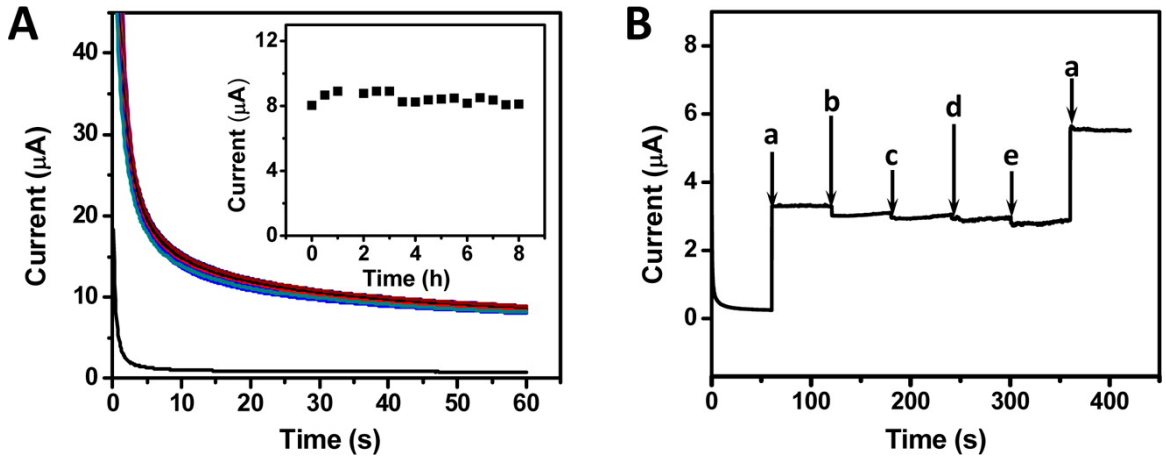


Figure 5.1.3: (A) Stability of the response of the tattoo biosensor to 8 mM lactate at 30 min intervals over a 8 h period. The inset is the corresponding current–time plot of the chronoamperometric response. The tattoo sensor kept at ambient conditions between such successive runs. (B) Selectivity study: Response to (a) 4 mM lactate, (b) 84 μM creatinine, (c) 10 μM ascorbic acid, (d) 0.17 mM glucose, and (e) 59 μM uric acid at +0.05 V (vs Ag/AgCl). (Reprinted with permission from ref. 12. Copyright 2015 American Chemical Society.)

The specificity of the biosensor was further examined by considering that perspiration consists of a plethora of metabolites and electrolytes. Among these constituents, ascorbic acid, uric acid, glucose, and creatinine can affect the response of the sensor and lead to inaccurate readings. The tattoo biosensors were thus evaluated in the presence of these interfering agents at physiological levels found in the perspiration. As shown in Figure 5.1.3B, the device responds favorably and rapidly to 4 mM lactate, while the contributions imparted by the selected interfering agents were negligible (less than 5% compared to the response associated

with lactate). The high selectivity is also illustrated below from control experiments employing an epidermal sensor lacking the LOx enzyme. Such high selectivity reflects the low operating potential and the composition of the reagent layer.

The human epidermis regularly experiences deformations due to bodily movements. Such epidermal deformations are a major cause of concern for wearable devices wherein the devices undergo disfigurations similar to the skin. This is especially true for epidermal sensors since these devices contact the epidermis directly. As the human body engages in locomotion, the epidermal layer can undergo bending, stretching, and twisting stresses. Accordingly, the robustness of the temporary transfer tattoo sensor was evaluated by applying it to flexible GORE-TEX textile. The temporary transfer tattoo sensor was flexed to a 90° angle for 120 iterations; the sensor response was recorded every 20 bending iterations. This was followed by stretching the same sensor by 10% for a total of 80 iterations; data was recorded every 10 stretching iterations. Each bending/stretching cycle consisted of bending or stretching for 5 s followed by a 5 s relaxation period. As indicated from Figure 5.1.4, the response of the temporary transfer tattoo sensor in both the bending (part A) and stretching (part B) studies remained highly uniform, and the corresponding normalized data (parts C and D) are highly stable with an RSD of 1.24% and 1.50%, respectively. The minimal deviation of the sensor response even after subjecting it to a large number of stress cycles can be attributed to the dispersed carbon fibers within the carbon and Ag/AgCl inks, which provide an interleaved conductive backbone. The transparent insulator, covering most of the sensor surface, further enhances the structural integrity (by facilitating adhesion among the printed pattern). As will be illustrated in the following epidermal evaluations, the resulting temporary transfer tattoo lactate biosensor performs desirably in the face of various mechanical stressors characteristic to epidermal operation.

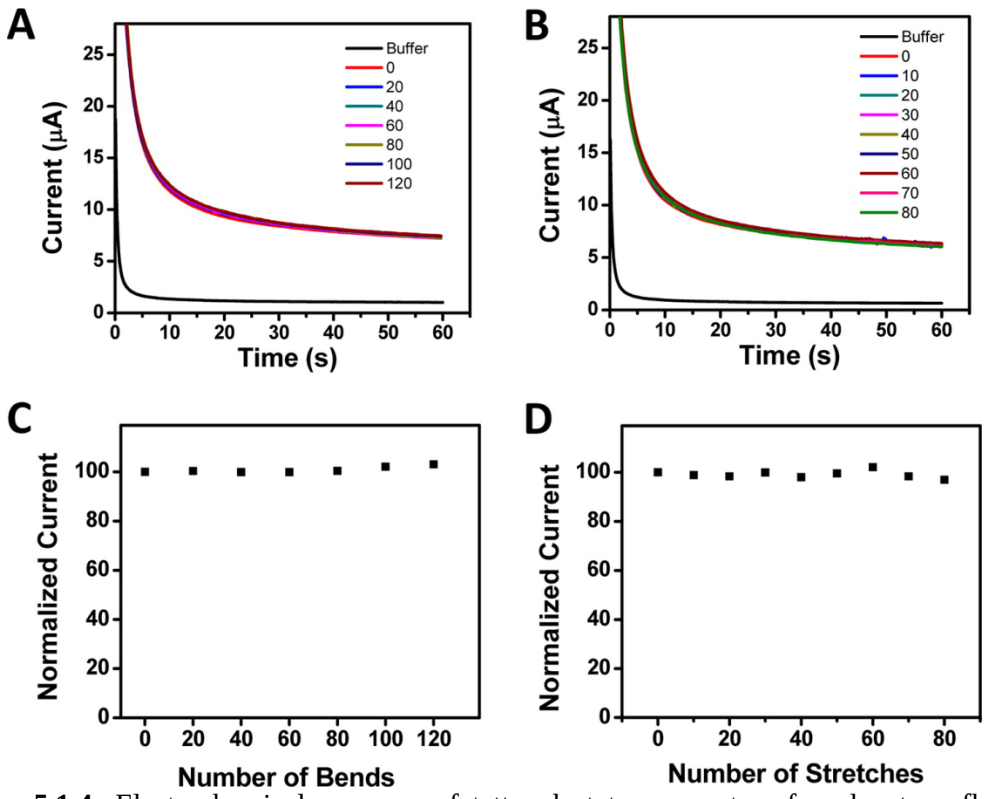


Figure 5.1.4: Electrochemical response of tattoo lactate sensor transferred onto a flexible GORE-TEX textile undergoing repeated bending (A) and stretching (B) to 8 mM lactate at +0.05 V (vs Ag/AgCl) and their normalized current (C) and (D), respectively. (Reprinted with permission from ref. 12. Copyright 2015 American Chemical Society.)

c. Epidermal evaluation:

Prior to epidermal lactate-sensing evaluation, the temporary transfer tattoo biosensors were examined for their ability to adhere to the epidermal surface under various forms of mechanical strain. Visual evaluation of a temporary transfer tattoo biosensor on the human neck region was performed in connection to different strain deformations. The device underwent repeated stretching, bending, and twisting stressors for a total of 100 iterations each. Figure 5.1.5 displays images of the sensor during these studies. The left column provides a top-view of the device during the various deformations. The right column displays photos of the devices at the conclusion of each study. The images clearly demonstrate that the tattoo biosensors are quite resilient to these flexions.

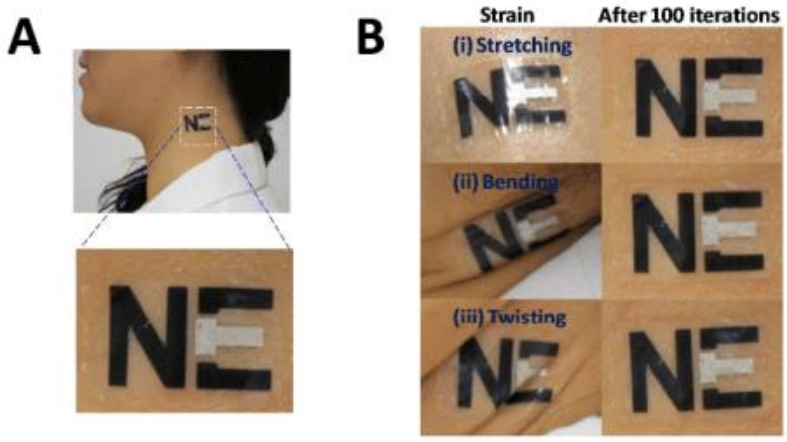


Figure 5.1.5: Photos of a bare 'NE' tattoo on a human neck (A) endured by mechanical strain tests (B) during and subsequent to 100 stretching (i), bending (ii) and twisting (iii) iterations. (Reprinted with permission from ref. 12. Copyright 2015 American Chemical Society.)

Proceeding with the operational characterization of the devices under practical scenarios, real-time epidermal lactate levels in 10 consenting subjects (recruited in strict compliance with IRB protocols delineated in the Experimental Section) were monitored utilizing the temporary transfer tattoo biosensors. Dynamic changes in sweat lactate levels were thus measured continuously during a 30 min bout of intense cycling while the exercise resistance/intensity was adjusted in pre-established intervals. Specifically, in order to ensure that the anaerobic metabolism was invoked, subjects were asked to mount a stationary cycle and maintain a steady cycling cadence while the resistance/intensity profile, illustrated in Figure 5.1.6A, was instituted. The temporary transfer-tattoo biosensor was applied to the volunteer's right deltoid (Figure 5.1.6B), and a custom-designed thin-film flexible connector was utilized to interface the three-electrode biosensor with a hand-held electrochemical analyzer. Medical grade adhesive was utilized to secure the electrical connection to the surface of the sensor connectors. In order to validate the ability of the biosensor to monitor lactate selectively, two temporary transfer tattoos were applied simultaneously on the subjects' deltoid in close vicinity, one containing the LOx enzyme and the other absent of this enzyme (serving as the control).

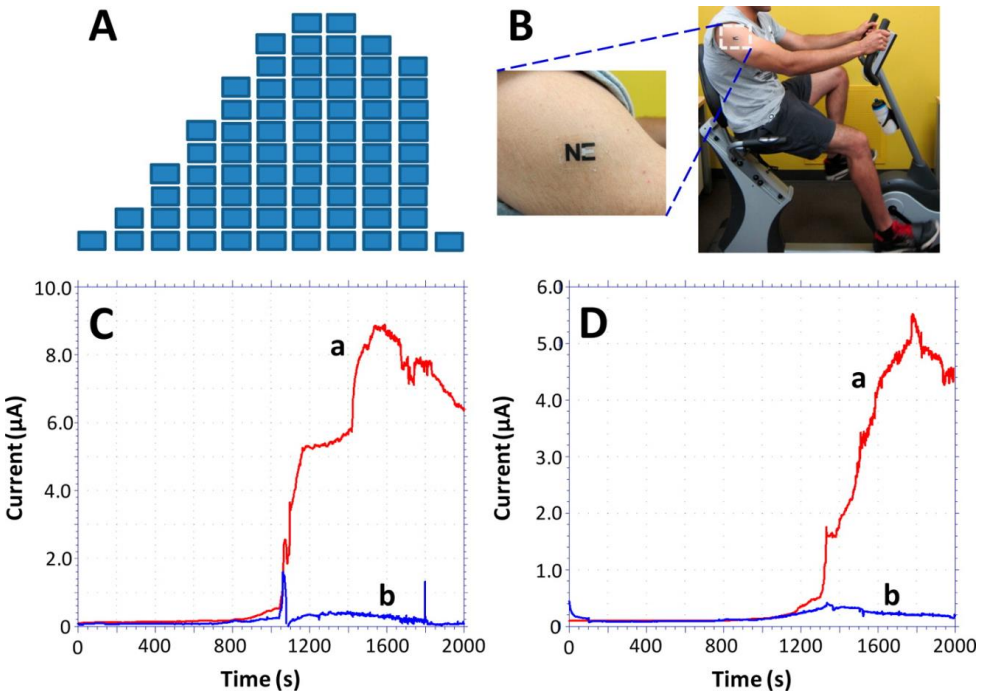


Figure 5.1.6: Monitoring of sweat lactate during 33 min of cycling exercise while changing the work intensity. (A) Exercise resistance profile on a stationary cycle. Subjects were asked to maintain a constant cycling rate while the resistance was increased every 3 min for a total evaluation of 30 min. A 3-min cool down period followed the exercise. (B) An "NE" lactate biosensor applied to a male volunteer's deltoid; (C and D) Response of the LOx- (a) and enzyme-free (b) tattoo biosensors during the exercise regimen (shown in part A) using two representative subjects. Constant potential, +0.05 V (vs Ag/AgCl); measurement intervals, 1 s. (Reprinted with permission from ref. 12. Copyright 2015 American Chemical Society.)

Figure 5.1.6C,D displays the continuous raw amperometric data (screen captures from the recording instrumentation without any postprocessing) of two representative subjects, among the larger group of volunteers. In each figure, the output of the LOx-functionalized (a, red) and control "enzyme-free" (b, blue) tattoo biosensors are overlaid. As indicated from these plots, unlike the control sensors, the LOx-functionalized biosensors displayed facile biocatalytic ability toward lactate oxidation in the perspiration. Moreover, the background current level and the corresponding noise level are minimal. The extremely low noise level, observed directly on the body, reflects the quality of the amperometric signal transduction and corresponding electrical contacts. During the initial period of the cycling exercise, no apparent faradaic current is observed at both electrodes, reflecting the lack of perspiration present on

the epidermis. As the exercise ensued, the skin became moist (albeit sweat formation was not yet observed), imparting electrical conductivity at the sensing surface, thereby contributing to the slow current rise observed at 850 and 1150 s, for subjects C and D, respectively. Additional sharper increases in the background current are observed only at the moment that the subject began to perspire (around 1000 and 1250 s for subjects C and D, respectively). At this point, owing to an electrolytic fluid (sweat) covering the biosensor surface, the lactate level could be assessed. Furthermore and more interestingly, for subject C, a lactate threshold, corresponding to the buildup of lactate in the perspiration at the transition from aerobic to anaerobic respiration, is clearly observed at ∼1450 s.[21] Subject D, on the other hand, a notably less "fit" individual, demonstrated such a transition earlier in their fitness routine, shortly after the onset of sweating at ∼1350 s. It should be noted that for both cases, the observed temporal profiles, corresponding to instantaneous lactate readings in the perspiration, reflect the resistance/intensity profile (of Figure 5.1.6A) and hence substantiate that the sweat lactate levels change dynamically in response to varying levels of physical exertion. Similar current–time profiles were obtained among the other subjects, all of whom demonstrated the onset of the lactate threshold during the controlled fitness routine, albeit at different time scales, reflective of their respective aerobic capacity.[22] The final stage (over the last 3 min) of the controlled exercise bout consisted of a cool-down. During this period, the subjects cycled with less intensity and were encouraged to reduce their cadence to a comfortable rate.

The epidermal amperometric data, shown in Figure 5.1.6C,D, reveal a similar pattern where a slight decrease in the signal is observed during the cool-down period, hence substantiating that the observed epidermal lactate profiles closely track the exercise intensity with near instantaneous response. In contrast, the "control" tattoo sensors (without LOx) worn by the two subjects display negligible current fluctuations throughout the entire exercise regimen (b), reflecting the absence of biocatalytic activity. The lack of response at the

"enzyme-free" sensors is also indicative of the remarkable selectivity of the tattoo sensing device and its intrinsic ability to address potential interference from electroactive constituents present in the perspiration. The results, therefore, clearly support that the profiles observed at the LOx-functionalized temporary-transfer tattoo biosensors are solely due to dynamic changes in sweat lactate levels associated with the exercise intensity. Such attractive performance and high selectivity make the new epidermal biosensor extremely attractive for assessing the wearer's physical exertion and fitness. In addition, no signs of skin irritation or inflammatory response were observed among the subjects following the exercise.

To further validate the lactate excretion profile, sweat samples were collected from a volunteer during cycling. As illustrated in Figure 5.1.7A, a similar lactate profile was obtained for an additional subject with a lactate rise onset time of less than 10 min due to the high exercise intensity. A sharp increase in the response was observed at 20 min, possibly reflecting the greater effort to maintain the speed in the wake of increasing exercise resistance/intensity. In order to estimate the real-time lactate concentration, the biosensor was calibrated at 37 °C to emulate it's effect of the physiological temperature on the enzyme's activity (Figure 5.1.7B). As expected, the sensitivity of the biosensor was approximately 1.4 times greater (s_x = 0.916 μA/mM or 14.66 μA/mM cm^2) than that measured at room temperature. Accordingly, the resulting calibration curve (of Figure 5.1.7B) can be leveraged to correlate the measured current during epidermal evaluation to the absolute lactate concentration (as shown in Figure 5.1.7A). To corroborate the accuracy of the biosensor, sweat samples were collected from the volunteer's deltoid at approximately 24, 28, and 30 min following the initialization of the exercise routine, and their lactate level was examined at 37 °C with a new tattoo biosensor. The corresponding lactate concentrations, shown as red marks in Figure 5.1.7A, indicate a strong correlation between the in vivo response and the in vitro data (~10–15% deviation). Sweat samples from another volunteer were also examined in

the same fashion and a ~6% deviation was observed, further validating the sensor's epidermal response. Such small variation between the in vivo and in vitro data may be attributed to the perspiration collection methodology where sweat was collected over a 1 min duration, leading to an integrated lactate in vitro response rather than an instantaneous one, as measured in vivo.

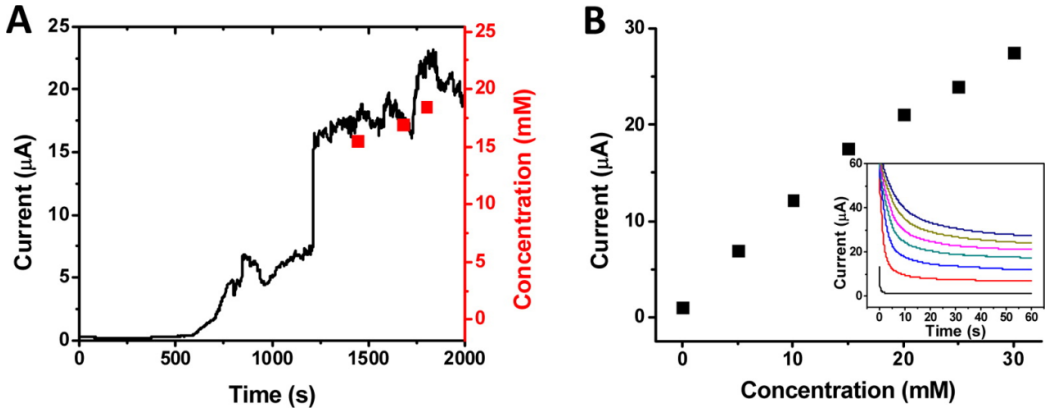


Figure 5.1.7: (A) Real-time response of the tattoo biosensor during a cycling exercise (left y-axis) and corresponding lactate concentrations (right y-axis); red dots represent the lactate concentrations in the sweat collected at these times. (B) In vitro calibration curve of tattoo biosensor at 37 °C; inset, amperometric response to different lactate concentrations up to 30 mM with 5 mM increments. (Reprinted with permission from ref. 12. Copyright 2015 American Chemical Society.)

5.1.4 Conclusion

We have demonstrated the first example of an epidermal electrochemical biosensor which provides real-time analysis of sweat lactate during exercise. Such direct epidermal monitoring of lactate has been realized through the use of flexible printed temporary-transferred tattoos functionalized with lactate oxidase. The resulting epidermal data has been shown to monitor sweat lactate dynamics closely tracking exercise intensity. Compared with traditional blood draws for lactate, the epidermal biosensor is noninvasive, is simple-to-operate, and causes no hindrance to the wearer. Furthermore, the tattoo biosensors endure repetitive mechanical deformations experienced by the epidermis during exercise. Future efforts are aimed at further miniaturization and integration of the electronic interface, data

processing, and wireless transmission of the results. While the on-body results gathered in this study are preliminary in scope, future efforts will be directed at more detailed physiological studies. Such studies will account for differences in temperature and relative humidity in conjunction with a larger cohort of subjects in order to assess the utility of the epidermal sensing concept for assessing physical performance among the general population. Moreover, future studies will seek to concurrently correlate lactate levels measured in the perspiration with those measured in the blood during a controlled fitness routine. In order to realize ubiquitous sensing, future efforts will also migrate the electronics required for control and readout of the sensor onto the same temporary transfer tattoo substrate. The new amperometric epidermal biosensing concept can readily be expanded toward skin-worn monitoring of other clinically relevant sweat metabolites and could thus find important applications for athlete or soldier performance assessment as well as in the generalized healthcare domain.

5.2 Wearable glucose sensor

5.2.1 Introduction

Diabetes is one of the most widely spread modern lifestyle diseases affecting hundreds of millions of people and is among the leading causes of deaths globally.[23, 24] Frequent monitoring of glucose is essential for optimal management of the disease and avoiding its associated problems.[25] Extensive research has led to the introduction and widespread use of self-testing blood glucose meters.[26] However, such self-testing methods rely on inconvenient and painful blood sampling from the finger tip that compromises the patient's compliance. Efforts aimed at addressing this drawback have resulted in several commercial continuous glucose monitoring systems. These enzyme-based microneedle sensors are inserted under the skin to measure glucose levels in the skin interstitial fluid (ISF) fluid.[27, 28] Such

minimally-invasive sensing methods are based on the correlation between glucose levels in the ISF and in blood.[29] Completely non-invasive glucose sensing systems are highly desired to address the limitations of these subcutaneous systems (e.g., fingerstick validation, biofouling, microbial infection and frequent replacement) and are thus ideal for diabetes management.

Extensive efforts have thus been aimed at developing non-invasive glucose sensors that rely on optical, spectroscopic, ultrasound, heat, electrical or electrochemical techniques.[30] Among these, electrochemical techniques have shown the greatest promise. Cygnus Inc. introduced the GlucoWatch® electrochemical glucose sensor for non-invasive glucose monitoring.[31] This platform relied on reverse iontophoresis technique to extract ISF glucose to the surface of the skin followed by the detection via an enzymatic electrochemical glucose sensor. Reverse ionotophoresis involves applying a mild current to the epidermis causing ions to migrate across the skin and towards the electrodes. Sodium ions are the major charge carriers due to the negative charge of the human skin at neutral pH. The migration of sodium ions from across the skin to the cathode leads to electro-osmotic flow of the ISF towards the cathode. During this ISF flow, glucose is also transported towards the cathode. Thus, this technique can be used for non-invasive monitoring of ISF glucose levels.[31] However, the device was later discontinued as patients experienced skin irritation. This limitation has been addressed recently by employing a lower current density for the glucose extraction in connection to new non-invasive reverse iontophoresis glucose sensors.[32] However, these protocols have either been carried out under in-vitro conditions[33] or require off-site glucose detection.[34]

The goal of this work is to demonstrate a proof-of-concept skin-worn temporary-tattoo based non-invasive glucose monitoring platform coupling an amperometric biosensor with a reverse iontophoresis operation (Figure 5.2.1).[35] Our team has recently introduced body-compliant wearable electrochemical devices based on temporary tattoos that combine highly

favorable substrate-skin elasticity with an attractive electrochemical performance.[36] The devices have been successfully applied for epidermal monitoring of sweat electrolytes (such as sodium)[37] and metabolites (such as lactate).[38] The new skin-worn tattoo-based glucose detection system uses a lower current density to extract the ISF glucose followed by selective amperometric biosensing using a glucose oxidase (GOx)-modified Prussian Blue transducer at a low potential as compared to GlucoWatch®. Such flexible, low-cost and aesthetically pleasing iontophoretic-biosensing tattoo platform can be easily mated with the human skin with least levels of intrusion to the wearer's routine. To realize both extraction and sensing operations using such printable skin-worn tattoo platform, additional Ag/AgCl reverse-iontophoresis electrodes (along with the agarose hydrogel coating), have been incorporated for efficient delivery of ISF close to the working and counter/reference electrodes (Figure 5.2.1A). The biocatalytic reagent layer was optimized for imparting the sensitivity needed for detecting low (micromolar) glucose concentrations in the extracted ISF and high specificity in the presence of common interfering electroactive species.

Following the in-vitro optimization and demonstration of the sensor sensitivity and selectivity, the tattoo-based iontophoretic-biosensing system was evaluated towards non-invasive glucose monitoring in human subjects, and was validated by simultaneous blood fingerstick measurements using a commercial glucose meter. The specificity of the tattoo GOx sensor was validated by applying it simultaneously with an enzyme-free tattoo sensor (no GOx control) on human subjects. The requirement of performing reverse iontophoresis prior to detection was demonstrated by analyzing the sensor response with and without active extraction of glucose ISF towards the sensor surface. These proof-of-principle on-body demonstrations reveal that the tattoo-based iontophoretic-biosensing platform holds considerable promise for non-invasive glucose monitoring in real-life situations. The attractive

features of the new skin-worn system also highlight its potential for on-body monitoring of other target chemicals present in the interstitial fluid.

5.2.2 Experimental section

a. Reagents and instrumentation:

Glucose oxidase (GOx) from *Aspergillus niger*, Type X-S (EC 1.1.3.4), chitosan, bovine serum albumin (BSA), sodium phosphate monobasic (NaH_2PO_4), sodium phosphate dibasic (Na_2HPO_4), D(+)-glucose, L(+)-ascorbic acid, uric acid, acetaminophen and agarose were obtained from Sigma-Aldrich (St. Louis, MO). Acetic acid was obtained from EMD Chemicals Inc. (Gibbstown, NJ). All reagents were used without further purification. Electrochemical characterizations were performed at room temperature using a CH Instruments electrochemical analyzer (model 1232A, Austin, TX) and PGSTAT 101 from Metrohm Autolab (Netherlands).

b. Tattoo fabrication, modification and transfer process:

The fabrication process of the glucose tattoo was similar to our earlier work.[14] Briefly, sensor patterns were designed in AutoCAD (Autodesk, San Rafael, CA) and outsourced for fabrication on stainless steel through-hole 12 in. × 12 in. framed stencils (Metal Etch Services, San Marcos, CA). Papilio temporary transfer tattoo base paper was purchased from HPS LLC (Rhome, TX). A sequence of the Prussian blue conductive carbon (C2070424P2, Gwent Group, Pontypool, UK), silver/silver chloride (Ag/AgCl) ink (4001, Engineered Conductive Materials, LLC, Delaware, OH), and insulator (Dupont 5036, Wilmington, DE) inks were patterned on the substrate employing an MPM-SPM semiautomatic screen printer (Speedline Technologies, Franklin, MA). As illustrated in Figure 5.2.1A, the tattoo sensor design consists of a pair of reverse iontophoresis electrodes (Ag/AgCl ink), a pseudo reference/counter (Ag/AgCl ink) and working electrodes (Prussian Blue ink). A transparent insulator was screen

printed over the surface of the electrode pattern to confine the electrode and contact areas. The Ag/AgCl ink was cured at 130 °C for 3 min, while the Prussian Blue ink was cured at 80 °C for 10 min in a convection oven.

Following the printing of the tattoo electrode transducers, the working electrode was functionalized with the reagent layer. The enzyme GOx solution (34 mg/mL containing 10 mg/mL BSA stabilizer) was mixed with chitosan solution (0.5 wt% in 0.1 M acetic acid) in 1:1 v/v ratio. Subsequently, a 2 μL droplet of the above solution was casted on the electrode and dried under ambient conditions.

c. In vitro characterization:

These studies were performed using a 0.1 M phosphate buffer (pH 7.0) solution containing 133 mM NaCl. The operating potential for the tattoo glucose sensor was selected by using cyclic voltammetry. The amperometric response was recorded after 1 min incubation in the sample solution, using a potential step to -0.1 V (vs Ag/AgCl) for 60 s. The sensor specificity was examined in the presence of relevant electroactive constituents, namely, 10 μM each of ascorbic acid, uric acid and acetaminophen.

d. On-body glucose monitoring:

An agarose hydrogel, covering all the electrodes, was applied to the tattoo sensor. The hydrogel was prepared by heating a continuously stirred agarose solution (4% w/v) in 0.1 M phosphate buffer (pH 7) at 120 °C for 15 min. The solution was then cooled down to 60 °C and 100 μL of the solution was casted on the sensor area to form a uniform hydrogel layer covering all the three electrodes of both the anodic and cathodic contingents. The epidermal biosensor evaluation was performed in strict compliance with a protocol approved by the institutional review board (IRB) at the University of California, San Diego. A total of 7 consenting healthy volunteers (4 males and 3 females between the ages of 20 and 40), with no prior medical history of heart conditions, diabetes, or chronic skeletomuscular pain, were

recruited for participation in the study. The subjects were requested to arrive at the lab in fasting state. The epidermal studies comprised of transferring the tattoo sensor to the skin followed by applying a constant current of 0.2 mA/cm^2 between the two reverse-iontophoresis electrodes for 10 min to extract ISF to the surface of the skin and finally recording the amperometric glucose response at an applied potential of -0.1 V (vs Ag/AgCl) for 5 min. A current density of 0.2 mA/cm^2 was selected for reverse iontophoresis based on a preliminary on-body study which revealed that lower current densities resulted in a slow ISF glucose extraction and hence in a delayed sensor response. The reverse-iontophoresis/detection cycle was performed first in the fasting state followed by consumption of a carbohydrate-rich meal. Thereafter, each subject was requested to wait for 5 min before a similar reverse-iontophoresis/detection cycle was repeated to measure the post-meal sensor response. The entire procedure is shown schematically in Figure 5.2.1C. The crucial role of reverse iontophoresis was examined by analyzing the response obtained from two glucose tattoo biosensors (applied simultaneously to subjects) with and without reverse iontophoresis. The selectivity of the on-body sensor to glucose was evaluated using two tattoos, one containing the GOx enzyme while the other devoid of it, applied simultaneously on the subjects' deltoid. For each human trial, simultaneous fingerstick blood glucose measurements were performed using commercial glucose strips (Accu-Chek Aviva Plus®) to establish the correlation between the response of the tattoo sensor and that obtained from the commercial glucose meter.

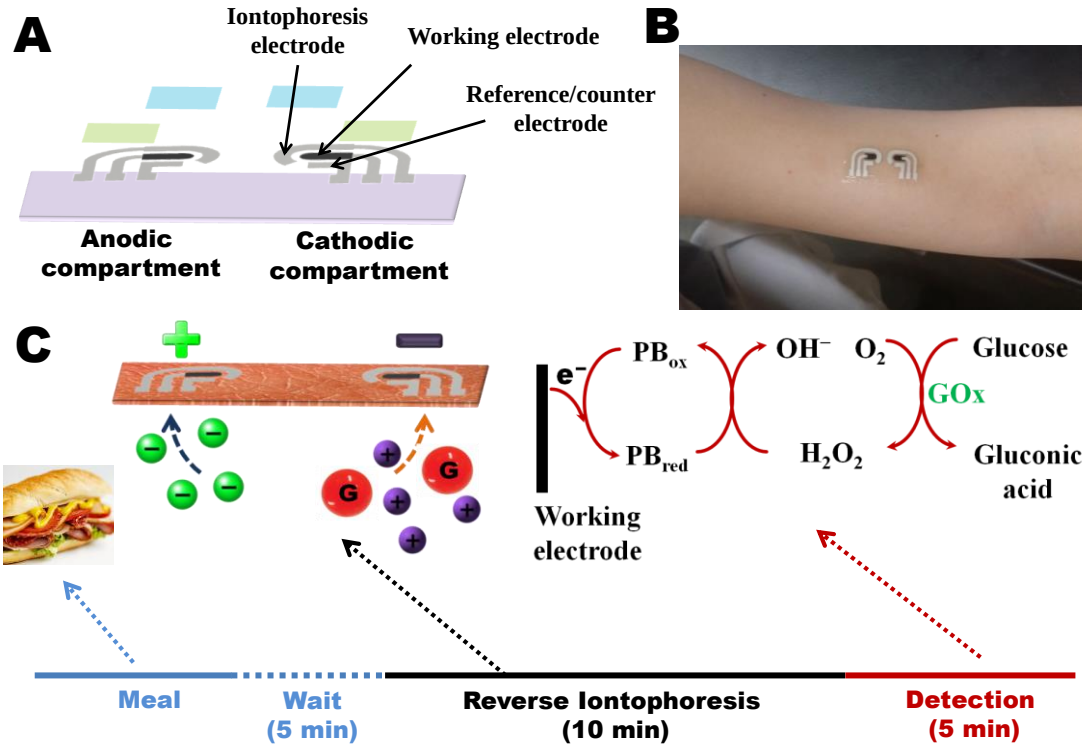


Figure 5.2.1: Tattoo-based platform for non-invasive glucose sensing. (A) Schematic of the printable iontophoretic-sensing system displaying the tattoo-based paper (purple), Ag/AgCl electrodes (silver), Prussian Blue electrodes (black), transparent insulating layer (green) and hydrogel layer (blue). (B) Photograph of a glucose iontophoretic-sensing tattoo device applied to a human subject. (C) Schematic of the timeframe of a typical on-body study and the different processes involved in each phase. (Reprinted with permission from ref. 34. Copyright 2015 American Chemical Society.)

5.2.3 Results and discussion

a. Rationale for tattoo design and enzyme modification:

The new iontophoretic-biosensing system requires a different electrode pattern that includes the iontophoretic electrodes, compared to the 3-electrode design of earlier tattoo-based electrochemical biosensors.[38] Each glucose tattoo sensor consisted of the anodic and cathodic contingents (Figure 5.2.1A). Each contingent comprised of an Ag/AgCl electrode that performed as a counter/reference electrode. A printable Prussian-Blue transducer was employed in view of its high selectivity towards hydrogen peroxide, the detectable product of

the GOx enzymatic reaction.[39] Each contingent consisted of an additional Ag/AgCl reverse iontophoretic electrode which encompassed the working and the counter/reference electrodes for efficient extraction of ISF close to the working and counter/reference electrodes. During the reverse iontophoresis operation, glucose is extracted at the cathodic contingent[31] and hence the working electrode of the cathodic contingent was modified with the GOx enzyme for selective glucose detection. Chitosan was utilized as a polymeric matrix for immobilizing the enzyme on the transducer surface. While performing reverse iontophoresis, care must be taken to ensure proper contact between the skin and the sensor for efficient glucose extraction and to avoid skin irritation. This requirement was satisfied by evenly coating a layer of biocompatible agarose gel on each contingent to cover all the electrodes. Preliminary on-body studies revealed that the absence of the hydrogel layer caused perceptible skin irritation and burning. However, applying the agarose gel to the glucose sensor circumvented this issue. This could be attributed to the enhanced electrical contact between the sensor and the skin offered by the gel. The resulting glucose tattoo sensor can be easily applied to the skin, adhering and conforming to the the contours of the epidermis, similar to a typical rub-on temporary tattoo (Figure 5.2.1B).

b. In vitro studies:

The glucose level in the ISF is in the same concentration range as that in the blood.[40] However, the concentration of the ISF glucose extracted via reverse iontophoresis is approximately two orders lower than that of the corresponding ISF glucose level.[34] Keeping this in view the response of the new glucose tattoo sensor was evaluated over the 0-100 µM glucose concentration range (Figure 5.2.2A). These well-defined chronoamperometric responses to 10 µM glucose additions (a-l) revealed that the sensor responded linearly and favorably over this range (sensitivity: 23 nA/µM; limit of detection: 3 µM), and could thus be utilized for detecting relevant ISF glucose levels extracted during on-body applications.

Specificity of a sensor is of utmost importance for avoiding false alarms. Hence, the effect of physiologically relevant concentrations of common co-existing interfering electroactive species on the sensor response was examined. The results, displayed in Figure 5.2.2B, highlight the high specificity of the sensor towards glucose (Figure 5.2.2B, plot 'a') in presence of ascorbic acid, uric acid and acetaminophen (Figure 5.2.2B, plot 'b'-'d'). Overall, the high sensitivity and selectivity demonstrated in Figure 2 reflect the coupling of the specific biocatalytic reaction with the low-potential amperomertic transduction at the Prussian-Blue transducer, as compared to the high detection potential utilized in GlucoWatch® that could lead to compromised selectivity.[31]

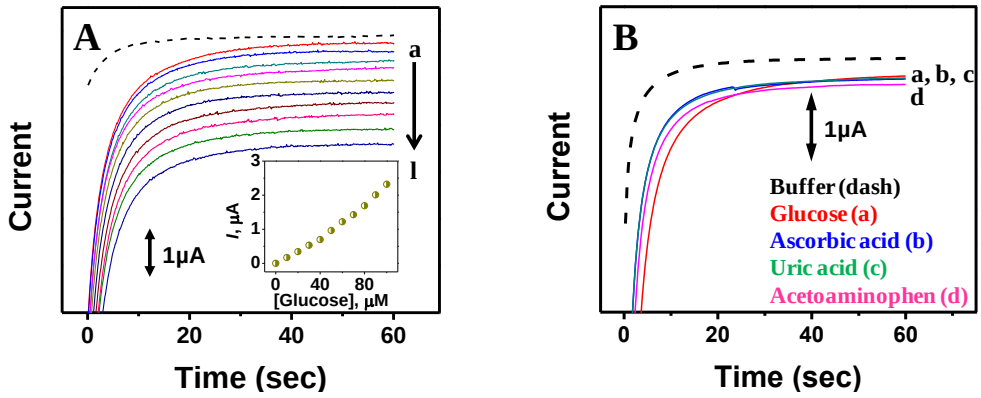


Figure 5.2.2: (A) Chronoamperometric response of the tattoo-based glucose sensor to increasing glucose concentrations from 0 µM (dash) to 100 µM (plot 'l') in buffer in 10 µM increments. (B) Interference study in presence of 50 µM glucose (plot 'a'), followed by subsequent 10 µM additions of ascorbic acid (plot 'b'), uric acid (plot 'c') and acetaminophen (plot 'd'). Potential step to -0.1 V (vs Ag/AgCl). Medium, phosphate-buffer with 133 mM NaCl (pH 7). (Reprinted with permission from ref. 34. Copyright 2015 American Chemical Society.)

c. On-body glucose monitoring:

After demonstrating in-vitro the ability of the tattoo sensors to selectively measure micromolar glucose levels, we examined the on-body detection of ISF glucose levels in human subjects under real-life scenarios with the system worn over the skin. Meal consumption triggers a rapid rise in blood glucose levels that may lead to detrimental effects on diabetic patients. Hence, the present proof-of-concept study aimed at demonstrating the

ability of the non-invasive tattoo sensor to monitor such sudden glycemic spikes. The first task was to identify the most appropriate time to perform the post-meal glucose sensing. Post-meal blood glucose levels of two subjects (1 male and 1 female) were thus measured at 10 min intervals over a 1 hour period following carbohydrate-rich meal. Based on these findings and literature data indicating approximately 15-20 min lag time between ISF and blood glucose levels,[41] a 5 min waiting period (followed by 10 min of IP extraction) was considered for the post-meal glucose sensing. None of the subjects reported perceptible discomfort during these on-body studies. Only a mild tingling feeling at the skin under the iontophoresis electrodes was experienced by few subjects for less than 10 s at the beginning of the test.

Two important control experiments were carried out to corroborate the validity of the reverse iontophoresis-based glucose tattoo sensing system: (1) detection of passively diffused ISF glucose by a GOx-modified sensor (*No-IP* sensor), and (2) use of an unmodified (enzyme-free) sensor under active reverse-iontophoretic extraction of ISF (*No-GOx* sensor). Subjects were selected randomly to participate in each set of control experiments. For each subject the control tattoo sensor was applied adjacent to a glucose tattoo sensor on the deltoid with a spatial gap of approximately 1.5 cm. The response of the control sensor was recorded in tandem with the glucose tattoo sensor.

Figure 5.2.3 displays data obtained from two subjects simultaneously adorning the glucose tattoo sensor and the *No-IP* sensor. It can be clearly noted that the respective glucose tattoo sensor display a distinct increment in the post-meal current response (Figure 5.2.3 A, A' plot b) as compared to the fasting state (Figure 5.2.3 A, A' plots a). In contrast, the respective *No-IP* sensors show minimal change in the current response before and after the meal (Figure 5.2.3 B, B' plots; a vs b). This study underpins the importance of active reverse iontophoretic extraction of ISF glucose for performing non-invasive glucose detection. Simultaneous blood glucose measurements using a commercial Accu-Chek Aviva Plus® glucose meter and

comparison with the response obtained from the tattoo sensors reveal the correlation between the non-invasive tattoo sensor and the blood glucose measurements.

Additional control experiments were carried out for other subjects wearing the glucose tattoo sensor along with a *No-GOx* sensor. In this set of studies, the response from glucose tattoo sensors was also significantly higher compared to that of the enzyme-free sensors, highlighting the specificity of the sensor to detect the glucose substrate in presence of potential interfering species. Figure 5.2.4 displays a collection of amperometric signals recorded with the glucose sensors (plots 'a_i', 'a_{ii}' and 'a_{iii}'), *No-GOx* sensors (plots 'b_i', 'b_{ii}' and 'b_{iii}') and the *No-IP* sensors (plots 'c_i', 'c_{ii}' and 'c_{iii}') for different human subjects. These data clearly illustrate the ability of the tattoo sensors to detect spikes in the glucose level occurring due to food consumption. Another control experiment was performed to identify the variation in the sensor response in absence of glucose spike. During this control experiment, a glucose tattoo sensor and a *No-GOx* sensor was applied simultaneously to a human subject. It was noted that both the blood glucose level as well as the response from the two sensors remained fairly stable, thus underscoring the sensor's ability to specifically detect blood glucose spikes (data not shown).

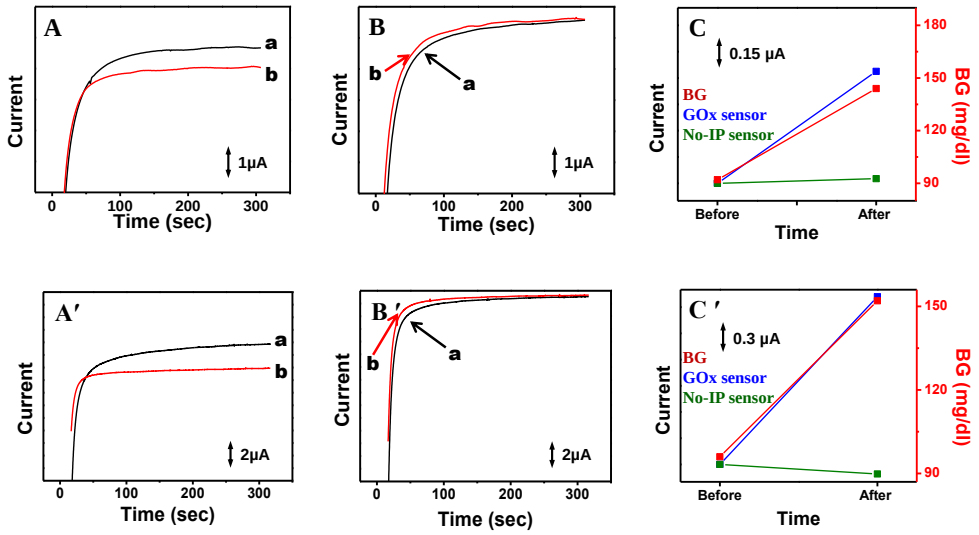


Figure 5.2.3: Amperograms obtained for non-invasive glucose detection obtained from two human subjects, wearing simultaneously the glucose tattoo sensor (A, A') with and (B, B') without the IP operation. (C,C') Correlation between data obtained from tattoo biosensors, with and without the IP procedure, and that obtained using a blood glucose (BG) meter. Potential step to -0.1 V (vs Ag/AgCl). (Reprinted with permission from ref. 34. Copyright 2015 American Chemical Society.)

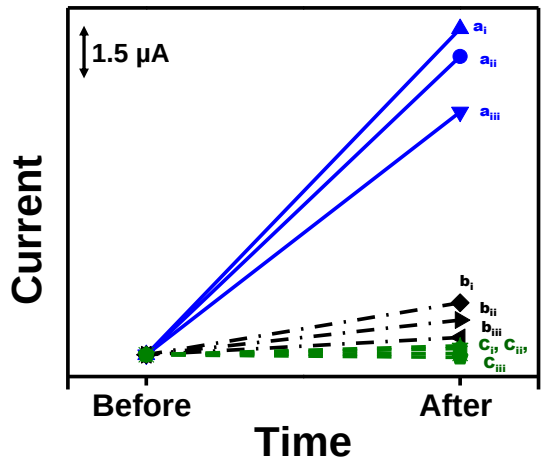


Figure 5.2.4.: Combined data obtained from glucose tattoo sensors (plots 'a_i', 'a_{ii}' and 'a_{iii}'), No-GOx sensors (plots 'b_i', 'b_{ii}' and 'b_{iii}') and No-IP sensors (plots 'c_i', 'c_{ii}' and 'c_{iii}') before and after meal consumption. Conditions, as in Figure 5.2.3. (Reprinted with permission from ref. 34. Copyright 2015 American Chemical Society.)

5.2.4 Conclusion

This proof-of-concept study supports the application of a skin-worn tattoo-based wearable electrochemical biosensor for the non-invasive glucose monitoring. The in-vitro

characterization of the tattoo sensors revealed their ability to detect micromolar levels of glucose in the presence of common interfering chemical species. On-body evaluation of the tattoo-based iontophoretic-biosensing platform further demonstrated the ability to detect the rise in the glucose level after a meal in a non-invasive fashion. Efforts are presently underway to build on this preliminary work to develop a tattoo-based biosensor for continuous non-invasive glucose monitoring. While key challenges remain towards such long operation, this preliminary proof-of-concept demonstration indicates the potential of the tattoo iontophoretic-biosensing platform for diabetes management. Future efforts are aimed at addressing these challenges and integrating the corresponding electronic backbone for powering the sensor, signal processing and wireless communication on a flexible wearable platform and performing a large-scale glucose monitoring study. The new tattoo-based iontophoretic-biosensing platform could be readily expanded towards the non-invasive monitoring of other chemical markers present in the interstitial fluid, and potentially for transcutaneous drug delivery.

This chapter is based, in part, on the material as it appears in Analytical Chemistry, 2013, by Wenzhao Jia, Amay J. Bandodkar, Gabriela Valdés-Ramírez, Joshua R. Windmiller, Zhanjun Yang, Julian Ramírez, Garrett Chan, and Joseph Wang; in part on the material as it appears in Analytical Chemistry, 2015, by Amay J Bandodkar, Wenzhao Jia, Ceren Yardımcı, Xuan Wang, Julian Ramirez, and Joseph Wang. The dissertation author was the primary investigator and corresponding author of these papers.

5.3 References

1. Milenković, A.; Otto, C.; Jovanov, E. *Comput. Commun.* **2006,** *29,* 2521.

2. Kim, D. H.; Lu, N.; Ma, R.; Kim, Y. S.; Kim, R. H.; Wang, S.; Wu, J.; Won, S. M.; Tao, H.; Islam, A.; Yu, K. J.; Kim, T.; Chowdhury, R.; Ying, M.; Xu, L.; Li, M.; Chung, H. J.; Keum, H.; McCormick, M.; Liu, P.; Zhang, Y. W.; Omenetto, F. G.; Huang, Y.; Coleman, T.; Rogers, J. A. *Science* **2011,** *333,* 838.

3. Chiarugi, F.; Karatzanis, I.; Zacharioudakis, G.; Meriggi, P.; Rizzo, F.; Stratakis, M.; Louloudakis, S.; Biniaris, C.; Valentini, M.; Di Rienzo, M.; Parati, G. *Comput. Cardiol.* **2008,** *35*, 901.

4. Buono, M. J.; Lee, N. V. L.; Miller, P. W. *J. Physiol. Sci.* **2010,** *60*, 103.

5. Robergs, R. A.; Ghiasvand, F.; Parker, D. *Am. J. Physiol. Regul. Integr. Comp. Physiol.* **2004,** *287*, 502.

6. Goodwin, M. L.; Harris, J. E.; Hernandez, A.; Gladden, L. B. *J. Diabetes Sci. Technol.* **2007,** *1*, 558.

7. Pilardeau, P. A.; Lavie, F.; Vaysse, J.; Garnier, M.; Harichaux, P.; Margo, J. N.; Chalumeau, M. T. *J. Sports Med. Phys. Fit.* **1988,** *28*, 247.

8. Biagia, S.; Ghimentib, S.; Onorc, M.; Bramantic, E. *Biomed. Chromatogr.* **2012,** *26*, 1408.

9. Polliack, A.; Taylor, R.; Bader, D. *J. Rehabil. Res. Develop.* **1997,** *34*, 303.

10. Faridnia, M. H.; Palleschi, G.; Lubrano, G. J.; Guilbault, G. G. *Anal. Chim. Acta* **1993,** *278*, 35.

11. Khodagholy, D.; Curto, V. F.; Fraser, K. J.; Gurfinkel, M.; Byrne, R.; Diamond, D.; Malliaras, G. G.; Benito-Lopez, F.; Owens, R. M. *J. Mater. Chem.* **2012,** *22*, 4440.

12. Jia, W.; Bandodkar, A. J.; Valdés-Ramírez, G.; Windmiller, J. R.; Yang, Z.; Ramírez, J.; Chan, G.; Wang, J. *Anal. Chem.* **2013,** *85*, 6553.

13. Bandodkar, A. J.; Hung, V. W. S.; Jia, W.; Valdés-Ramírez, G.; Windmiller, J. R.; Martinez, A. G.; Ramírez, J.; Chan, G.; Kerman, K.; Wang, J. *Analyst* **2013,** *138*, 123.

14. Bandodkar, A. J.; Hung, V. W. S.; Jia, W.; Valdes-Ramírez, G.; Windmiller, J. R.; Martinez, A. G.; Ramírez, J.; Chan, G.; Kerman, K.; Wang, J. *Analyst* **2013,** *138*, 123.

15. Harvey, C. J.; LeBouf, R. F.; Stefaniak, A. B. *Toxicol. in Vitro* **2010,** *24*, 1790.

16. Green, J. M.; Pritchett, R. C.; Crews, T. R.; McLester, J. R.; Tucker, D. C. *Eur. J. Appl. Physiol.* **2004,** *91*, 1.

17. Liu, H. Y.; Deng, J. Q. *Electrochim. Acta* **1995,** *40*, 1845.

18. Kulys, J.; Simkeviciene, V.; Higgins, I. J. *Biosens. Bioelectron.* **1992,** *7*, 495.

19. Kowalewska, B.; Kulesza, P. J. *Electroanalysis* **2009,** *21*, 351.

20. Wu, W.; Liu, L. Q.; Li, Y.; Guo, Z. X.; Dai, L. M.; Zhu, D. B. *Fullerenes, Nanotubes, Carbon Nanostruct.* **2003,** *11*, 89.

21. Marcinik, E. J.; Potts, J.; Schlabach, G.; Will, S.; Dawson, P.; Hurley, B. F. *Med. Sci. Sports Exerc.* **1991,** *23*, 739.

22. Yoshida, T.; Chida, M.; Ichioka, M.; Suda, Y. *Eur. J. Appl. Physiol. Occup. Physiol.* **1987,** *56*, 7.

23. Whiting, D. R.; Guariguata, L.; Weil, C.; Shaw, J. *Diabetes Res. Clin. Pract.* **2011,** *94*, 311.

24. Amos, A. F.; McCarty, D. J.; Zimme, P. *Diabetic Med.* **1997,** *14*, S7.

25. Newman, J. D.; Turner, A. P. F. *Biosens. Bioelectron.* **2005,** *20*, 2435.

26. Wang, J. *Chem. Rev.* **2008,** *108*, 814.

27. McGarraugh, G. *Diabetes Technol. Ther.* **2009,** *11*, S17.

28. Gross, T. M.; Bode, B. W.; Einhorn, D.; Kayne, D. M.; Reed, J. H.; White, N. H.; Mastrototaro, J. J. *Diabetes Technol. Ther.* **2000,** *2*, 49.

29. Tanenberg, R.; Bode, B.; Lane, W.; Levetan, C.; Mestman, J.; Harmel, A. P.; Tobian, J.; Gross, T.; Mastrototaro, J. *Mayo Clin. Proc.* **2004,** *79*, 1521.

30. Vashist, S. K. *Anal. Chim. Acta* **2012,** *750*, 16.

31. Tierney, M. J.; Kim, H. L.; Burns, M. D.; Tamada, J. A.; Potts, R. O. *Electroanalysis* **2000,** *12*, 666.

32. Sun, T. P.; Shieh, H. L.; Ching, C. T. S.; Yao, Y. D.; Huang, S. H.; Liu, C. M.; Liu, W. H.; Chen, C. Y. *Int. J. Nanomed.* **2010,** *20*, 343.

33. Ching, C. T. S.; Sun, T. P.; Huang, S. H.; Shieh, H. L.; Chen, C. Y. *Ann. Biomed. Eng.* **2010,** *38*, 1548.

34. McCormick, C.; Heath, D.; Connolly, P. *Sens. Actuators, B* **2012,** *166–167*, 593.

35. Bandodkar, A. J.; Jia, W.; Yardımcı, C.; Wang, X.; Ramirez, J.; Wang, J. *Anal. Chem.* **2015,** *87*, 394.

36. Bandodkar, A. J.; Wang, J. *Trends Biotechnol.* **2014,** *32*, 363.

37. Bandodkar, A. J.; Molinnus, D.; Mirza, O.; Guinovart, T.; Windmiller, J. R.; Valdés-Ramírez, G.; Andrade, F. J.; Schöning, M. J.; Wang, J. *Biosens. Bioelectron.* **2014,** *54*, 603.

38. Jia, W.; Bandodkar, A. J.; Valdes- Ramírez, G.; Windmiller, J. R.; Yang, Z.; Ramírez, J.; Chan, G.; Wang, J. *Anal. Chem.* **2013,** *85*, 6553.

39. Karyakin, A. A. *Electroanalysis* **2001,** *10*, 813.

40. Choleau, C.; Klein, J. C.; Reach, G.; Aussedat, B.; Demaria-Pesce, V.; Wilson, G. S.; Gifford, R.; Ward, W. K. *Biosens. Bioelectron.* **2002,** *17*, 647.

41. Stout, P. J.; Racchini, J. R.; Hilgers, M. E. *Diabetes Technol. Ther.* **2004,** *6*, 635.

Chapter 6 Printed Wearable Hybrid Sensors

6.1 Wearable lactate and electrocardiogram sensor

6.1.1 Introduction

Continuous monitoring of a person's health status can provide unprecedented levels of important data that can help users and health providers in maintaining one's well-being.[1] The medical interest for wearable systems arises from the need for monitoring patients over long periods of time. These devices have the potential to continuously collect continuously vital health information from a person's Wearable sensors present an exciting opportunity to measure human physiology in a continuous, real-time non-invasive manner.[1, 2] Recent advances in hybrid fabrication techniques have enabled the design of wearable sensing devices in thin, conformal form factors that naturally comply with the smooth curvilinear geometry of human skin[3] thereby enabling intimate contact necessary for robust physiological measurements. Development of such epidermal electronic sensors has enabled devices that can monitor respiration rate,[4] heart rate,[5] electrocardiograms (ECGs),[6] blood oxygenation,[7] skin temperature,[8] bodily motion,[9] brain activity,[10] and blood pressure.[11]

To date, most systems have targeted only a single measurement at a time, and most such sensors measure only physical and electrophysiological parameters, significantly limiting the monitoring information and diagnostic opportunities. For example, the human body undergoes complex physiological changes during physical activities such as exercise,[12] and monitoring the physiologic effect of physical activity can be important for a wide variety of subjects ranging from athletes to the elderly[13] and patients. Yet current devices that only measure heart rate, motion, and ECG provide an incomplete picture of the complex

physiological changes taking place. As a result, further progress in the area of wearable sensors must include new, relevant sensing modalities, and must integrate these different modalities into a single platform for continuous, simultaneous sensing of multiple parameters, relevant to a wide range of conditions, diseases, health, and performance states. Specifically, inclusion of chemical measurements can provide extremely useful insights into the performance level and health status of the individual not available from physical or electrophysiological sensors.[14]

While chemical information is currently acquired via clinical labs or Point-of-Care (PoC) devices,[15] such approaches do not support continuous, real-time measurements, limiting their utility to applications where stationary, infrequent tests are sufficient. Researchers, including us, have demonstrated that chemicals such as electrolytes and metabolites can be measured continuously using epidermal electronics on the skin,[16] or through non-invasive monitoring of other bodily fluids,[17] these devices measure only a single parameter at once, and are not integrated with other sensing modalities. Recently, Gao et al demonstrated a wearable patch that can simultaneously track levels of metabolites and electrolytes in the human sweat.[18] However, no efforts were directed to integrate sensing modalities that can monitor simultaneously electrophysiological as well as chemical parameters on the same device. Such sensor fusion is crucial to obtain a comprehensive knowledge about a wearer's well-being. Here we introduce a wearable device that can simultaneously measure chemical and electrophysiological parameters in the form factor of a single epidermal patch, thus fusing on-body chemical sensing with the monitoring of vital signs into single wearable platform.[19] The hybrid wearable, termed here as a Chem-Phys patch, comprises a screen-printed three-electrode amperometric lactate biosensor and two ECG electrodes, enabling concurrent real-time measurements of lactate and ECG. When used in physical exertion monitoring, ECG measurements can help monitor heart health and function, while sweat lactate can be used to

track an individual's performance and exertion level during physical activity.[19] Sweat lactate is an important biomarker for tissue oxygenation and can act also as marker for pressure ischemia.[20] Although, past works have demonstrated separate wearable ECG and lactate sensors, these devices were fabricated on separate platforms and thus mandate applying multiple single sensor wearable patches on the human body in order to monitor multiple physiological parameters. By combining a lactate biosensor and an ECG sensor, the new Chem-Phys hybrid wearable patch represents a powerful platform capable of simultaneously tracking both physicochemical and electrophysiological changes of a human body, thus providing a more comprehensive view of a person's health status than current wearable fitness monitors.

The Chem-Phys hybrid patch has been fabricated by leveraging screen printing technology on a thin, highly flexible polyester sheet that conforms well with the complex three dimensional morphology of the human skin to provide a low-noise signal. The working electrode of the lactate biosensor is functionalized and coated with a biocompatible biocatalytic layer (Lactate Oxidase-modified Prussian Blue). The three amperometric electrodes are separated from the Ag/AgCl ECG electrodes via a printed hydrophobic layer to maximize sensor stability and signal-to-noise ratio even in the presence of significant perspiration. The Chem-Phys hybrid patch has been judiciously designed to attain a compact form-factor with the three lactate biosensor electrodes in the center, and the two ECG electrodes at each corner. The dimensions of the electrodes and the inter-electrode distances have been optimized based on human trails to acquire a clean ECG signal and lactate response with minimal interference between the two sensors. The two sensors are interfaced to a custom printed circuit board (PCB) featuring a potentiostat, an ECG analog front-end (AFE), and a Bluetooth Low-Energy (BLE) radio for wireless telemetry of the results to a mobile platform, such as a smartphone or laptop. Preliminary studies of the hybrid sensor patch revealed that

the lactate sensor has optimal sensitivity and linear detection range to determine lactate levels in human perspiration while the ECG electrodes could capture signals that correlated well with that obtained from commercial ECG electrodes. Ultimately, the device was reduced to practice by applying it to three human subjects and simultaneously monitoring sweat lactate levels and ECGs in a continuous fashion. Results presented in the following sections show that lactate and ECG can be measured simultaneously on human subjects, and that lactate measurements do not adversely interfere with high-impedance ECG measurements. The on-body tests also prove that the ECG signals remain undistorted irrespective of the wearer's perspiration state. The heart-rate, extracted from the ECG signals, was also correlated with that obtained from a commercial wrist-band based heart-rate monitor. Additionally, a control experiment comprising of applying an enzyme-free amperometric sensor to a perspiring human subject corroborated the lactate sensor's selectivity towards lactate detection. The promising data obtained in this work thus supports the possibility of developing more advanced hybrid wearable sensors that involve complex integration of several physical and chemical sensors on the same platform for monitoring body dynamics.

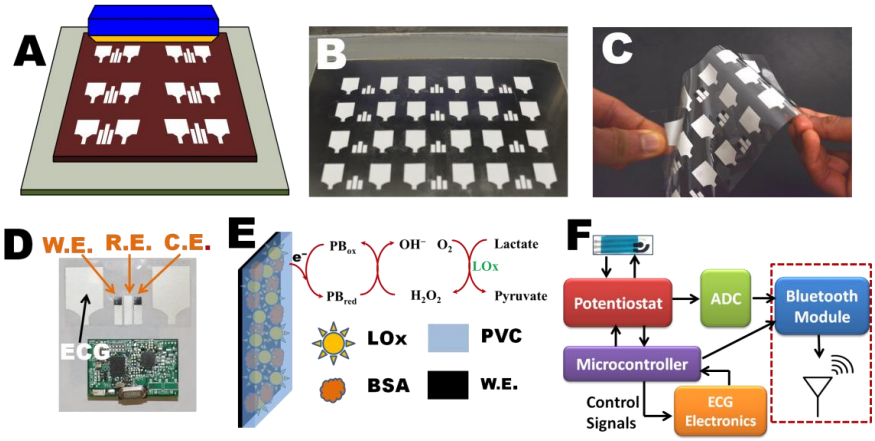


Figure 6.1.1: Fabrication and function of the Chem–Phys hybrid sensor patch.(a) Schematic showing the screen-printing process. (b) Image of the Chem–Phys printing stencil. (c) An array of printed Chem–Phys flexible patches. (d) Image of a Chem–Phys patch along with the wireless electronics. (e) Schematic showing the LOx-based lactate biosensor along with the enzymatic and detection reactions. (f) Block diagram of the wireless readout circuit. (Reprinted with permission from ref.19. Copyright 2016 Nature Publishing Group.)

6.1.2 Experimental section

a. Reagents and materials:

Chitosan, acetic acid, polyvinyl chloride (PVC), tetrahydrofuran (THF), bovine serum albumin (BSA), L-lactic acid, sodium phosphate monobasic, and sodium phosphate dibasic were obtained from Sigma-Aldrich (St. Louis, MO). L-Lactate oxidase (LOx) (activity, 101 U/mg) was procured from Toyobo Corp. (Osaka, Japan). All reagents were used without further purification. Prussian blue conductive carbon (C2070424P2), Ag/AgCl (E2414) and insulator (Dupont 5036) inks were procured from Gwent Group (Pontypool, UK), Ercon Inc. (Wareham, MA.) and Dupont (Wilmington, DE). ECG hydrogel conductive adhesive (RG63B, 35-mil thick) was purchased from Covidien. Polyester sheets (MELINEX® 453, 50 µm thick) were provided by Tekra Inc. (New Berlin, WI).

b. Instrumentation:

The Chem-Phys patch was printed by employing an MPM-SPM semiautomatic screen printer (Speedline Technologies, Franklin, MA). Sensor patterns were designed in AutoCAD (Autodesk, San Rafael, CA) and outsourced for fabrication on stainless steel through-hole 12 in. × 12 in. framed stencils (Metal Etch Services, San Marcos, CA). Electrochemical characterization was performed at room temperature using a CH Instruments electrochemical analyzer (model 630C, Austin, TX). A CONTEC MS400 Multi-parameter Patient Simulator, ECG simulator has been utilized for testing of ECG instrumentation circuits. 3M Red Dot Multi-Purpose Monitoring electrodes are used for verification of collected signal using the fabricated ECG sensors.

c. Fabrication of Chem-Phys hybrid device:

The Chem-Phys hybrid patch was fabricated via screen printing technology while the wearable electronic board was realized by relying on standard 4-layer PCB fabrication and assembly protocols.

d. Printing and functionalization of Chem-Phys hybrid patch:

The Chem-Phys patch was fabricated in-house by printing a sequence of Ag/AgCl, Prussian Blue and insulator inks were patterned on the highly flexible transparent polyester substrate by employing the custom designed stencils and screen printer. The Ag/AgCl and insulator ink was cured at 90 °C for 10 min, while the Prussian Blue ink was cured at 80 °C for 10 min in a convection oven.

Upon printing of the hybrid patch, the working electrode of the amperometric sensor was functionalized with LOx enzyme. The LOx solution (40 mg/mL containing 10 mg/mL BSA stabilizer) was mixed with a chitosan solution (0.5 wt% in 1 M acetic acid) in a 1:1 v/v ratio. Subsequently, 8 μL droplet of the above solution was casted on the electrode and dried under ambient conditions. Thereafter, 4 μL of PVC solution (3 wt% in THF) was drop casted and allowed to dry under ambient conditions for at least 3 h before use. The ECG electrodes were covered with conductive hydrogel adhesive. The patch was then affixed to a medical grade adhesive sheet required for applying to human skin. The patch was stored at 4 °C when not in use.

e. PCB fabrication:

The 4-layer Bluetooth-enabled PCB employed a Texas Instrument (TI) CC2541 BLE System-on-Chip for communication and processing. An ADS1293 analog front end chip was employed for biopotential measurements to record the electrocardiogram (ECG) signals from the fabricated ECG electrodes. An LMP91000 analog front end, programmable through an I2C interface driven by the CC2541, was used as the on-board potentiostat for lactate concentration determination. The data from each sensor was collected by the CC2541 and

transmitted to a Bluetooth 4.0-enabled receiver. A graphical interface was developed using Python to demonstrate measurement results on a PC. A Johanson Technology 2.45 GHz chip antenna (2450AT42A100) and impedance-matched balun (2450BM15A0002) were employed for wireless transmission. A CR2032 button cell lithium battery (3 V, 220 mAh) was utilized as a power source, regulated for the electronics via a TPS61220 boost converter. In the "active mode", the board consumed, on average, 5 mA from a 3 V supply (15 mW).

f. In-vitro studies:

i. Characterization of amperometric lactate sensor:

These studies were performed using a 0.1 M phosphate buffer (pH 7.0) solution. The operating potential for the lactate sensor was selected by using cyclic voltammetry. The amperometric response was recorded after 1 min incubation in the sample solution, using a potential step to -0.1 V (vs Ag/AgCl) for 60 s.

ii. Characterization of the ECG sensor:

ECG monitoring has been performed using both commercial 3M Red Dot Multi-Purpose monitoring electrodes, as well as fabricated ECG electrodes to verify the functionality of the printed Ag/AgCl ECG sensors.

g. On-body characterization of Chem-Phys patch:

All experiments were performed in strict compliance with the guidelines of Institutional Review Boards (IRB) and were approved by Human Research Protections Program at University of California, San Diego (Project name: Epidermal Electrochemical Sensors and Biosensors. Project number: 130003). The study was deemed by the IRB as posing "no greater than minimal risk" to the prescreened subjects who were recruited for the investigation. A total of 3 healthy male volunteers (recruited in response to follow-up from flyers) with no prior medical history of heart conditions, diabetes, or chronic skeletomuscular pain were recruited for participation in the study, and informed, signed consent was obtained

from each individual following a rigorous prescreening procedure. A typical study comprised of applying the Chem-Phys hybrid patch on fourth intercostal space of a subject's chest in order to record the ECG signal between V1 and V2 positions.

Subjects were then asked to mount a stationary cycle and begin cycling at a steady, comfortable cadence. Subjects were instructed to maintain their cadence while an increasing resistance was applied at 3 min intervals. The absolute resistance level and duration was selected according to subject's fitness level while the same intensity profile was used throughout the human studies. This ensured that the anaerobic metabolism was invoked at similar time scales, hence augmenting the excretion of lactate in the perspiration in a controlled fashion. Following the intense fitness bout, the volunteers were asked to gradually reduce their cadence during a 3 min "cool-down" period whereby the resistance was reduced from maximal levels.

h. Characterization of instrumentation circuits:

The printed circuit board was assembled and tested in-vitro to validate the functionality and performance. The potentiostat circuit was verified together with the lactate biosensor through an in-vitro amperometric experiment. The ECG AFE was characterized using a CONTEC MS400 Multi-parameter Patient Simulator (ECG simulator). The output signal of the ECG simulator was read using ADS1293 analog front end chip, and transferred through BLE link to a BLE-enabled device.

6.1.3 Results and discussion

a. Hybrid patch design rationale and fabrication:

The Chem-Phys hybrid multi-sensor system must be compact and easy to wear in a location that offers adequate access to both ECG signals and perspiration for lactate measurements. The design must also minimize sensor-body motion, must minimize co-

interference between the sensing modalities, and be low-cost. These requirements motivate a flexible epidermal electronic design that can be worn on the chest and fabricated using screen printing technology.

The design of the sensing system is shown in Figure 6.1.1. The biosensors were fabricated via conventional low-cost screen printing technique (conceptually illustrated in Figure 6.1.1A) utilizing custom-designed stencils (photograph in Figure 6.1.1B). The biosensing patches were printed onto a highly flexible, thin polyester sheet (50 μm thickness) for realizing highly conformable sensor patch that adheres well to the human skin without causing any discomfort. An array of fabricated sensors is shown in Figure 6.1.1C. The total patch size was dictated by the bipolar ECG electrodes, which must be separated by a minimum distance in order to attain a high quality signal. Typically, single-lead monitoring systems such as the present design are used for basic heart monitoring, arrhythmias diagnosis, or studying the effect of exercise on the heart, and are placed in the vicinity of the conventional V1-V6 chest lead locations. Electrode size, separation, and placement parameters were determined through a series of experiments involving placement of Ag/AgCl-based ECG electrodes of various sizes (1 x1 cm^2, 1.5 x 1.5 cm^2, 1.5 x 1 cm^2 and 2 x 2 cm^2) and separation distances (1 to 6 cm) on subjects with different chest sizes, and observing the resulting ECG waveforms. The study revealed that a compact patch that provides favorable ECG signal could be realized by placing 1.5 x 1.5 cm^2 ECG electrodes across the V1 and V2 lead sites with an inter-electrode distance of 4 cm, thereby measuring from the vantage point of the septal surface of the heart as suitable for diagnostics of arrhythmias and the effects of exercise on the heart. This sets an upper-end size of the patch to be 7 x 2 cm^2. The chest region is not only convenient for measurement of ECG, but also has a high sweat rate during physical excursion,[21] and can thus serve as an appropriate location to also measure lactate levels in human perspiration. Additionally, the epidermis and muscle tissues over these locations do not

experience complex three dimensional strains and remain fairly stable even during intense physical activities, making measurements here especially convenient. Since the performance of amperometric lactate electrodes is not compromised by reducing their dimension, they were fabricated between the two ECG electrodes, as shown in Figure 6.1.1D. Each of the three electrodes have an active area of 3 mm x 2.5 mm. The working electrodes were printed using Prussian Blue ink due to the high selectivity of Prussian Blue towards hydrogen peroxide, a byproduct of the enzymatic oxidation of lactate[22] (Figure 6.1.1E). The reference electrode was printed using Ag/AgCl. Since sweat can provide an alternate electrically-conductive pathway between the ECG electrodes and also between the ECG and amperometric electrodes, thus leading to potential distortion of the recorded ECG signal, a printed hydrophobic layer of Ecoflex® was used to separate the amperometric biosensor from the ECG electrodes to obviate direct electrical contact between the ECG and amperometric electrodes via sweat, thus minimizing the cross-talk between the two sensors. The entire Chem-Phys patch is highly flexible and can be smoothly mated on curved surfaces. Such flexibility is crucial for achieving unobtrusive wearable devices that cause no hindrance or irritation to the wearer.

The Chem-Phys patch was interfaced to a custom printed circuit board (PCB) featuring a potentiostat and analog-to-digital converter (ADC) for amperometric data acquisition, an analog front-end (AFE) for ECG data acquisition, and a Bluetooth Low Energy chip for wireless transmission (Figure 6.1.1D and F).

b. In-vitro characterization of lactate biosensor:

Lactate concentration in human sweat depends on a person's metabolism and level of exertion, and typically ranges from 0 to 25 mM.[23] A wide linear detection range coupled with a fast response time is thus essential for continuous epidermal monitoring of lactate. The operating potential of -0.1V (vs to Ag/AgCl) was selected based on the onset potential for electro-oxidation of lactate by the fabricated biosensor, obtained during cyclic voltammetry

studies. When the biosensor comes in contact with lactate, the immobilized LOx enzyme catalyzes the oxidation of lactate to generate pyruvate and H_2O_2. The Prussian Blue transducer, then selectively reduces the H_2O_2 to generate electrons to quantify the lactate concentration (Figure 6.1.1E). Figure 6.1.2A shows the amperometric response of the lactate biosensor to increasing lactate concentrations in the physiological range of 0-28 mM. It is evidenced from this figure that the biosensor responds linearly to the lactate concentrations in this range with a sensitivity of 96 nA/mM.

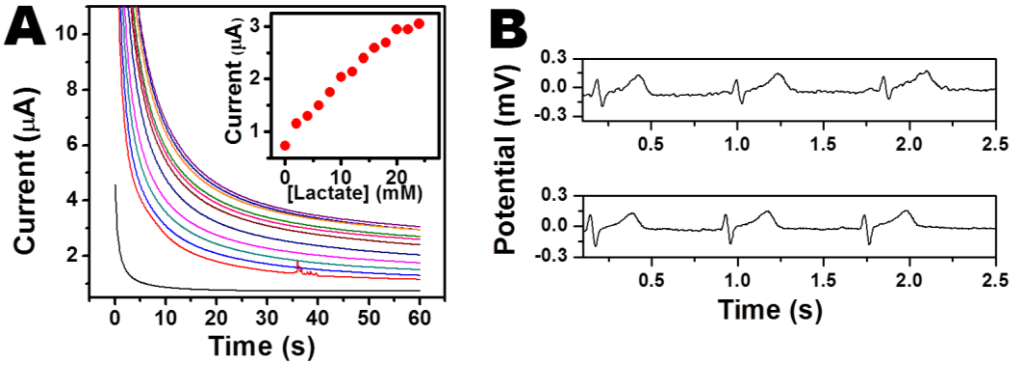


Figure 6.1.2: In-vitro characterization of Chem–Phys hybrid patch.(a) Amperometric response to increasing lactate concentration from 0 to 28 with 2 mM additions in phosphate buffer (pH 7.0). Applied voltage -0.1 V versus Ag/AgCl. (b) Electrocardiogram signals using 3M Red Dot electrodes (top), and printed electrocardiogram sensor (bottom). (Reprinted with permission from ref. 19. Copyright 2016 Nature Publishing Group.)

c. On-body characterization of ECG sensor:

All experiments were performed in strict compliance with the guidelines of Institutional Review Boards (IRB) and were approved by Human Research Protections Program at University of California, San Diego (Project name: Epidermal Electrochemical Sensors and Biosensors. Project number: 130003). The ability of the printed ECG electrodes to record ECG signals was validated by comparing recordings from the fabricated electrodes to commercially-available 3M™ Red Dot™ ECG electrodes. As illustrated in Figure 6.1.2B, ECG signals recorded for the same subject using commercial and fabricated electrodes at the same location have similar morphologies when acquired using the same AFE circuitry.

d. Epidermal evaluation of the Chem-Phys patch:

The Chem-Phys hybrid patch (Figure 6.1.3A) was fabricated and applied to three healthy male subjects on the fourth intercostal space of the chest (Figure 6.1.3B). Dynamic changes in sweat lactate levels and ECG signals were measured continuously during a bout of intense cycling. In order to ensure that the anaerobic metabolism was invoked, subjects were asked to mount a stationary cycle and maintain a steady cycling cadence while the cycling resistance increased periodically as illustrated in Figure 6.1.3C.

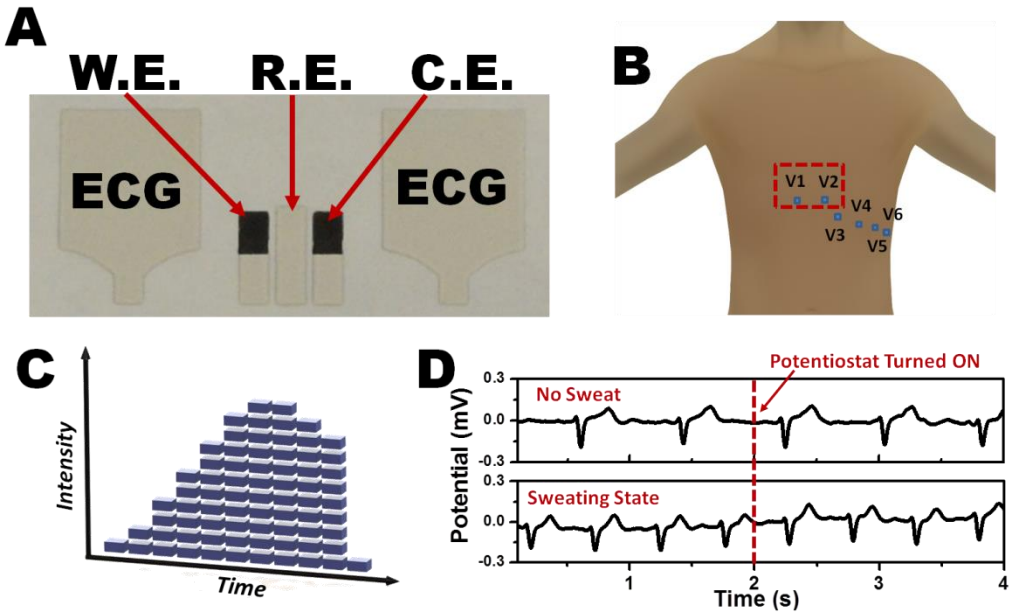


Figure 6.1.3: On-body test configuration.(a) A photograph of Chem–Phys hybrid patch. (b) Location of the Chem–Phys patch for mounting on the human body—the fourth intercostal space of the chest. (c) Cycling resistance profile for on-body tests. (d) Effect of amperometric measurement on the electrocardiogram signal before cycling (no sweat state) and during cycling (sweating state). (Reprinted with permission from ref. 19. Copyright 2016 Nature Publishing Group.)

Since ECG measurements were made via bipolar high-impedance electrodes, and lactate measurements were made by applying a constant potential via a low-impedance potentiostat output and measuring current, there is a possibility that a change in the applied potentiostat voltage (for example during start-up) could interfere with ECG measurements

during the settling time of the potentiostat. At the same time, sweat consists of many ions and could thus act as an electrically conductive medium that can shunt the lactate and ECG sensors, or the two ECG electrodes together. Co-sensor interference and shunting effects were mitigated by geometrically separating the lactate and ECG electrodes and printing two vertically-oriented hydrophobic layers were next to the lactate biosensor, thereby facilitating flux of new perspiration across the biosensor itself, while minimizing shunting between the lactate and ECG sensors. To validate performance under concurrent hybrid sensing scenarios, the Chem-Phys sensor was mounted on a human subject and set to continuously record ECG prior to, during, and immediately after turning on the -0.1 V potentiostat output. Experimental results, obtained via a wireless Bluetooth link as shown in Figure 6.1.3D, reveal that the potentiostat has a negligible effect on the morphology of the ECG signals, irrespective of whether the subject was in a resting or cycling state.

To validate performance under realistic conditions, the Chem-Phys patch was tested on three subjects during 15-30 minutes of intense cycling activity; continuous time-series results during each experiment are shown in Figure 6.1.4. At the commencement of the cycling activity, each subject's heart rate, extracted from ECG data, was within the normal resting range of 60 to 120 beat per minute (BPM).[24] At the same time, a negligible current response was measured by the lactate biosensor due to the lack of perspiration. With time, the resistance for cycling was increased, causing the subjects to exert increasing levels of effort to maintain constant cycling speed. This resulted in increasing heart rate and generation of sweat. At the onset of perspiration, lactate is released from the epidermis, and is selectively detected by the LOx-based biosensor. As the resistance increases, the sweat lactate concentration too increases, as illustrated in Figure 6.1.4A-C, showing a correlation between physical exertion, heart rate, and lactate generation. As the cycling continued, the sweat rate for each subject increased, leading to the well-documented phenomenon of dilution factor that causes decrease

in the lactate concentration.[25] The final stage of the cycling bout involved a 3 minute cool down period. During this phase, as expected, the heart rate normalized back near to the normal resting heart rate. At the same time, the lactate concentration measured by the lactate biosensor continued to decrease.

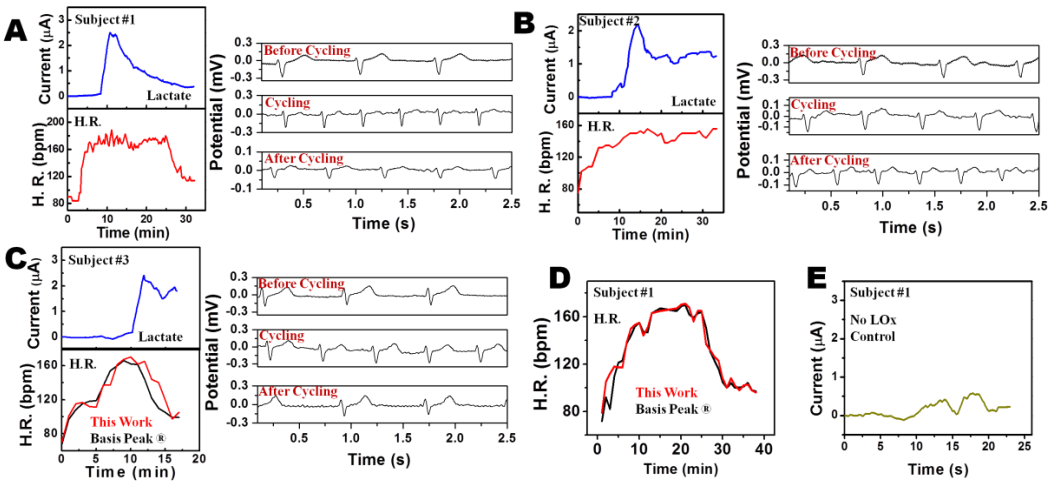


Figure 6.1.4: Real-time on-body evaluation of the Chem-Phys hybrid patch showing the lactate levels and H.R. for three human subjects. The corresponding 'blue plots' represent the real-time lactate concentration profiles for each subject, while, the 'red plots' depict the H.R. data obtained by the ECG electrodes of the Chem-Phys patch. The 'black plots' correspond to the H.R. data recorded by the Basis Peak® heart rate monitor. Typical real-time ECG data obtained before, during and after the cycling bout for each subject is also shown in A, B and C. Panel D provides more data for H.R. verifications. Panel E demonstrates response of the control amperometric sensor (without Lox enzyme) for subject #1. (Reprinted with permission from ref. 19. Copyright 2016 Nature Publishing Group.)

The lactate biosensor data for each subject resembles the expected sweat lactate profile for increasing intensity workouts. To validate that lactate, not other sweat constituents, was specifically measured, a control experiment in which an unmodified (LOx-free) amperometric biosensor was used under the same experimental conditions as above to subject #1. As shown in Figure 6.1.4E, the control biosensor leads to a negligible current response without the presence of LOx, confirming the high selectivity of the lactate biosensor. To validate ECG data over long time series, even under the presence of experimentally-induced motion, heart rate as extracted from the ECG data is benchmarked against a commercial

wristband heat rate monitor (BASIS®) for subjects 1 and 3. Extracted heart rate data matched the wrist-worn device with a Pearson correlation coefficient of r = 0.975. These on-body studies illustrate that the hybrid patch could monitor sweat lactate and ECG in a continuous simultaneous manner and that the hydrophobic barrier between the sensors assisted in minimizing potential cross-talk between the two sensing modalities. The data also demonstrates that such a barrier had minimal effect on the supply of oxygen to the enzyme electrode required for biocatalytic detection of lactate.

6.1.4 Conclusions

The Chem-Phys sensor patch described in this study represents a hybrid system that fuses the monitoring of vital signs with on-body chemical sensing into single fully printable wearable platform. On-body epidermal testing in a realistic fitness environment revealed that ECG sensing is in-line with existing wearable devices, and is not adversely affected by simultaneous measurement of lactate via constant-potential amperometry. The lactate control study using an enzyme-free amperometric sensor and correlation of the heart rate data of the hybrid patch to that recorded by a commercial heart rate monitor underscore the promise of the Chem-Phys patch to monitor simultaneously ECG signals and sweat lactate levels for tracking the wearer's physicochemical and electrophysiological status. This device represents an important first step in the research and development of multi-modal wearable sensors that fuse chemical, electrophysiological, and physical sensors for more comprehensive monitoring of human physiology.

This chapter is based on the material as it appears in Nature Communications, 2016, by Somayeh Imani, Amay J. Bandodkar, A. M. Vinu Mohan, Rajan Kumar, Shengfei Yu, Joseph Wang, and Patrick P. Mercier. The dissertation author and Prof. Patrick Mercier were the co-principle investigators and co-corresponding authors of this paper.

6.2 References

1. Kim, D. H.; Ghaffari, R.; Lu, N.; Rogers, J. A. *Annu. Rev. Biomed. Eng.* **2012,** *14*, 113.

2. Bandodkar, A. J.; Wang, J. *Trends Biotechnol.* **2014,** *32*, 363.

3. Kim, D.-H.; Lu, N.; Ma, R.; Kim, Y.-S.; Kim, R.-H.; Wang, S.; Wu, J.; Won, S. M.; Tao, H.; Islam, A.; Yu, K. J.; Kim, T.-i.; Chowdhury, R.; Ying, M.; Xu, L.; Li, M.; Chung, H.-J.; Keum, H.; McCormick, M.; Liu, P.; Zhang, Y.-W.; Omenetto, F. G.; Huang, Y.; Coleman, T.; Rogers, J. A. *Science* **2011,** *333*, 838.

4. Merritt, C. R.; Nagle, H. T.; Grant, E. *IEEE Sens. J.* **2009,** *9*, 71.

5. Chiarugi, F.; Karatzanis, I.; Zacharioudakis, G.; Meriggi, P.; Rizzo, F.; Stratakis, M.; Louloudakis, S.; Biniaris, C.; Valentini, M.; Rienzo, M. D.; Parati, G. In *Measurement of heart rate and respiratory rate using a textile-based wearable device in heart failure patients*, 2008 Computers in Cardiology, 14-17 Sept. 2008; 2008; pp 901.

6. Lee, S. M.; Byeon, H. J.; Lee, J. H.; Baek, D. H.; Lee, K. H.; Hong, J. S.; Lee, S.-H. *Sci. Rep.* **2014,** *4*, 6074.

7. Rothmaier, M.; Selm, B.; Spichtig, S.; Haensse, D.; Wolf, M. *Opt. Express* **2008,** *16*, 12973.

8. Bian, Z.; Song, J.; Webb, R. C.; Bonifas, A. P.; Rogers, J. A.; Huang, Y. *RSC Adv.* **2014,** *4*, 5694.

9. Son, D.; Lee, J.; Qiao, S.; Ghaffari, R.; Kim, J.; Lee, J. E.; Song, C.; Kim, S. J.; Lee, D. J.; Jun, S. W.; Yang, S.; Park, M.; Shin, J.; Do, K.; Lee, M.; Kang, K.; Hwang, C. S.; Lu, N.; Hyeon, T.; Kim, D.-H. *Nat. Nano.* **2014,** *9*, 397.

10. Löfhede, J.; Seoane, F.; Thordstein, M. *Sensors* **2012,** *12*, 16907.

11. Cong, P.; Ko, W. H.; Young, D. J. *IEEE Sens. J.* **2010,** *10*, 243.

12. Wasserman, K.; Van Kessel, A. L.; Burton, G. G. *J. Appl. Physiol.* **1967,** *22*, 71.

13. Pollock, M. L.; Franklin, B. A.; Balady, G. J.; Chaitman, B. L.; Fleg, J. L.; Fletcher, B.; Limacher, M.; Piña, I. L.; Stein, R. A.; Williams, M.; Bazzarre, T. *Circulation* **2000,** *101*, 828.

14. Yarasheski, K. E.; Zachwieja, J. J.; Bier, D. M. *Am. J. Physiol.* **1993,** *265*, E210.

15. Soper, S. A.; Brown, K.; Ellington, A.; Frazier, B.; Garcia-Manero, G.; Gau, V.; Gutman, S. I.; Hayes, D. F.; Korte, B.; Landers, J. L.; Larson, D.; Ligler, F.; Majumdar, A.; Mascini, M.; Nolte, D.; Rosenzweig, Z.; Wang, J.; Wilson, D. *Biosens. Bioelectron.* **2006,** *21*, 1932.

16. Windmiller, J. R.; Wang, J. *Electroanalysis* **2013,** *25*, 29.

17. Bandodkar, A. J.; Jia, W.; Yardımcı, C.; Wang, X.; Ramirez, J.; Wang, J. *Anal. Chem.* **2015,** *87*, 394.

18. Gao, W.; Emaminejad, S.; Nyein, H. Y. Y.; Challa, S.; Chen, K.; Peck, A.; Fahad, H. M.; Ota, H.; Shiraki, H.; Kiriya, D.; Lien, D.-H.; Brooks, G. A.; Davis, R. W.; Javey, A. *Nature* **2016,** *529*, 509.

19. Imani, S.; Bandodkar, A. J.; Mohan, V.; Kumar, R.; Yu, S.; Wang, J.; Mercier P. P. *Nat. Commun.* **2016** (accepted).

20. Biagia, S.; Ghimentib, S.; Onorc, M.; Bramantic, E. *Biomed. Chromatogr.* **2012,** *26*, 1408.

21. Harrigan, R. A.; Chan, T. C.; Brady, W. J. *J. Emerg. Med.* **2012,** *43*, 1038.

22. Karyakin, A. A. *Electroanalysis* **2001,** *10*, 813.

23. Green, J. M.; Pritchett, R. C.; Crews, T. R.; McLester, J. R.; Tucker, D. C. *Eur. J. Appl. Physiol.* **2004,** *91*, 1.

24. Kostis, J. B.; Moreyra, A. E.; Amendo, M. T.; Di Pietro, J.; Cosgrove, N.; Kuo, P. T. *Circulation* **1982,** *65*, 141.

25. Buono, M. J.; Lee, N. V. L.; Miller, P. W. *J. Physiol. Sci.* **2010,** *60*, 103.

Chapter 7 Conclusions and Future Prospects

The present doctoral thesis work attempts to overcome some of the challenges experienced by wearable chemical sensors. Particularly, through this research the first examples of soft, highly stretchable all-printed electrochemical sensors have been demonstrated. These devices can easily withstand strains upto 500% with minimal impact on their electrochemical properties. Such soft biosensors have major implications in the field of wearables since they can be intimately integrated with the human skin for rea-time monitoring of biochemicals with causing skin irritation. Efforts have also been made towards developing all-printed self-healing electrochemical devices to address the issue related to mechanical stress –induced device failure. Cracking will eventually occur in wearable devices due to regular body motions. Thus, self-healing printed devices can hold the answer to this problem. In-vitro characterizations of the self-healing electrochemical devices reveal that the printed device regains its original electrochemical properties within a few seconds even after it has been completely severed.

The following chapters focus on real-life applications of wearable all-printed electrochemical sensors for personalized health monitoring. Chapter 4 discusses the development of epidermal tattoo-based potentiometric pH and sodium sensors. Preliminary in-vitro tests performed on these all-solid-state potentiometric sensors reveal that these sensors have reversible response to varying concentrations of analyte. At the same time, these can survive repeated mechanical deformations common to the human skin. On-body tests of these sensors demonstrate the viability of these patches to record transient pH and sodium levels in the human sweat in a non-invasive fashion. Chapter 5 is aimed at discussing the fabrication of tattoo-based amperometric sensors for non-invasive detection of lactate and glucose for fitness

monitoring and diabetes management respectively. Similar to potentiometric sensor studies, each of the amperometric system was first tested for its detection range, effect of intereferring chemicals on sensor response and effect mechanical deformation on performance. Thereafter, the devices were reduced to practice by applying them to consenting human subjects for validating the sensor performance in real-life scenarios. These epidermal studies illustrate that the sensors detect lactate and glucose with high selectivity and sensitivity. Finally, Chapter 6 is focused on the work demonstrating the first example of a hybrid wearable sensor patch that integrates a lactate (biochemical) sensor with an ECG (electrophysiological) sensor for simultaneous monitoring of a wearer's sweat lactate levels and ECG signals. Such multi-parameter sensors are crucial in order to obtain a holistic view of a person's well-being.

Significant progress has thus been made in recent years in the field of wearable chemical sensors. Such devices are poised to grow very rapidly over the next decade. Yet, the field of wearable chemical sensors has many challenges to address and technological gaps to fill before realizing its full potential. Addressing these challenges will accelerate the commercial viability of wearable chemical sensors that are low-power and easily integrated with the human body, and provide valuable information in a user-friendly and secure manner to the wearer in a continuous fashion. Several of the challenges facing researchers in the field of wearable chemical sensors can only be solved by innovative cross-disciplinary research, involving researchers not only from standard STEM fields but also from Humanities.

Such cross-disciplinary efforts will lead to technologically advanced wearable devices that a wide variety of consumers will be excited to use in their routine daily lives. For example, materials scientists should work on developing novel materials that will enable the transformation of conventional chemical sensors into wearable formats. Sensor stability, accuracy, response time, shelf-life are some of the most pressing needs of wearable chemical sensors. Solving these issues will require a dramatically different approach that what has been

employed by researchers in the chemical sensors field. This is true, since the requirements for the wearables field is quite different from that mandated by laboratory settings.

In addition to the core sensor challenges, one must also look at the other sub-systems that are an integral part of the wearable sensors. For example, researchers working in the energy field should focus on developing wearable and biocompatible power sources that have high energy density and long life, as well as incorporating multi-source energy harvesting systems. At the same time, engineers involved in developing wireless communication systems should develop devices that will allow high density of wearable electronics to interact uninterruptedly with high bit rates. With greater market penetration, wearable sensors are bound to generate huge volumes of personal data and thus data security and user privacy are a matter of major concern. Thus, cryptologists must work on next generation algorithms that will secure the data generated by the wearable sensors.

Besides solving the issues faced by the various above mentioned sectors associated with wearable chemical sensors, one must also work on the seamless integration of these sub-systems. Such integration requires ingenious systems engineering skills since the roadblocks faced by wearable sensors domain are unique, and also because all the sub-systems are deeply interconnected with each other. Challenges for integration arise due to different fabrication processes for various physical components of the whole system. Difference in packaging of the sub-components also leads to ineffective device integration. For example, the chemical sensor must be exposed to the biofluid, while the supporting electronics must be completely sealed from any exposure to moisture. The interface between different sensor components is usually where the entire system is most susceptible to fail. Flawless integration of all these sub-systems is thus extremely critical for the development of wearable chemical sensors. In addition to the need for engineers and scientists to work together, the field of wearable sensors also requires intimate coordination and collaboration with medical practitioners. Wearable

sensors are expected to generate personal health data that was impossible to obtain earlier. Such health monitoring thus requires close collaboration with physicians to correctly interpret the data. It is clear that the wearable chemical sensor field offers exciting collaborative opportunities and that the commercial success of this rapidly growing field will ultimately rely on the abilities of the researchers to continue to innovate and collaborate to address the existing challenges faced by wearable chemical sensors.